

# Design of High Temperature Engineering Test Reactor (HTTR)

2

*Yusuke Fujiwara, Minoru Goto, Kazuhiko Iigaki, Tatsuo Iyoku,  
Hai Quan Ho, Taiki Kawamoto, Makoto Kondo, Kazuhiko Kunitomi,  
Keisuke Morita, Satoru Nagasumi, Shigeaki Nakagawa,  
Tetsuo Nishihara, Naoki Nojiri, Masato Ono, Akio Saikusa,  
Nariaki Sakaba, Taiju Shibata, Yosuke Shimazaki, Atsushi Shimizu,  
Masayuki Shinozaki, Junya Sumita, Yukio Tachibana, Shoji Takada,  
Daisuke Tochio, Takahiro Uesaka and Shohei Ueta*

Sector of Fast Reactor and Advanced Reactor Research and Development, Japan Atomic Energy Agency, Ibaraki, Japan

The HTTR is the first and the only HTGR in Japan, which is installed at the Oarai Research and Development Institute of JAEA. In this chapter, the design details of the HTTR are described as follows:

- 1. Overview of HTTR design features** The general philosophy and specific aspects of the HTTR design and its major characteristics together with history, back ground and objective.
- 2. Nuclear design** Nuclear characteristics, such as reactivity control, power distribution, reactivity coefficients, etc., were evaluated. The reactor can be shut down safely by either the control rods or the reserved shutdown system. The reactor possesses power suppressing safe characteristic due to negative reactivity coefficients.
- 3. Core thermal-hydraulics** The maximum fuel temperature at normal operation and anticipated operation occurrences and the coolant flow rate distribution were evaluated. The safety analysis clarified the maximum fuel temperatures at normal operation and at any anticipated operation occurrences do not exceed the each design limit.
- 4. Graphite components** The design criteria for the graphite components have been developed by JAEA because there were no available design criteria for brittle materials such as graphite. An outline of quality control specified in the design criteria is also described.
- 5. Metallic components** Hastelloy XR was developed for the very high temperature structures such as the heat transfer tubes of the intermediate heat exchanger (IHX) through optimizing or lowering contents of several elements of Hastelloy X. The high temperature structural design guidelines for Hastelloy XR, 2½Cr–1Mo steel, SUS316 and SUS321 austenitic stainless steels and 1Cr–0.5Mo–V steel were established based on the existing design guidelines.
- 6. Core components and reactor internals** Design requirements were settled and extensive design efforts and R&D were performed in order to maintain the integrity of the core components and reactor internals. Assessment of fuel integrity was made comprehensively and the fuel integrity was confirmed as to normal operating and transient conditions of the HTTR. The structural integrity of the graphite components was also ascertained by performing the analytical evaluations.

7. **Seismic design** The validity of the core seismic analysis code called SONATINA-2V was confirmed. Impact load characteristics for the dowel–socket and key–keyway systems and core support posts were clarified quantitatively. The structural integrity of the graphite components against earthquake was also confirmed throughout the seismic tests and the analysis.
8. **Cooling system** The schematic flow diagram of the primary and secondary cooling systems and design requirements of key components such as the primary pressurized water cooler, the IHX, the helium gas circulator and the concentric hot gas duct are described.
9. **Reactivity control system** A design requirement of control rods used in the very high temperature environment is described. Alloy 800H was chosen for the metallic parts of the control rods, because the maximum temperature of the control rods reaches about 900 °C at reactor scrams. The design guideline for the HTTR control rod was made based on ASME Code Case N-47-21. Observing the guideline, temperature and stress analysis were conducted; it can be confirmed that the target life of the control rods of 5 years can be achieved.
10. **Instrumentation and control system** The design outline of the instrumentation, control equipment and safety protection systems and the schematic diagram of control system were described. Their performance such as the in-core temperature monitoring, the reactor power control, the reactor outlet coolant temperature control, etc. was clarified at the rise-to-power test.
11. **Containment structures** The design specifications of the reactor containment vessel, the service area and the emergency air purification system are described. The measured leakage rates of the reactor containment vessel were enough less than the specified leakage limit of 0.1 %/d confirmed during the commissioning tests and annual inspections. The service area was kept in a way that the design pressure becomes well below its allowable limitation by the emergency air purification system.
12. **Other systems** The design specifications of the auxiliary helium systems such as the helium purification, the helium sampling, the helium storage and supply systems, and the fuel handling and storage system.
13. **Safety design** A safety design philosophy of the HTTR considering the major design features of HTGR is described. The strategy of defense in depth was implemented so that the safety engineering functions such as control of reactivity, removal of residual heat and confinement of fission products shall be well performed to ensure safety. The analytical codes for the safety evaluation are also introduced.

## 2.1 Overview of HTTR design features

### 2.1.1 Introduction

JAEA has carried out the research and development on HTGR and high-temperature heat applications since the 1960s. Based on the Long-term Program for Research, Development and Utilization of Nuclear Energy revised by the Atomic Energy Commission of Japan in 1987, the construction of the HTTR was determined and initiated at the Oarai Research and Development Institute of JAEA in 1991. The HTTR attained the first criticality on November 10, 1998, and achieved the full power of 30 MW with the reactor outlet coolant temperature of 850°C on

December 7, 2001. After series of safety demonstration tests, it will be used as heat source of a hydrogen production system [1].

The purpose of the HTTR project is to establish HTGR and nuclear heat utilization technologies and to carry out basic researches on high temperature irradiation. Recently, JAEA has stressed the importance of research and development on the hydrogen production considering significance of hydrogen as an energy carrier for energy security and prevention of global climate change. In order to achieve early deployment of a hydrogen society, which is beneficial for human health and the environment, JAEA is acting as the prominent organization for the HTGR and hydrogen production technologies, and the HTTR is used as a keystone for the development of these technologies.

The HTGR technology is now being established through the accumulation of the operation experience and various test data of the HTTR. As for the nuclear heat application research, development of a hydrogen production system to be connected to the HTTR has been conducted, aiming at realizing the hydrogen production using the nuclear heat. Especially, hydrogen production by the water splitting iodine–sulfur (IS) method that has been developed for a long time by JAEA is seen as the efficient and ultimate clean system, and thus the IS process is considered as the primary candidate to be connected to the HTTR. The GTHTR300 system for generating electricity with high thermal efficiency of about 46%, combining a HTGR and a gas turbine generator system, is also being developed. The basic researches include the development of new materials and the development of high temperature in-core instrumentation technologies.

The HTTR project enables the HTGR and related nuclear heat application technologies to be deployed. As a result, the nuclear heat will be applicable to various fields such as chemical industries, which currently emit large amount of carbon dioxide. The hydrogen production using nuclear heat will completely cut the emission of carbon dioxide and make it possible to realize an ultimate clean hydrogen society. The system for generating electricity with high thermal efficiency of about 46% is expected to be a safe and economically competitive system. The HTGR and related heat application technologies can contribute to the environmental preservation by reducing dependence on fossil fuels and effectively using the nuclear energy.

### **2.1.2 *History and future plan of HTTR project***

Fig. 2.1 shows the history of the HTTR project. For establishing and upgrading HTGR technologies, JAEA decided to construct the high temperature engineering test reactor based on the Long-term Program for Development and Utilization of Nuclear Energy, which was revised in 1987. JAEA obtained the installation permit for the HTTR from the government in November 1990. JAEA received the first approval of the HTTR design and construction methods from the Science and Technology Agency (STA) in January 1991 and started the construction work for the HTTR in March 1991. Excavation was completed in August 1991 and the construction of the concrete base mat was completed in May 1992.

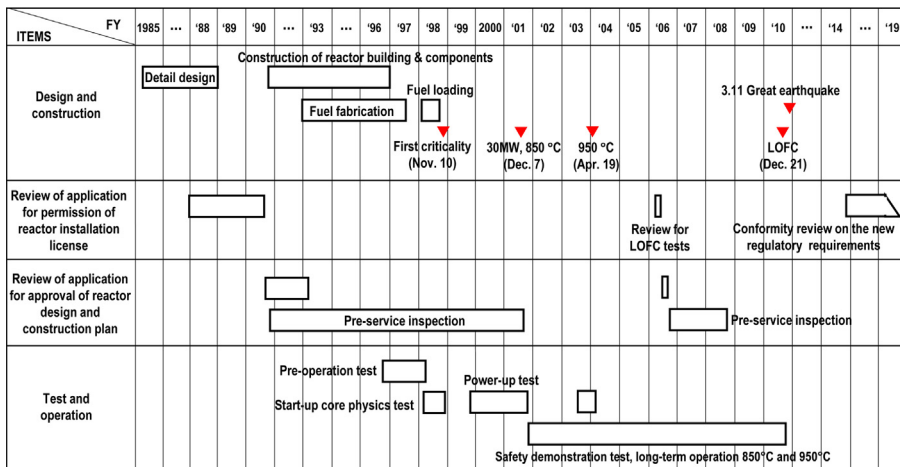


**Figure 2.1** History of HTTR project.

The reactor containment vessel was installed and passed proof pressure and leakage tests successfully in November 1992. The reactor pressure vessel (RPV), intermediate heat exchanger (IHX), primary helium circulators, and primary-pressurized water cooler (PPWC) were installed in the reactor containment vessel in 1994. The first pressure test for the primary cooling system was carried out successfully in October 1995. Construction of the reactor building was completed by closing the temporary opening for carrying in large components in December 1995.

JAEA obtained the uranium material for the first loading fuel in 1994, and manufacture of the fuel rods was completed in October 1997. Assembly of fuel elements was carried out in the reactor building and was completed in December 1997.

Comprehensive and functional tests for each system were started in October 1996, and several malfunctions such as a temperature rise of the upper concrete biological shield of the RPV were found. The improvements were finished by March 1998 [2].

Preparation for the first fuel loading of the HTTR was started in April 1998. During this preparation, some design problems were found in the fuel handling machine. After countermeasures against these problems were finished, the first fuel loading was started on July 1, 1998. The first criticality was achieved in a core of 19 columns at 14:18 on November 10, 1998. Loading of all 150-fuel assemblies was completed on December 16. The criticality tests of the full-loaded core were carried out in January 1999. The criticality tests confirmed the core characteristics of the HTTR. Improvement of the HTTR reactor system and confirmation tests was carried out until August, then the reactor was considered to be ready for the rise-to-power test.

The rise-to-power test was started on September 28, 1999, and the HTTR achieved the full power of 30MW at a reactor outlet coolant temperature of about 850°C on December 7, 2001. The operation permit of the HTTR was issued on March 6, 2002 from the Ministry of Education, Culture, Sports, Science and Technology (MEXT). The following extensive tests using the HTTR were started in

FY 2002. The high temperature test operation was carried out and the reactor outlet coolant temperature of 950°C was achieved on April 19, 2004.

The long-term high temperature operation was successfully completed by using the HTTR at the rated power 30 MW by maintaining the reactor outlet temperature at 950°C for 50 days from January to March, 2011, subsequently after the long-term rated power operation at 850°C for 30 days. The potential of stable high-temperature heat supply to the heat utilization system such as the planned HTTR-IS hydrogen production system was demonstrated. The technical basis of HTGRs was established through the evaluation of the test data [3] concerning the core physics [4], the fission product (FP) retention performance of coated fuel particles (CFPs) [5], the impurity control in coolant helium [6], and the operation and maintenance technology [7].

The safety demonstration tests have been carried out to verify the inherent safety features of the HTGR. It was revealed that the negative feedback effect of the core brings the reactor power lower as the core temperature rises, finally to a safe and stable power level without a reactor scram through the tests simulating the anticipated operation occurrences (AOOs). The control rod withdrawal tests and the coolant flow reduction tests have been successfully carried out to verify the safety evaluation method to reveal the inherent safety of HTGRs [8]. As a result, a loss of forced cooling (LOFC) test using the HTTR was licensed by regulatory authority in 2006 to verify the inherent safety of HTGR under the condition of LOFC while the reactor shutdown system is disabled. The LOFC test simulates the anticipated transients without scram (ATWS), including a LOFC in the core with deactivation of all trains of cooling in vessel cooling system (VCS). The first LOFC test was carried out at thermal power of 30% by using the HTTR in December 2010 [9]. Subsequently, the test of the LOFC with a partial loss of cooling in the VCS was carried out at thermal power of 30% in January 2011. A part of the tests is carried out as an international joint research for safety of innovative reactors organized by the OECD/NEA, the OECD/NEA LOFC project, in March 2011.

JAEA has carried out the inspections of the structures and systems, etc. in parallel with the seismic analysis by using the actual seismic waves measured on the reactor during the earthquake on March 11, 2011, which are needed before restarting the reactor [10].

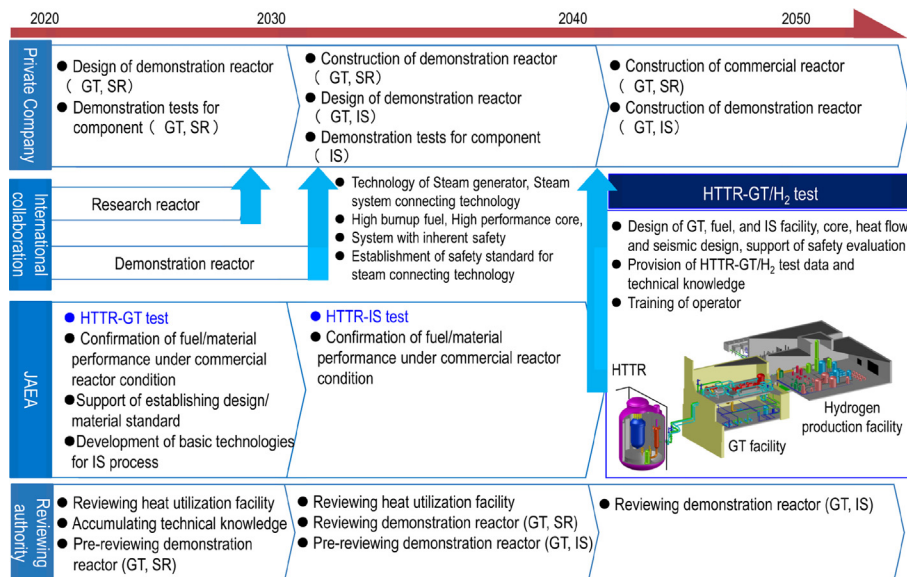
A new regulation standard issued on December 18, 2013, by Nuclear Regulation Authority (NRA). JAEA submitted the evaluation results satisfying the new regulation standard to the NRA on November 26, 2014, which has been reviewed by the NRA.

Fig. 2.2 shows the R&D of HTGR using HTTR and Introduction Plan.

### 2.1.2.1 Evaluation of reactor performance

Based on the HTTR operational data, the HTGR reactor performance has been evaluated and analytical computer codes are verified or modified for predicting realistic reactor performance under steady-state and operational transient conditions.

The evaluation is focused on: (1) core physics in relation with thermal response and control system, (2) thermal analysis for fuel, reactor internals, and high temperature



**Figure 2.2** Present and future plan of the HTTR project.

components, (3) fuel performance on FP release and degradation of the coating layers to contain the FPs, (4) structural integrity of reactor internals and high temperature components, (5) decay heat and residual heat removal characteristics. The fruits from the HTTR operational data and their evaluation are expected to be utilized for the design of the future Japanese advanced HTGR.

### 2.1.2.2 Safety demonstration test

It is well known that safety of medium-size HTGRs can be maintained even in the case of no forced cooling systems functioned with failure of reactor shutdown because of its strong negative feedback, large heat capacity of the core, etc. It is of great importance and one of the best ways for the wide public acceptance to demonstrate such inherent safety of the HTGR using an actual HTGR. It is, therefore, planned in the HTTR to conduct a safety demonstration test. The safety demonstration test may not be enough to convince the public to accept the safety of the HTGR; however, it is helpful from the standpoint of the public acceptance. The obtained test results are useful for validation of HTGR safety analysis codes. The safety demonstration test is divided into two phases.

The first phase test, which simulates anticipated operational occurrences, includes primary coolant flow reduction test and a control rod withdrawal test at power operation. In the primary coolant flow reduction test, coolant flow rate is reduced by running down one and two gas circulators out of three. This test demonstrates that rapid decrease of coolant flow rate brings reactor power to stable level by the negative reactivity feedback of the core without a reactor shutdown. Due to these tests, the basic characteristics of the HTTR are confirmed and analytical codes for reactor transients are validated. The second phase test simulating accident

conditions will be conducted after completion of the first phase test. The second phase test contains LOFC test and VCS stop test.

### ***2.1.2.3 Development of process heat application system***

To enhance the nuclear energy application for heat process industries, JAEA has continued extensive efforts for development of hydrogen production systems using nuclear heat from an HTGR. In the hydrogen production by well-established steam reforming of natural gas, the emission of CO<sub>2</sub> is inevitable because natural gas of methane is used as feed gas. Therefore the final goal of the hydrogen production system using HTGR is to produce hydrogen from water without emission of CO<sub>2</sub>.

For this purpose, the thermochemical iodine–sulfur process is under study. After the successful completion of laboratory-scaled test, an engineering basic test is under way aiming to develop the process control technique. Continuous hydrogen production tests with the test facility made of industrial materials such as metal and ceramics are currently under way. A process heat application system will be coupled to the HTTR in the future, and hydrogen will be produced directly by using nuclear energy.

### ***2.1.3 Major design features of HTTR***

The major specifications of the HTTR are summarized in [Table 2.1](#). The HTTR consists of the reactor core, a reactor cooling system, engineered safety systems, instrumentation, and control system. [Figs. 2.3–2.5](#) show the cutaway view of HTTR reactor building, the schematic view of reactor components and reactor core structures and the RPV, and the cooling system of the HTTR, respectively [11,12].

**Table 2.1** Major specification of HTTR [11].

Thermal power (MW)	30
Outlet coolant temperature (°C)	850/950
Inlet coolant temperature (°C)	395
Fuel	Low-enriched UO <sub>2</sub>
Fuel element type	Prismatic block
Direction of coolant flow	Downward flow
Pressure vessel	Steel
Number of main cooling loop	1
Heat removal	Intermediate heat exchanger (IHX)
	Pressurized water cooler (PWC)
Primary coolant pressure (MPa)	4
Containment type	Steel containment
Plant lifetime	About 20 years

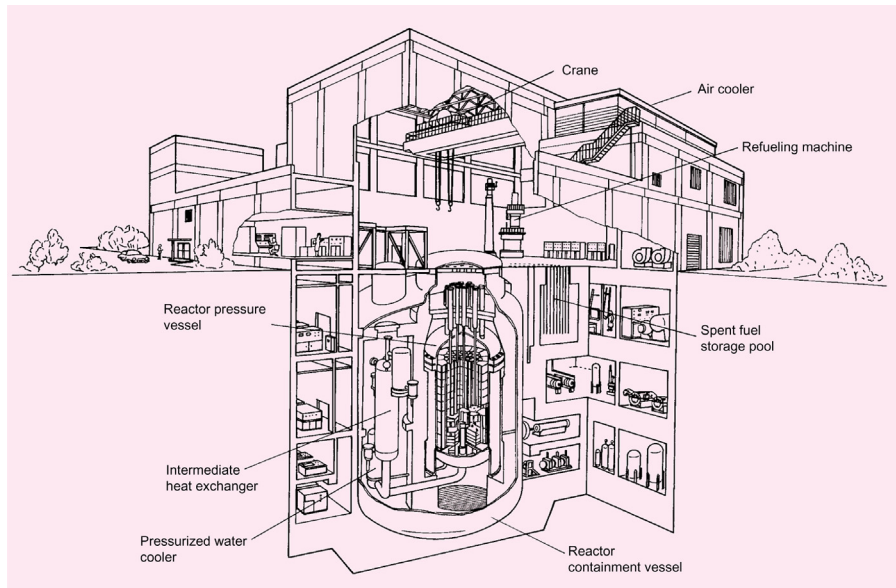


**Figure 2.3** Cutaway view of HTTR reactor building [11].

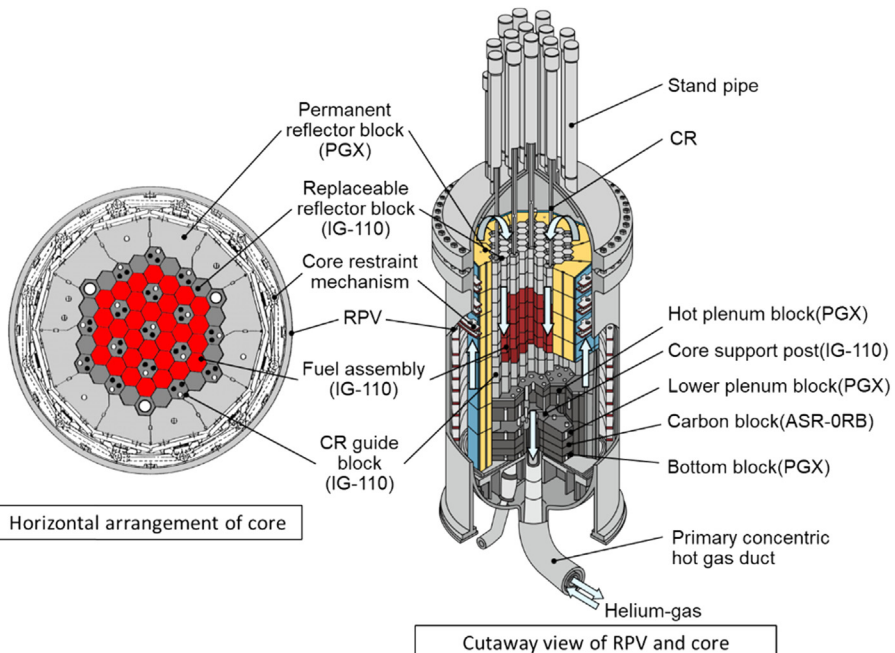


**Figure 2.4** Schematic view of components and reactor core vessel of HTTR [11].

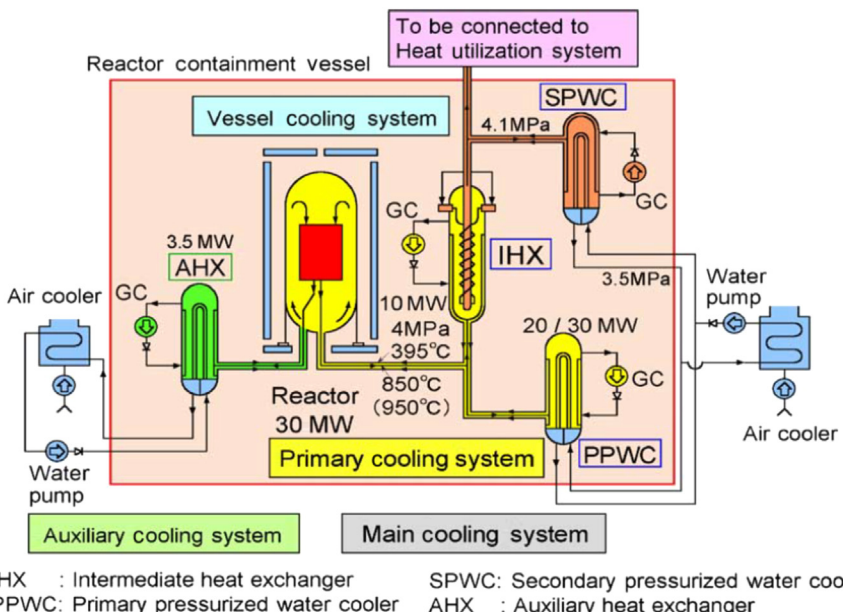


Figure 2.5 Cooling system of HTTR [12].

### 2.1.3.1 Reactor core

The reactor core is composed of core components, reactor internals, reactivity control system, and the RPV as shown in Fig. 2.3.

#### 2.1.3.1.1 Core components

The reactor core consists mainly of hexagonal fuel blocks, control rod guide blocks, and replaceable reflector blocks. The active core, which is 2.9 m in height and 2.3 m in diameter, consists of 30 fuel columns and 7 control rod guide columns. One column is made up of five fuel blocks and four replaceable reflector blocks above and below the fuel blocks. The active core is surrounded by replaceable reflector blocks and permanent reflector blocks. The permanent reflector blocks are fixed tightly by the core restraint mechanism.

A fuel assembly consists of fuel rods and a hexagonal graphite block, 360 mm across flats and 580 mm in height, as shown in Fig. 2.6. The fuel assembly has three dowels on the top and three mating sockets at the bottom to align the fuel assemblies. TRISO-CFPs with UO<sub>2</sub> kernel, about 6 wt.% average enrichment and 600 µm in diameter, are dispersed in the graphite matrix and sintered to form a fuel compact. Fuel compacts are contained in a fuel rod, 34 mm in outer diameter and 577 mm in length. Fuel rods are inserted into vertical holes in the graphite block. Helium gas coolant flows through gaps between the holes and the rods.

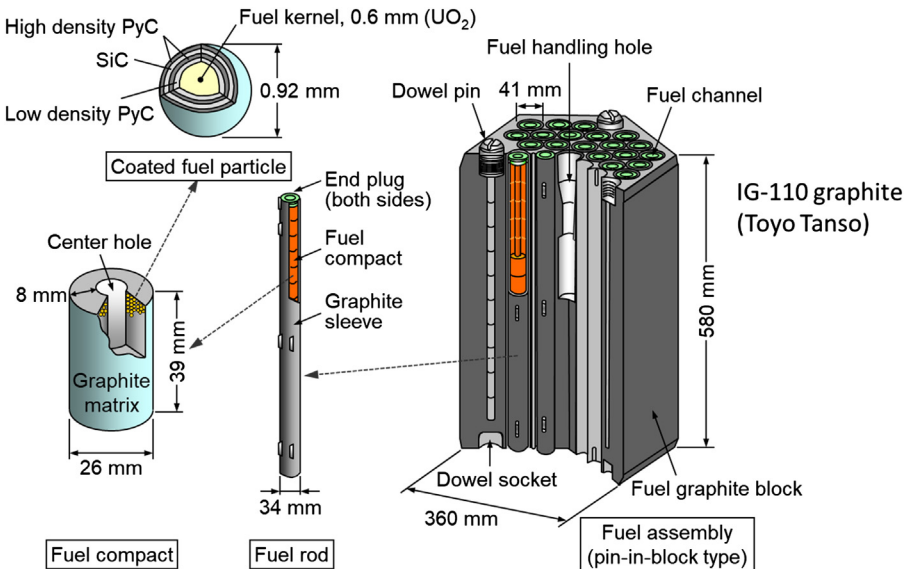


**Figure 2.6** Fuel assembly of HTTR [11].

#### 2.1.3.1.2 Reactor internals

The reactor internals consist of graphite core support structures, metallic core support structures, and the other components as shown in Fig. 2.7.

The graphite support structures consist of hot plenum blocks, core bottom structures (CBSSs), core support posts, etc. The hot plenum blocks provide lateral and vertical positioning and support of the core array. The blocks contain flow paths, which guide the primary coolant from the outlet of the fuel columns and distribute it into the hot plenum beneath the hot plenum blocks. The core support posts are designed so as to support the core and hot plenum block arrays, which form the hot plenum. The permanent reflector block is a graphite structure surrounding the replaceable reflector blocks and control rod guide blocks located in the circumference of the active core. The metallic core support structures are composed of core support plates, a core support grid, and the core restraint mechanisms. The core support plate and the core support grid are placed below the thermal insulation layers. The core restraint mechanism surrounds the permanent reflector blocks.

#### 2.1.3.1.3 Reactivity control system

The control rods are individually supported by control rod drive mechanisms located in stand pipes connected to the hemispherical top head of the reactor vessel. The control rods are inserted into the channels in the active core and replaceable reflector regions around the active core. The control rod drive mechanism withdraws and inserts a pair of the control rods. Reactor shutdown is made at first by inserting nine pairs of control rods into the reflector region, and then by inserting the other seven pairs of the control rods into the active core 40 min later or

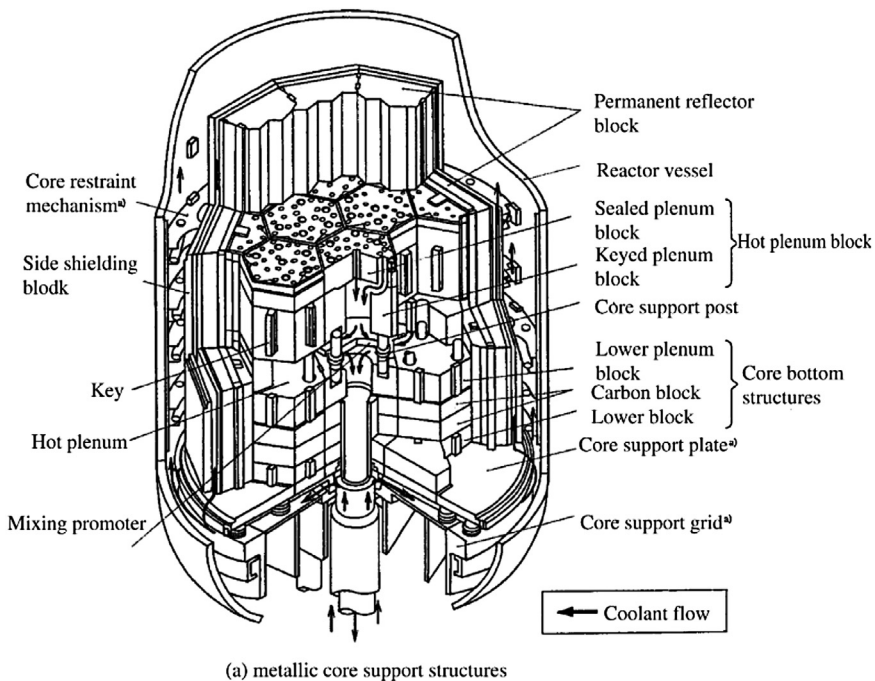


**Figure 2.7** Reactor core internals of HTTR [1].

after the outlet coolant temperature is down to 750°C so that the control rods should not exceed their design temperature limit. Reserve shutdown capability is provided by insertion of B<sub>4</sub>C/C pellets into holes in the control rod guide blocks.

#### 2.1.3.1.4 Reactor pressure vessel

The RPV, 13.2 m in height and 5.5 m in diameter, is made of 2½Cr–1Mo steel. The 2½Cr–1Mo steel has better creep strength at high temperature than Mn–Mo steel, which is widely used in the pressure vessels of light water reactors. The top head of the RPV is bolted to the flange of the cylindrical shell. Thirty-one stand pipes, including the control rod and the irradiation stand pipes, are welded to the top head. A stand pipe closure is installed on the top of each stand pipe and is removed during refueling.

#### 2.1.3.2 Reactor cooling system

The main cooling system of the HTTR is composed of a primary cooling system, a secondary helium cooling system, and a pressurized water-cooling system as schematically shown in Fig. 2.5. The primary cooling system, which has gas circulators and two heat exchangers, that is, a helium–helium IHX and a PPWC, removes the heat from the reactor core to the secondary helium cooling system and pressurized water-cooling system. Primary helium gas is transferred from the core to the helium–helium IHX and the PPWC through a primary concentric hot duct. The

secondary helium cooling system, composed of the secondary pressurized water cooler (SPWC) and a gas circulator, removes the heat from the primary helium gas through the helium–helium IHX. The pressurized water-cooling system consists of an air cooler and water pumps. The air cooler cools the pressurized water for both the PPWC and the SPWC, and transfers the heat from the reactor core to the final heat sink, that is, the atmosphere.

### ***2.1.3.3 Engineered safety systems***

#### ***2.1.3.3.1 Auxiliary cooling system***

The auxiliary cooling system consists mainly of the auxiliary heat exchanger, auxiliary gas circulators, and an air cooler as shown in Fig. 2.5. The auxiliary cooling system has a heat transfer capacity of about 3.5 MW. The auxiliary cooling system automatically starts up when the reactor is scrammed and the main cooling system is stopped by accidents. Core cooling by a forced circulation is possible with the auxiliary cooling system. The auxiliary cooling system consists of redundant dynamic components such as gas circulators, water pumps, and valves that are also operated with emergency power supply.

#### ***2.1.3.3.2 Vessel cooling system***

The VCSs consist of upper, lower, and side cooling panels, around the RPV, and cooling water circulation systems. The VCSs are used as a residual heat removal system when the forced circulation in the primary cooling system cannot be maintained due to the rupture of the inner pipe or both pipes in the concentric hot gas duct. The VCSs are also an engineered safety feature composed of two independent complete sets that are backed up with emergency power supply.

#### ***2.1.3.3.3 Containment structure***

The containment structure consists of a reactor containment vessel, service area, and an emergency air purification system, which reduce the release of FPs to the environment during the postulated accidents. The containment vessel is designed to withstand the temperature and pressure transients and to be leak-tight within the specified limits in the case of primary gas duct rupture. The service area is the space surrounding the containment vessel, where the fuel handling and storage systems and the primary and the secondary helium purification systems are located. The emergency air purification system removes airborne radioactivity and maintains pressure slightly lower than that of the atmosphere in the service area during the accidents.

### ***2.1.3.4 Instrumentation and control system***

#### ***2.1.3.4.1 Instrumentation system***

The nuclear instrumentation system of the HTTR is composed of a wide range monitoring system and a power range monitoring system. The wide range monitoring system is available as a postaccident monitor under accident conditions such as rupture of the primary concentric hot gas duct. The wide range monitoring system is used to measure the neutron flux from  $10^{-8}\%$  to 30% of rated power. Three

fission chambers are installed in the permanent reflector blocks through the stand pipes. The power range monitoring system is used to measure the neutron flux from 0.1% to 120% of rated power. The power range monitoring system is also used as the sensor for the reactor power control system. The detectors of the power range monitoring system are located outside the RPV. Therefore the detectors have high sensitivities so as to detect the neutron flux at a very low level. In order to monitor the core outlet temperature of the primary coolant, seven thermocouples are arranged in the hot plenum blocks below the reactor core. N-type thermocouples (Nicrosil–Nisil) are selected because the temperature of the primary coolant in the hot plenum reaches about 1000°C at rated power operation. The fuel failure detection system is composed of precipitators, a preamp, and a control box. The precipitator is used to detect  $\beta$ -rays radiated from short-lived gaseous FPs such as  $^{88}\text{Kr}$ ,  $^{89}\text{Kr}$ , and  $^{138}\text{Xe}$ .

#### 2.1.3.4.2 Control system

The reactor control system is designed to assure high stability and reasonably damped characteristics against various disturbances during operation. The main control system of the HTTR consists of the operational mode selector, the reactor power control, and plant control systems. The operational mode selector is designed to select several mode operations such as the rated power operation, the high temperature test operation, the safety demonstration test operation, and the irradiation test. The reactor power control system consists of the power control and reactor outlet coolant temperature control devices. The reactor outlet coolant temperature control device gives demand of reactor power to the power control device so that the outlet coolant temperature can be controlled to a certain value. The plant control system controls the plant parameters such as the reactor inlet coolant temperature, the primary coolant pressure, and differential pressure between the primary cooling system and the pressurized water-cooling system or secondary helium cooling system.

#### 2.1.3.4.3 Safety protection system

The safety protection system consists of the reactor protection and engineered safety features actuating systems. It is designed with a 2-out-of-3-circuit logic and 2-trains. The reactor protection system of the HTTR automatically initiates a reactor scram by inserting the control rods and simultaneously stops gas circulators. The engineered safety features actuating system of the HTTR is designed to arrest the release of the FP and to ensure the integrity of the core, the reactor coolant pressure boundary, and the containment vessel boundary against unexpected conditions during abnormal operational transients and accidents such as a primary cooling system pipe rupture.

### 2.1.4 R&D programs for HTTR

#### 2.1.4.1 Fuel

Fabrication technology of high-quality CFPs with low failure fraction and high irradiation resistance was developed. Irradiation tests on the fuel performance under normal operating conditions were conducted using the Oarai Gas Loop No. 1

(OGL-1), the gas-swept capsules, and the closed capsules at the Japan materials testing reactor (JMTR), and the closed capsules at the Japan research reactor-2 (JRR-2). In parallel, the fuel behavior under accident conditions was also investigated in out-of-pile ramped and isothermal-heating tests on irradiated CFPs.

#### **2.1.4.2 Graphite**

High-grade graphite IG-110 with high strength, corrosion, and irradiation resistance was developed and graphite structural design guideline was established. The studies on mechanical properties and nondestructive test of the nuclear grade graphite were performed to support the design and acceptance inspection for the HTTR core and core support components.

#### **2.1.4.3 Metallic materials**

Heat and corrosion-resistant superalloy Hastelloy XR was developed, which can be used at temperatures as high as 950°C at normal operation and 1000°C in accidents, and high temperature structural design guideline for high temperature metallic components was established. Comprehensive qualification tests such as creep, fatigue, and corrosion on Hastelloy XR were carried out to accumulate the test data for structural design and safety evaluation. On the other hand, R&D on a long-term target alloy, Ni–Cr–W superalloy, was carried out for application at service temperatures around 1000°C.

#### **2.1.4.4 Reactor physics**

Reactor physics experiments were conducted using a very high temperature reactor critical assembly (VHTRC). Seven different cores having radial and axial reflectors were assembled at the VHTRC to study the detailed neutronic characteristics of the HTTR core. The VHTRC-1 and -2 cores were loaded mainly with 4 wt.%-enriched fuel and the VHTRC-3 core was loaded mainly with 6 wt.%-enriched fuel. These three cores had an axially uniform loading pattern. On the other hand, VHTRC-4, -5, -6, and -7 cores were loaded with 2, 4, and 6 wt.%-enriched fuel rods in axially zoning patterns.

#### **2.1.4.5 Reactor instrumentation**

In the field of nuclear instrumentation for reactor operation and control, high-temperature fission counter-chambers (HTFCs), gamma-compensated ionization chambers (CICs), and high-sensitive gamma-uncompensated ionization chambers (HSUICs) were developed. The HTFCs and the HSUICs are adopted to the wide range monitoring system and the power range monitoring system of the HTTR, respectively. As for in-core temperature sensors, the advanced Ni–Cr thermocouples, that is, Nicrosil–Nisil thermocouples (N-type TCs), were developed. The N-type TCs have a Nicrosil sheath with a heat-resistant ceramic coat of about

200  $\mu\text{m}$  in thickness. They showed stable electromotive force characteristics under out-pile tests at 1200°C for 20,000 h and in-pile irradiation tests at 1000°C.

#### **2.1.4.6 Heat transfer and fluid dynamics**

##### **2.1.4.6.1 Air ingress process following primary-pipe rupture**

When the primary-pipe rupture accident occurs, the high-pressure helium gas coolant in the reactor is forced out into the reactor containment vessel through the breach. Gas pressure would be balanced between inside and outside of the RPV after a few minutes. After that, it is supposed that air enters the reactor core from the breach due to molecular diffusion and natural convection of a multicomponent gas mixture. In the first stage of the accident, density of the gas mixture in the reactor gradually increases as air enters by the molecular diffusion and natural convection of the gas mixture. Finally, natural circulation of the air occurs suddenly throughout the entire reactor and the second stage of the accident starts. The process of air ingress during the first and second stages was investigated experimentally and numerically. According to the test results, the rate control process of air ingress in the first stage is the molecular diffusion and the very weak natural circulation, which results in a small amount of air ingress rate. On the other hand, air flows into the reactor by the ordinary natural circulation in the second stage, which results in a large amount of air ingress rate.

##### **2.1.4.6.2 Graphite oxidation in case of air ingress into reactor core**

Graphite corrosion rates were investigated experimentally as well as theoretically with a particular focus on corrosion by high temperature gas stream. A coefficient of the graphite corrosion rate was calculated and measured in wide range of gas temperature and O<sub>2</sub> concentration. Experiments of the graphite oxidation at the mass transfer controlled regime (high temperature region) were performed during the natural circulation in the air ingress accidents. The mass transfer coefficients and the generation ratio of CO and CO<sub>2</sub> were obtained.

#### **2.1.4.7 Components and structures at high temperature**

The helium engineering demonstration loop (HENDEL) was constructed for performing full-scale demonstration tests on the core internals and high temperature components for the HTTR. In the fuel stack test section (T<sub>1</sub>) of the HENDEL, thermal and hydraulic performances of helium gas flowing through a fuel rod channel and a fuel stack were investigated for the HTTR core thermal design. In addition, functioning reliability of a control rod drive mechanism and a control rod assembly was confirmed using a mockup model. On the other hand, demonstration tests were conducted to verify thermal and hydraulic characteristics and structural integrity related to the CBS using a full-scale test facility named as the in-core structure test section (T<sub>2</sub>). For example, sealing performance tests revealed that leakage of low temperature helium gas through gaps between the permanent reflector blocks to the core is at very low level compared with the HTTR design value and no change of the leakage flow rate was observed after a long-term operation.

## 2.2 Nuclear design

### 2.2.1 Introduction

The HTTR is a block-type HTGR, designed for 950°C outlet gas temperature. The high outlet gas temperature may increase the FP release from fuel because of increased fuel temperature. Therefore it was important in the nuclear design to suppress the fuel temperature rise by optimizing the power distribution, which was carried out in the following steps.

First, we planned to replace each fuel block with a fresh fuel block after every burn-up cycle. The axial and radial power distribution was optimized to flatten by allocating optimally the fuel blocks with 12 different uranium enrichments of fresh fuel throughout the core.

Second, the loading of fresh fuel blocks throughout the core caused large initial excess reactivity, which resulted in the deep insertion of control rods into the core and resulted in high fuel temperatures. Greater excess reactivity was necessary because fast reactivity depletion resulted from the low conversion ratios of the low-enriched uranium fuel. Thus it was important for the nuclear design of the HTTR to reduce the excess reactivity adequately. The problem with the excess reactivity was solved by optimizing burnable poisons (BPs) in the core. The optimization kept the excess reactivity to the minimum necessary for reactor operations.

Third, deviation from the optimum power distribution due to burnup of fissile materials was avoided by optimizing the specifications of BPs, namely, the poison atom density and the radius for each local area. The excess reactivity of the core was maintained constant. It becomes possible, then, to operate the reactor without changing the insertion position of control rods during power operation at 950°C.

Based on the above design policy, the design requirements, analytical methods, and nuclear characteristics of the HTTR were determined, and the analytical methods were improved based on experimental results [13,14].

### 2.2.2 Design requirement

The main physical parameters of the HTTR core are listed in [Table 2.2](#). The nuclear design must satisfy the following requirements.

#### 2.2.2.1 Excess reactivity

Excess reactivity must be determined taking into account the following effects:

- temperature increase from the cold shutdown state to the rated power operation state;
- build-up of FPs, such as  $^{135}\text{Xe}$  and  $^{149}\text{Sm}$ ;
- burnup of fuel;
- margins including the irradiation tests; and
- uncertainty for nuclear calculations.

#### 2.2.2.2 Reactor shutdown margin

The control rods must be so designed as to provide a reactor shutdown margin of more than  $0.01 \Delta k/k$ , even if one pair of control rods having the maximum

**Table 2.2** Specifications of HTTR [14].

Thermal power (MW)	30
Outlet coolant temperature (°C)	950
Inlet coolant temperature (°C)	395
Primary coolant pressure (MPa)	4
Core structure	Graphite
Equivalent core diameter (m)	2.3
Effective core height (m)	2.9
Average power density (W/cm <sup>3</sup> )	2.5
Fuel	UO <sub>2</sub>
Uranium enrichment (wt.%)	3–10
Type of fuel	Pin-in-block
Burnup period (days)	660
<i>Fuel compact</i>	
Outer diameter (cm)	2.6
Inner diameter (cm)	1.0
Length (cm)	3.9
Packing fraction of CFPs (vol.%)	30
Density of graphite matrix (g/cm <sup>3</sup> )	1.7
Impurity in graphite matrix (ppm)	<1.2 (boron equivalent)
<i>CFP</i>	
CFP diameter (μm)	920
Kernel diameter (μm)	600
Density (g/cm <sup>3</sup> )	10.41
Coating material	PyC/PyC/SiC/PyC
Layer thickness (μm)	60/30/25/45
<i>Coolant</i>	
Material	Helium gas
Flow in core	Downward
<i>Reflector thickness</i>	
Top (m)	1.16
Side (m)	0.99
Bottom (m)	1.16
Number of fuel blocks	150
Number of fuel columns	30
Number of pairs of control rods	16

reactivity worth is completely withdrawn and cannot be reinserted. The reserved shutdown system must be designed to allow for a reactor shutdown margin of 0.01 Δk/k or more, even if the control rod system is not available.

### 2.2.2.3 Reactivity addition rate

The maximum reactivity addition rate with the control rods must be limited to such extent that a related power excursion does not impair the integrity of the core, the reactor internal structures, the primary cooling system, etc. In order to satisfy these conditions, the control rod system shall be so designed that the withdrawal length in one step is limited below 50 mm and the maximum reactivity addition rate does not exceed  $2.4 \times 10^{-4} \Delta k/k/s$ , even if the control rods are withdrawn with the permissible maximum speed.

### 2.2.2.4 Reactivity coefficient

An important reactivity coefficient is the power coefficient of reactivity, which is dominated by the Doppler and the moderator temperature coefficients. The reactor core must have a negative reactivity feedback characteristic, which dampens the power level change. To achieve this condition, the reactor core must be designed in such a way that the power coefficient of reactivity is negative for any operation condition.

### 2.2.2.5 Power distribution

The power distribution must be so determined that the fuel temperature does not exceed the limited value during operation. To obtain this condition, the fuel and BP must be loaded so that the maximum fuel temperatures are kept as low as possible.

### 2.2.2.6 Burnup

The maximum average burnup in a fuel element must not exceed 33,000 MWd/t. To achieve the outlet coolant temperature of 950°C,  $^{235}\text{U}$  enrichment distribution and BP distribution in the core are optimized. Therefore burnup of fuel becomes low.

## 2.2.3 Analytical method

The shutdown margin, control rod worth, reactivity coefficient, and power distribution must satisfy the design requirements. Therefore they should be evaluated with a nuclear design code system (NDCS) of sufficient accuracy. The calculation accuracy of the system was evaluated from the measured values of the VHTRC.

### 2.2.3.1 Design codes

The NDCS for the HTTR [15] consists of the computer codes DELIGHT, TWOTRAN-2 [16], and CITATION-1000VP [17]. The program structure of the system is shown in Fig. 2.8. DELIGHT is a one-dimensional lattice burnup cell calculation code, which has been developed in JAERI especially for the nuclear design of the HTTR. This code is used to provide group constants of fuel blocks and graphite blocks for the succeeding core calculation. TWOTRAN-2 is a transport code, which is used to provide the average group constants of a graphite block where control rods are inserted. CITATION-1000VP is a reactor core analysis code, which has been improved from CITATION in JAERI to perform the nuclear characteristics analysis with a whole core model of the HTTR.

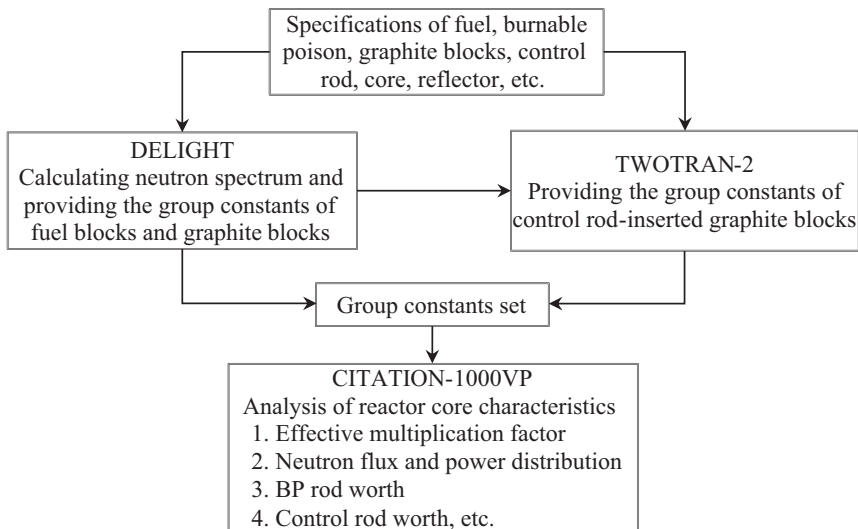


**Figure 2.8** Structure of the nuclear design code system for HTTR [14].

### 2.2.3.2 Validation of design code using very high temperature reactor critical assembly

The critical assembly VHTRC was constructed to obtain data for validation of the NDCS. Calculation errors of effective multiplication factor, neutron flux distribution, BP reactivity worth, control rod worth, and temperature coefficients by the NDCS were confirmed for the NDCS. Calculation errors of Monte Carlo code were also evaluated. The Monte Carlo code showed good agreement with experimental data of the VHTRC [18,19]. The Monte Carlo code could also be applied for the evaluation of HTGR's design.

## 2.2.4 Evaluation of nuclear characteristics

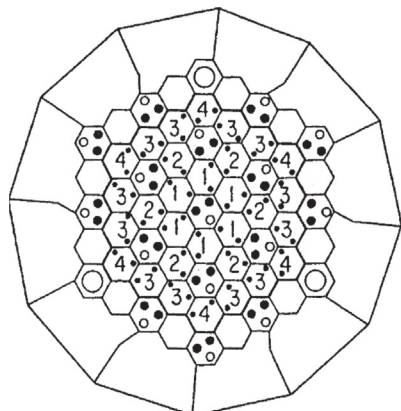
### 2.2.4.1 Excess reactivity and nuclear shutdown margin

The reactivity of the core is controlled by the control rods, BP rods, and reserved shutdown system. The control rods are used for power regulation and shutdown during normal operation because the primary coolant flow rate is kept constant during operation. The BP rods are used to obtain an adequate initial excess reactivity for the operation. The locations of the control rods, BP rods, and reserved shutdown system in the core are shown in Fig. 2.9.

The excess reactivity, reactor shutdown margin and functions of the control rods, BP rods, and reserved shutdown system are described in the following.

#### 2.2.4.1.1 Excess reactivity

The excess reactivity was determined to compensate for reactivity losses. The details of the reactivity losses and excess reactivity are as follows.



Layer <sup>*3</sup>	Fuel zone number <sup>*1</sup>				BP <sup>*2</sup>
	1	2	3	4	
1	6.7	7.9	9.4	9.9	2
2	5.2	6.3	7.2	7.9	2.5
3	4.3	5.2	5.9	6.3	2.5
4	3.4	3.9	4.3	4.8	2
5	3.4	3.9	4.3	4.8	2

\*1 235U enrichment (wt%)

\*2 Natural boron concentration (wt%)

\*3 The number indicates the layer number from the top fuel block

**Figure 2.9** Fuel and BP configuration plan of HTTR core [14].

## Reactivity losses

1. Reactivity loss from the cold shutdown state to the rated power operation state.
2. Build-up of rapidly saturating FPs, such as  $^{135}\text{Xe}$  and  $^{149}\text{Sm}$ .
3. Depletion of fissile material and the build-up of heavy metal isotopes.
4. Build-up of slowly saturating FPs.
5. Reactivity margin of irradiation tests.

The reactivity losses of (1) and (2) are about  $0.064 \Delta k/k$  and  $0.024 \Delta k/k$ , respectively. The sum of the reactivity losses of (3) and (4) is about  $0.043 \Delta k/k$ . The total of the reactivity losses is about  $0.131 \Delta k/k$ .

**Excess reactivity** The excess reactivity is determined to compensate for the reactivity losses and provide a reactivity margin for operation. The reactivity margin for operation is about  $0.003 \Delta k/k$ . The excess reactivity is then about  $0.165 \Delta k/k$  in consideration of calculation uncertainties ( $0.016 \Delta k/k$ ) and reactivity increase due to the irradiation test of fuel ( $0.015 \Delta k/k$ ).

### 2.2.4.1.2 Burnable poison rods

If the core does not contain the BP rods, the excess reactivity of the core becomes too high to control the reactivity by the control rods only. The excess reactivity is reduced by the neutron absorption effect of the BP rods to an adequate value as

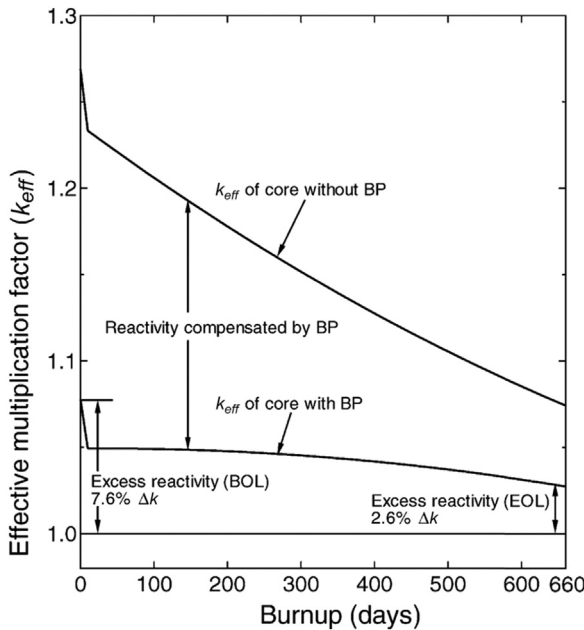


**Figure 2.10** Change in excess reactivity in rated power operation state where control rods are fully withdrawn [14].

shown in Fig. 2.10. In cold condition, the reactivity compensated by the BP rods is 0.113  $\Delta k/k$  at beginning of life (BOL).

#### 2.2.4.1.3 Controllable reactivity and shutdown margin

**Control rod** Seven pairs of the control rods are inserted into the active core, and nine pairs into the removable reflector region. The control rods are designed so that the controllable reactivity is larger than the excess reactivity to achieve a sufficient shutdown margin. The controllable reactivity of the control rods corresponds to the core reactivity, which is held by full insertion of all control rods except for two pairs. One is the pair at the core center. This pair is dismantled during irradiation tests. The other is a pair of the control rods neighboring the core center. This pair has the maximum reactivity worth among all pairs of the control rods, and it should be considered for the shutdown margin evaluation to be inoperable at the fully withdrawn position. The controllable reactivity, in this case, is at least 0.18  $\Delta k/k$  taking into the calculation uncertainties, and the shutdown margin more than 0.015  $\Delta k/k$ .

**Reserved shutdown system** The absorbers of the reserved shutdown system are pellets produced by sintering  $B_4C$  powder and graphite. These pellets can be released from the storage hoppers into the reserved shutdown system holes in the control rod guide columns to act as a backup system for the control rod system. The reserved shutdown system in the core center is not involved in measuring the controllable reactivity worth since the control rod guide column is not used for the reserved shutdown

system during the irradiation test. The controllable reactivity of the reserved shutdown system is at least  $0.18 \Delta k/k$  for any operating control rod configuration including consideration of calculation uncertainty. The reserved shutdown system must be capable of compensating the reactivity, which arises in the change from the full-power operation state to the cold shutdown state. This reactivity increase is less than  $0.088 \Delta k/k$  for any operation condition through a burnup cycle. The shutdown margin of the reserved shutdown system is about  $0.092 \Delta k/k$  for all operating conditions.

## 2.2.4.2 Reactivity addition rate and reactivity coefficient

### 2.2.4.2.1 Reactivity addition rate

The reactivity addition rate results from the driving speed and reactivity worth of a control rod. The maximum driving speed of the control rod is 60 cm/min. The maximum control rod reactivity worth per unit length is  $2.3 \times 10^{-4} \Delta k/k/cm$ . The maximum reactivity addition rate is then  $2.3 \times 10^{-4} \Delta k/k/s$ .

### 2.2.4.2.2 Reactivity coefficient

Reactivity coefficients include the Doppler, moderator temperature, and power coefficients. The Doppler coefficient is the rate of reactivity change due to a change in the average fuel temperature, and is negative for any operating conditions as shown in Fig. 2.11. The moderator temperature coefficient is the rate of reactivity change due to a change in the moderator temperature. It is largely negative for all temperatures at BOL, but could become positive within a certain temperature range at end of life (EOL), as shown in Fig. 2.12. The power coefficient is the rate of reactivity change due to a

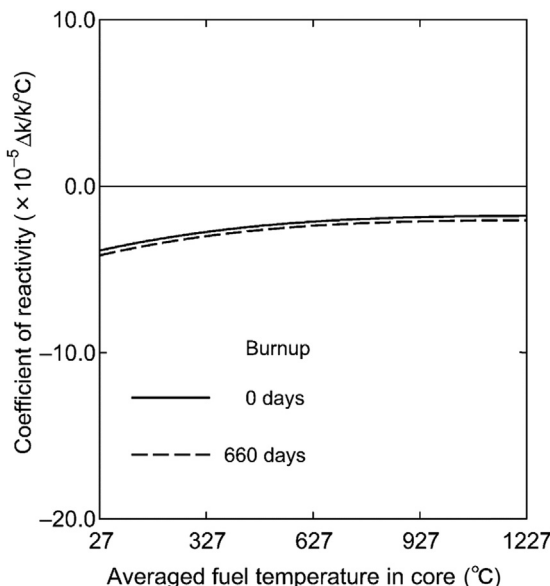


Figure 2.11 Doppler coefficients at BOL and EOL [14].

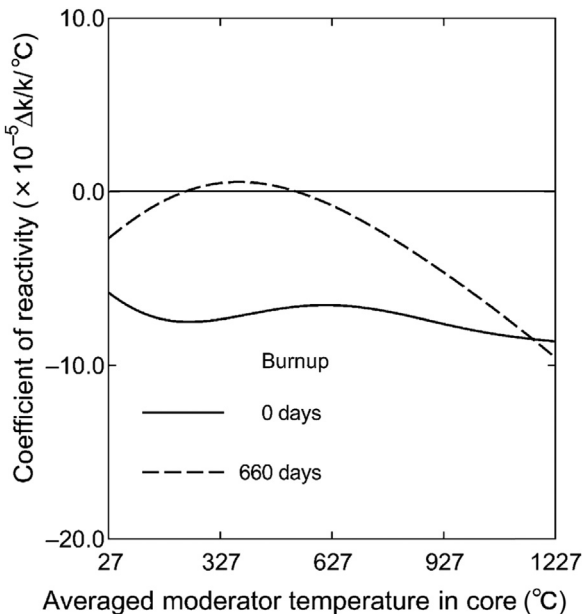


Figure 2.12 Moderator temperature coefficients at BOL and EOL [14].

change in the reactor power level. The power coefficient, dominated by the combination of the Doppler and the moderator temperature coefficients, remains negative at any temperature even if there is the possibility of positive moderator temperature coefficient.

### 2.2.4.3 Power distribution and burnup

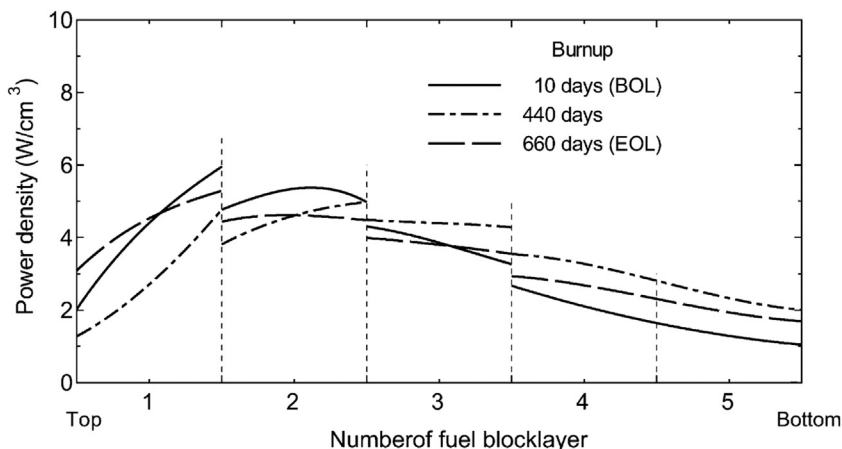
#### 2.2.4.3.1 Power distribution

To achieve the high reactor outlet coolant temperature of 950°C, the  $^{235}\text{U}$  enrichment and natural boron concentration of the BP rod in each fuel block are determined to keep the maximum fuel temperature as low as possible. The  $^{235}\text{U}$  enrichment and natural boron concentration are also shown in Fig. 2.9. To keep the radial power distribution unchanged through the burnup cycle, the  $^{235}\text{U}$  enrichment in the outer region has to be larger than in the inner region. To create an axial fuel temperature distribution as uniform as possible, the  $^{235}\text{U}$  enrichment in the upper region has to be larger than that in the lower region. This is due to the large temperature difference of 550°C between the inlet and outlet of coolant.

**Radial power distribution** The radial power peaking factors are estimated from the coarse power distribution for various burnup steps. Table 2.3 shows that the radial power peaking factor does not exceed 1.1. Thus the radial power distribution appears to be sufficiently flattened through all of the burnup cycles in uniform fuel temperature distribution. As for the effect of heterogeneity caused by the fuel rods, BP rods, etc., the correction factor of local radial power peaking is estimated and

**Table 2.3** Radial power peaking factor [14].

Burnup (days)	Fuel zone 1	Fuel zone 2	Fuel zone 3	Fuel zone 4
0	1.04	1.07	1.08	1.10
10	1.06	1.08	1.09	1.10
110	1.08	1.08	1.08	1.10
220	1.09	1.08	1.09	1.10
330	1.09	1.08	1.08	1.09
440	1.10	1.08	1.08	1.09
550	1.10	1.08	1.08	1.10
660	1.09	1.09	1.09	1.10

**Figure 2.13** Moderator temperature coefficients at BOL and EOL [14].

confirmed to be less than 7%. This correction factor is accounted for in the maximum fuel temperature evaluation.

**Axial power distribution** The axial power distribution for several burnup steps is shown in Fig. 2.13. At BOL, the power is larger in the upper region because the  $^{235}\text{U}$  enrichment is higher than that of the lower region. With burnup progress, the power in the upper region decreases considerably 440 days after BOL. Then the control rods are withdrawn gradually, and the power in the upper region increases again. In spite of these power changes, the distribution of the fuel temperature in the core remains very uniform. As for the effect of heterogeneity caused by the fuel and reflector block structure, the correction factor of local axial power peaking is estimated and confirmed to be below 4%. This correction factor is also accounted for in the maximum fuel temperature evaluation.

#### 2.2.4.3.2 Burnup

The average burnup of each fuel block at EOL is shown in Table 2.4. The maximum burnup appears in the second layer in the second fuel zone, and amounts to

**Table 2.4** Average burnup (MWd/t) of each fuel block at EOL [14].

Axial fuel layer	Fuel zone 1	Fuel zone 2	Fuel zone 3	Fuel zone 4
1	20,500	21,000	20,500	21,000
2	31,000	31,500	30,500	30,500
3	27,500	28,500	27,000	26,500
4	18,500	19,000	17,500	17,500
5	13,000	13,000	12,000	12,000

31,500 MWd/t. Thus even considering the uncertainty in the heavy metal inventory, the maximum burnup remains within the design limit of 33,000 MWd/t. The average burnup of the core is about 22,000 MWd/t. To achieve 950°C of outlet coolant temperature,  $^{235}\text{U}$  enrichment distribution and specification of BP are optimized. Therefore the burnup became relatively low.

## 2.3 Core thermal-hydraulics

### 2.3.1 Introduction

The HTTR is a helium-cooled, graphite-moderated high temperature reactor with 30 MW thermal power and a reactor outlet coolant temperature of 950°C. This maximum outlet coolant temperature of 950°C is achieved in the high temperature test operation mode.

The core thermal-hydraulic design is carried out considering specific characteristics of the HTTR such as a prismatic fuel element and coated fuel particles, the nuclear and core component design, hot-spot factors, fuel design limit, etc. Approximately 95% of the 30 MW thermal power is generated in the fuel elements and the rest in the graphite moderator. Thermal and irradiation conditions become severe for the graphite blocks at the outermost region of the core so that fuel elements in the region contain only 31 fuel rods instead of 33 to keep their structural integrity. The coolant, flowing downward in the annular space between a fuel rod and a hole in the graphite block, is heated to about 1000°C at the exit of the core.

Approximately 97% of the reactor thermal power is removed by the main cooling system with a helium flow of 12.4 kg/s at rated operation and 10.2 kg/s at the high temperature test operation. The rest of the heat is removed, mainly, by the VCS. After reactor scram, the residual heat of the core is removed by the auxiliary cooling system and/or the VCS.

This section describes outline of the core thermal-hydraulic design of the core and the analytical estimation of the maximum fuel temperature based on the experimental results of the HTTR [20].

### 2.3.2 Design requirements

As for the integrity of the fuel itself, it is necessary to maintain the maximum fuel temperature as low as possible under normal operation and any AOOs. The fuel

design limit is determined considering the experimental results of in-pile as well as out-of-pile fuel performance tests simulating reactor operation. The failure of CFPs is caused mainly by kernel migration (amoeba effect) and corrosion of the SiC layer by palladium at high temperatures and a high temperature gradient in the fuel compact. Major safety requirements for the fuel to be maintained intact, especially, in respect of the core thermal-hydraulic design, are as follows:

- The CFPs shall not fail significantly during normal operation.
- The maximum fuel temperature shall not exceed fuel design limit of 1600°C during any AOOs. It is confirmed experimentally that the coating layers of the CFPs would maintain their intactness below 1600°C.

To satisfy these requirements, the maximum fuel temperature limit for normal operation is specified as 1495°C.

### 2.3.3 Design details

[Fig. 2.14](#) shows a calculation flow diagram of the core design including the nuclear and thermal-hydraulic design. The coolant flow rate and coolant temperature distributions are evaluated by the flow network analysis code FLOWNET. The

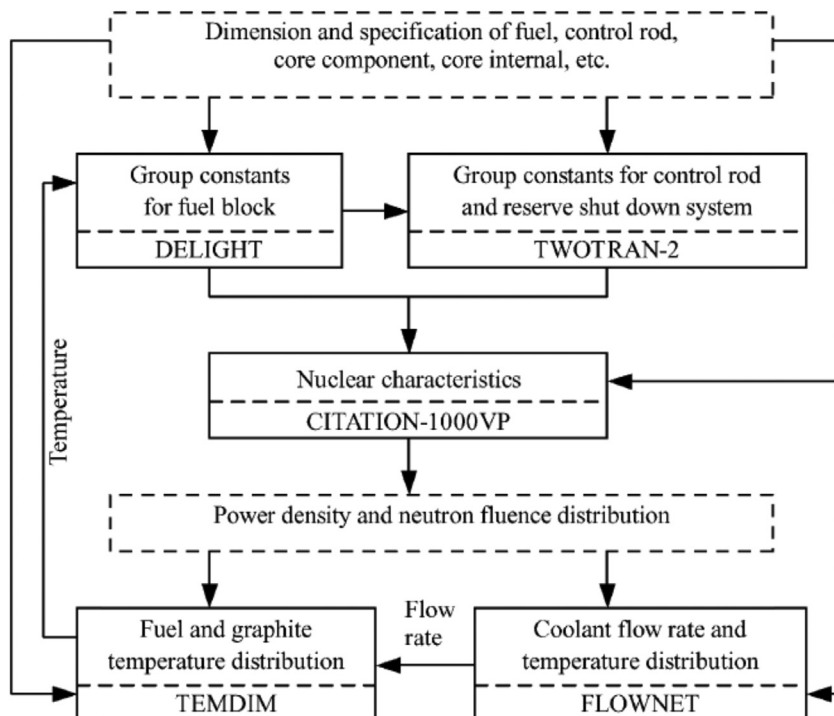


[Figure 2.14](#) Calculation flow of core design [20].

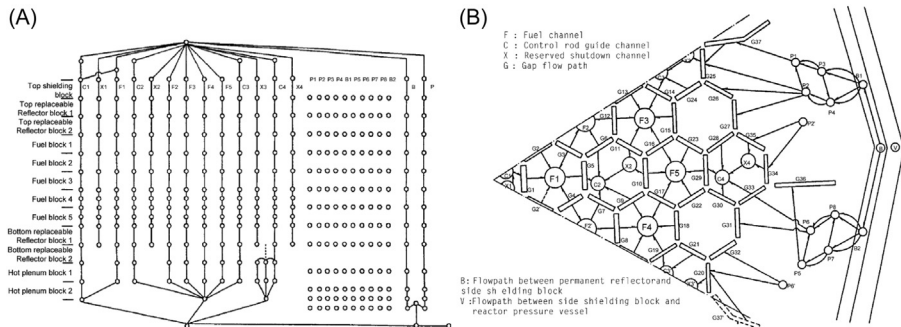


**Figure 2.15** FLOWNET analysis model for HTTR: (A) axial flow network model, (B) radial flow network model [20].

calculation model of FLOWNET consists of one-dimensional flow branches and pressure nodes, which are the junctions or terminals of the branches as shown in Fig. 2.15. Each branch is provided with an equivalent cross-section area, length, hydraulic diameter, and pressure loss coefficient of the actual passage. Pressure loss coefficients used in the calculation for the leakage flow between permanent reflectors and/or hot plenum blocks and the cross-flow between fuel elements, control rod guide blocks, and replaceable reflector blocks were derived from experimental results. A detailed coolant flow distribution is determined based on the power distribution obtained in the nuclear design and the dimensions of the core components and reactor internals. Flow paths, regarding the coolant flow analysis, are the main coolant flow in the graphite blocks, the bypass flow in the intercolumn gaps, the leakage flow through the permanent reflectors and the cross-flow in the horizontal interface gaps of the hexagonal graphite blocks.

To achieve a high reactor outlet coolant temperature of 950°C, it is important to keep the maximum fuel temperature as low as possible. Therefore in the core thermal-hydraulic design, the coolant flow, ineffective to direct fuel cooling, should be minimized. Since the reduction of the ineffective coolant flow such as leakage, cross and bypass flows cannot be eliminated completely in the design of a prismatic fuel core, the plan is to seal the core bypass flow at the outer part of the core. Pressure loss coefficients for each flow branch and the sealing mechanism are derived from experimental results.

The fuel temperature is calculated by the fuel temperature analysis code TEMDIM, using a cylindrical model, based on the power distribution including local power peaking, coolant flow distribution including redistribution in the fuel column, and hot-spot factors. The hot-spot factors or hot channel factors are considered in the core thermal-hydraulic design to evaluate the maximum fuel temperature not only during normal operation condition but also during any AOOs with an adequate conservativeness. They are also used to account for various uncertainties and to assure that the specified maximum fuel temperature in the core does not exceed the fuel design limit at any time and any location during the normal operation condition. Hot-spot factors consist of systematic factors (direct accumulation of conservatism) such as total reactor

power, coolant flow rate, and inlet coolant temperature, and random factors (statistically treated), such as manufacturing tolerances and uncertainties on physical properties.

### 2.3.4 Evaluation results of design

As a result of the coolant flow analysis, an effective core flow rate, as high as 88% of the total flow rate, is achieved for the minimum value. The effective core flow rate is calculated with the worst combination of flow passages and pressure loss coefficients.

The coolant flow rate in the fuel-cooling channel decreases in the flow direction due to the cross-flow. The minimum coolant flow rate occurs at the fourth layer of the fuel. The cross-flow in the upper part of the core flows out of the fuel-cooling channel; in the lower part it flows in the opposite direction. The total leakage flow through the gaps between the permanent reflector blocks is approximately 1.1% of the total coolant flow.

Moreover, the effects of deviations of the coolant flow rate from nominal value, which are caused by column bending, distribution of intercolumn gap width, manufacturing tolerances, etc., are estimated by the sensitivity analysis to determine hot-spot factors for the fuel temperature analysis. Approximately 3.0% of the coolant decreases from the nominal flow rate due to column bending, and is considered as one of the systematic factors relating coolant flow rate. The value of 3.2% is determined as the random factor due to the intercolumn gap width distribution and manufacturing tolerances.

The maximum fuel temperature corresponds to the inner surface temperature of the fuel compact and is shown in Fig. 2.16. The solid lines in the figure show nominal values and the dotted line, the maximum fuel temperature considering hot-spot factors.

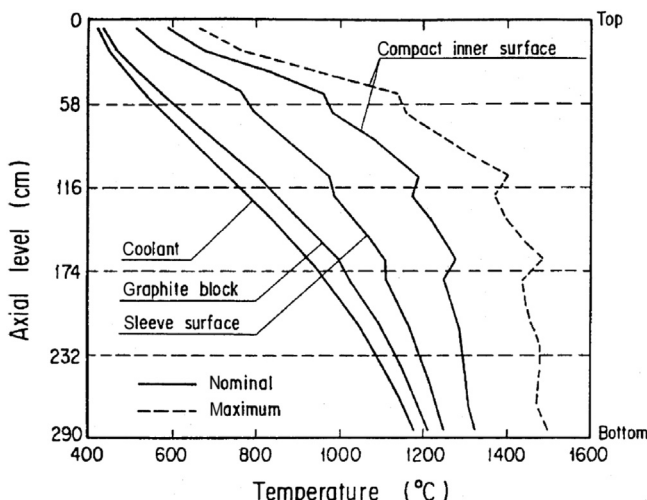


**Figure 2.16** Illustration of axial temperature distribution for 950°C operation [20].

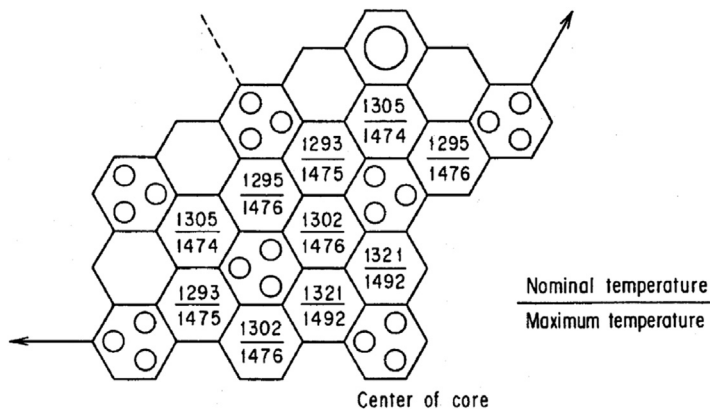


**Figure 2.17** Radial fuel temperature distribution at 950°C operation [20].

The maximum fuel temperature is achieved during the high temperature test operation, and is 1492°C after approximately 440 effective full-power operation days. It does not exceed the 1495°C of the fuel design limit for normal operation. Fig. 2.17 shows the radial temperature distribution at the high temperature test operation.

On the other hand, the maximum fuel temperatures for the rated and the irradiation test operation are 1420°C and 1456°C, respectively, and are less than the temperature for the high temperature test operation. It has also been confirmed that the maximum fuel temperature during an AOOs is 1555°C for a case of abnormal control rod withdrawal at rated operation. In this case, the reactor does not be scrammed because reactivity insertion is below cents.

### 2.3.5 Reevaluation of maximum fuel temperature with operational data

#### 2.3.5.1 Revision of calculation condition

In the thermal-hydraulic design, the maximum fuel temperature is evaluated by using the power distribution calculated by core physics codes, and the coolant flow rate in the fuel channel, calculated by the FLOWNET code, and taking account of hot-spot factors as shown in Section 2.3.4. To reconfirm the fuel integrity during the high-temperature test (950°C) operation mode, the fuel temperature was re-evaluated taking account of the measured data in the rise-to-power test of 850°C. The reevaluation of the maximum fuel temperature was performed with the same method as in the thermal-hydraulic design and the revised hot-spot factors by measurement data through rise-to-power test, gamma ray measurement of fuel block. As for the power distribution and coolant flow rate in the fuel channel, it was confirmed that the core calculation code and FLOWNET code gave valid calculation result as follows.

Power distribution in each fuel block was evaluated by gamma ray from each fuel block. Comparison of measured and calculated results of power distribution in

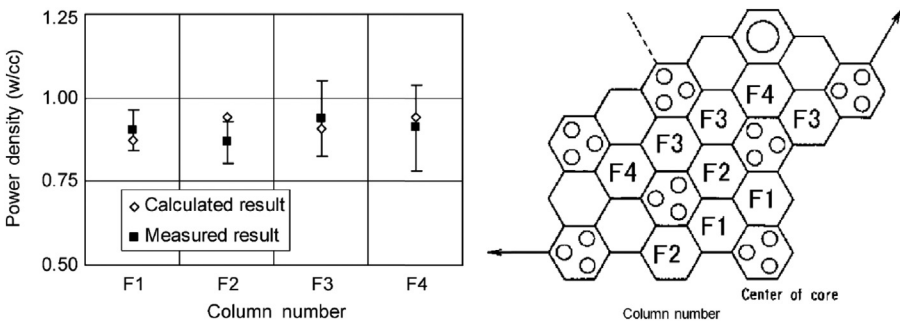


**Figure 2.18** Comparison of experimental and analytical results for power density [20].

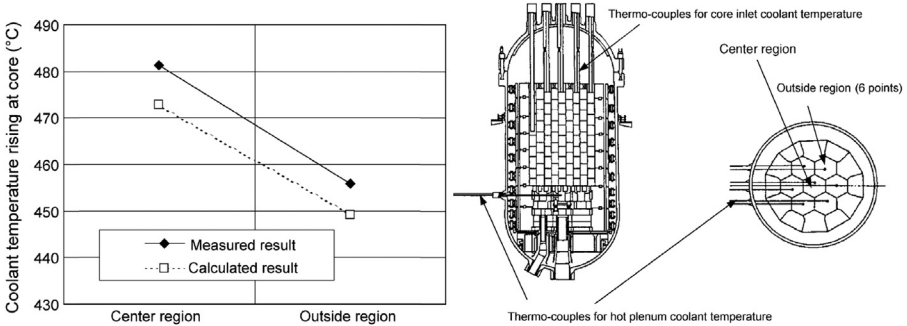


**Figure 2.19** Comparison of experimental and analytical results for coolant temperature rising at core [20].

each fuel column at 9 MW is shown in Fig. 2.18. There is no significant difference between measured and calculated results. Considering uncertainties of measurements of power distribution, calculated power distribution shows good agreement with measured results. Comparison of measured with calculated results of coolant temperature, in the hot plenum block, was carried out. The coolant temperatures in the hot plenum block were calculated by FLOWNET. Comparison of coolant temperatures, in the hot plenum block, is shown in Fig. 2.19. Measured results show higher values at the center. The calculated results also show higher values at the center and show similar temperature differences between the center and the outer region to the measured results. It is concluded that the flow distribution in the HTTR core calculated by FLOWNET code is reliable.

Hot-spot factors, such as reactor power estimation error and power distribution error, were revised based on measured data. For example, a hot-spot factor of uncertainty of reactor thermal power consisted in 2% of measurement error and 0.5% of control systems in the thermal-hydraulic design. In the reevaluation, this hot-spot factor was revised as 1.5% based on an error of measurement system and operation data of HTTR. Moreover, calculation conditions such as core inlet

temperature, total core flow rate, and control rod positions were revised by operation data of the HTTR for realistic evaluations.

### 2.3.5.2 Reevaluation result by operational data

As the result of reevaluation, maximum fuel temperature was estimated as 1463°C at the high temperature test operation at 160 days of effective full-power operation days. This result is below the limit temperature for normal operation of 1495°C; it is also below the results of the thermal-hydraulic design of the HTTR.

An effective core flow rate becomes 90% of the total flow rate. Compared to the results of the thermal-hydraulic design, ratio of coolant flow in a fuel-cooling channel is larger than that in the thermal-hydraulic design. It is due to the revision of calculation conditions of power distribution and flow rate distribution according to operational data.

Axial temperature distributions of coolant and fuel in a fuel column show maximum fuel temperature are depicted in Fig. 2.20.

While maximum fuel temperature occurs at the bottom of fuel column in the thermal-hydraulic design, as shown in Fig. 2.16, maximum fuel temperature occurs at middle of fuel column in the reevaluation. It is due to a change in axial power distribution. In the reevaluation of power distribution, the calculation conditions of control rod position are higher than that in the thermal-hydraulic design. The control rod position is found according to the experimental data. An axial power distribution that shows a “sign curve” is affected by the control rod position. The control rod position becomes higher; thus the position of the axial power peak becomes higher in the core. Therefore the position of the maximum fuel temperature moves to higher positions.

Maximum fuel temperature distribution in each fuel column is shown in Fig. 2.21. In the thermal-hydraulic design, fuel column in the core center shows

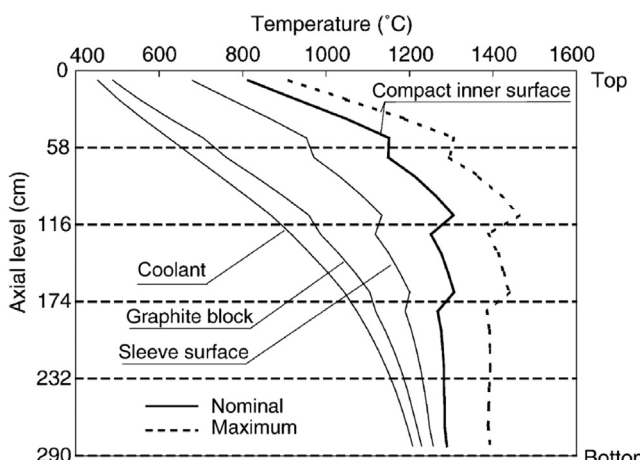


**Figure 2.20** Illustration of axial temperature distribution for 950°C operation [20].

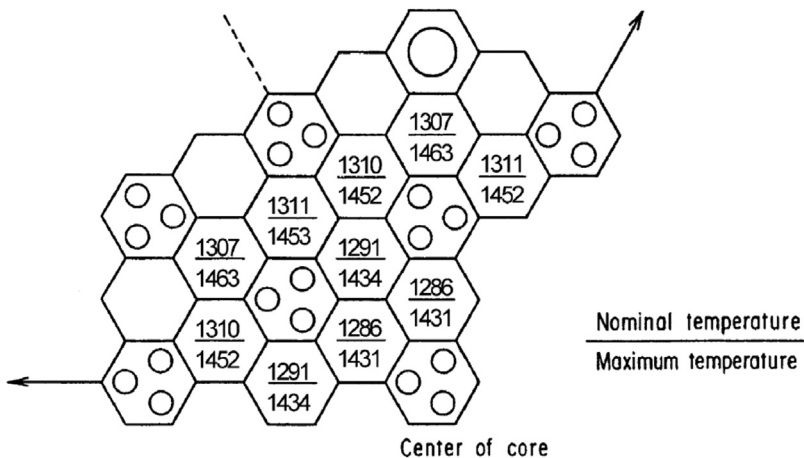


**Figure 2.21** Radial fuel temperature distribution at 950°C operation [20].

higher fuel temperature. In the reevaluation, the outer fuel column shows higher fuel temperature. In the HTTR, radial power distribution is adjusted to be flat during burnup period by a fuel enrichment distribution in the core. However, the radial power distribution changes slightly with increase in burnup. In the thermal-hydraulic design, a maximum fuel temperature of 1492°C appears at 440 days of burnup. The temperature distribution in Fig. 2.21 is the result at 160 days of burnup. The difference of position where maximum temperature occurs is due to the difference of radial power distribution for different burnup.

## 2.4 Graphite components

### 2.4.1 Introduction

The HTTR is a graphite-moderated and helium gas-cooled reactor with the core composed of prismatic fuel elements of hexagonal graphite blocks. The characteristics of graphite are quite different in stress-strain response from metals, since the ductility of graphite is significantly less than the ductility of metals. Needless to say, design codes for metal components cannot be applied directly to the graphite components. JAEA had to develop the design criteria taking account of the brittle fracture behavior. The concept and key specification of the developed graphite design criteria are described, and also an outline of the quality control specified in the design criteria is mentioned.

### 2.4.2 In-core graphite and carbon structure in high temperature engineering test reactor

The reactor core is an array of graphite blocks (fuel assemblies, control rod guide blocks, and replaceable reflector blocks), which provide the physical structure for arrangement and confinement of the fissile fuel materials, neutron moderation, heat

transfer, and the positioning of control/shielding absorber materials. The core is supported by the core support structures and fixed by the core restraint mechanism [11]. As shown in Fig. 2.4, the graphite components are divided into two kinds, one for the permanently installed graphite components of the core support structures and the other for the replaceable components of the reactor core. IG-110 graphite, PGX graphite, and ASR-0RB carbon are used for the in-core components.

#### 2.4.2.1 Core graphite components

The fuel graphite blocks are graphite hexagonal right prisms with an array of fuel holes. The fuel graphite blocks are 360 mm in across flats and 580 mm height as shown in Fig. 2.6. Three dowel pins are installed on the top face, and they engage with dowel socket in the bottom face of the block above. The dowel arrangement ensures the correct orientation of fuel graphite blocks within the column with respect to each other. They are fabricated from IG-110 graphite, isotropic fine grained nuclear grade graphite. Table 2.5 shows typical thermomechanical properties of the IG-110 and PGX graphite, and ASR-0RB carbon [21]. Control rod guide blocks and replaceable reflector blocks have the same external shape as the fuel blocks. They are also fabricated from the IG-110 graphite.

#### 2.4.2.2 Core support graphite components

The hexagonal hot plenum block array is made up of two axial layers. This structure provides lateral and vertical positioning and support of the core array. The hot plenum block assembly contains passages, which collect the primary coolant flow from the outlet of the columns and distribute it into the high temperature plenum beneath the hot plenum blocks. Hot plenum blocks operate at core outlet gas

**Table 2.5** Typical thermomechanical properties of graphite and carbon materials (unirradiated and unoxidized condition) [21].

	IG-10	PGX	ASR-0RB
Bulk density (kg/m <sup>3</sup> , 300 K)	$1.78 \times 10^3$	$1.73 \times 10^3$	$1.65 \times 10^3$
Mean tensile strength (MPa, 300 K)	25.3	8.1	6.8
Mean compressive strength (MPa, 300 K)	76.8	30.6	50.4
Young's modulus (GPa, 300 K) ( $\pm \% S_u$ ) <sup>a</sup>	7.9	6.5	8.7
Mean thermal expansion coefficient (293–673 K) ( $10^{-6}/\text{K}$ )	4.06	2.34	4.40
Thermal conductivity (W/mK, 600 K)	80	75	10
Ash (ppm)	Max. 100	Max. 7000	Max. 5000
Grain size ( $\mu\text{m}$ )	Mean 20	Max. 800	Max. 2000

<sup>a</sup>Determined from the cord joining two points (one point is the one-third of the specified minimum tensile strength and the other is the one-third of the specified minimum compressive strength) on the stress-strain curve.

temperature, 950°C. These blocks are fabricated from PGX graphite, a structural grade, medium-to-fine grained molded graphite.

The core support posts and seats are designed to structurally support the core and hot plenum block array while providing a flow plenum to receive the primary coolant flow exiting the core. The posts and seats are made of IG-110 graphite.

The thermal insulation layer at the core bottom consists of three blocks: lower plenum block, carbon block, and bottom block. The main function of the carbon block, which is fabricated from nuclear grade ASR-0RB carbon, is to keep the metallic core support structures below 500°C. The permanent reflector is a graphite structure immediately surrounding the replaceable reflector and control rod guide columns located in the circumference of the core. The permanent reflector is an assembly of graphite blocks making 12 circumferential segments and 8 axial layers.

### ***2.4.3 Concepts of graphite design criteria***

The design criteria were developed by partially modifying the ASME CE Code in the items of by-axes failure theory, buckling limit, oxidation effects on the basis of test data. The design criteria for the graphite components in the HTTR have been developed by JAEA [22]. The limits in the JAEA design criteria for HTTR are detailed in the following.

#### ***2.4.3.1 Component classification***

The graphite components have different use and functions as follows:

1. The core graphite components are replaced at regular intervals; on the other hand, the core support graphite components are permanent components, not replaced as shown in [Table 2.6](#).
2. The core support components have more serious structural functions than the core components, that is, the core support components are thought to be more important from a safety viewpoint.

Therefore the graphite components are divided into two components, core components and core support components, and the stress limit for the core support graphite components is specified to be more severe than for the core graphite components.

**Table 2.6** Differences between core and core support graphite components [21].

	<b>Core graphite components</b>	<b>Core support graphite components</b>
Main component	Fuel block	Hot plenum block
	Graphite sleeve	Permanent reflector block
	Control rod guide block	Core bottom structure
	Replaceable reflector block	Core support post
Replaceability	Routine	
Irradiation effects	Major	
Design life	3 years	

### 2.4.3.2 Fracture theory

Several fracture theories are proposed as applicable to the graphite strength. From taking into consideration of simplicity in design and conservative in evaluation, the maximum principal stress failure theory, partially introducing the modified Coulomb–Mohr theory, is adopted on the basis of strength data. As shown in Fig. 2.22 with reference data [23], the maximum principal stress failure theory should be applied in the first quadrant (tensile–tensile stress condition). This theory can be even extended partially into the fourth quadrant (tensile–compressive stress condition). In the lower part of the fourth quadrant where the compressive stress component is higher, the modified Coulomb–Mohr fits the data satisfactorily.

### 2.4.3.3 Stress classification

There are two kinds of stress categories, primary stress and secondary stress. The primary stress is produced by pressure load, dead load, etc., and this stress is not reduced by the deformation of components; instead, there is stress redistribution. On the other hand, the secondary stress is produced by thermal load, etc., and this stress is characterized by the stress decrease due to the deformation of components, self-limiting in character. Since the secondary stress is reduced by the plastic deformation for the metallic components, different stress limits for the primary and secondary stresses are regulated, as well known, in the metallic design criteria. On the contrary, graphite, a brittle material with negligible small fracture strain, cannot

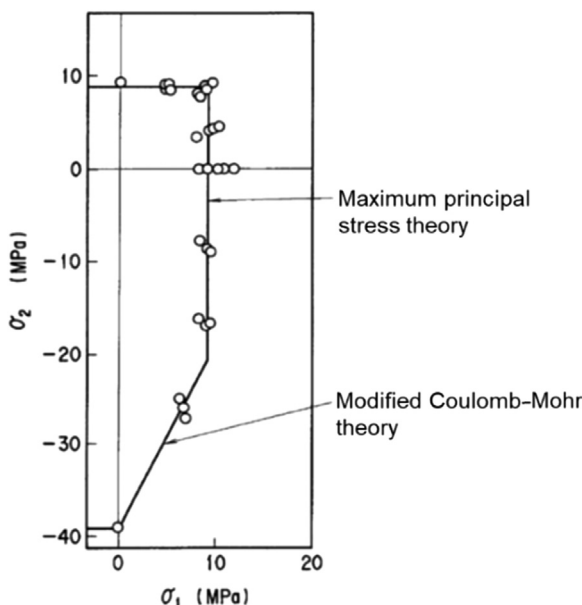
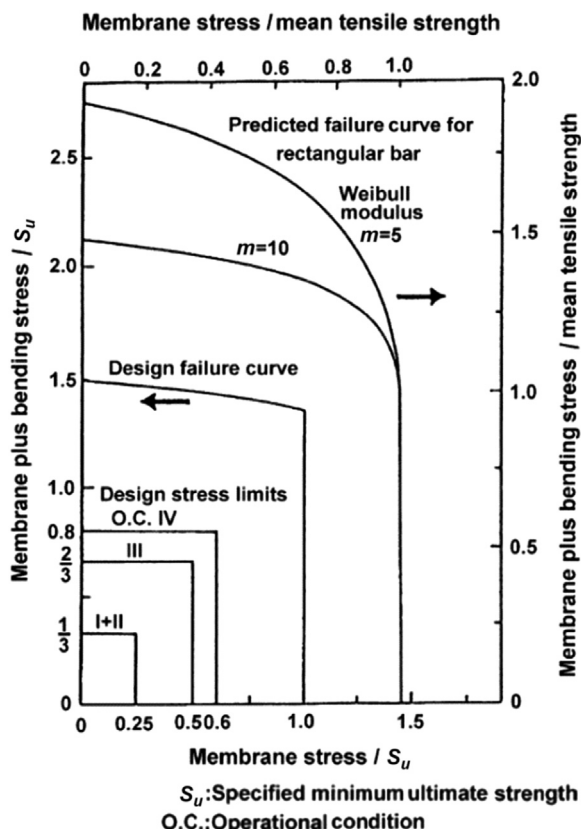


Figure 2.22 Biaxial stress theory of PGX graphite [21].

reduce secondary stress by the plastic deformation. Namely, the secondary stress, for example, thermal stress, will potentially produce cracks and then will produce fracture. The secondary stress is classified in the same manner as the primary stress to evaluate stress limitation conservatively. Namely, stress limitation is taken to the primary plus secondary stress.

#### 2.4.3.4 Stress limit

Peak stress is also limited in order to prevent crack initiation and growth even for a single stress (static fatigue). Bending tests show that graphite bars subject to pure bending exhibit strength higher than companion specimen brought to the same maximum stress in uniaxial tension, which can be derived from Weibull theory. A predicted failure by the theory is shown in Fig. 2.23. This suggests that higher stresses may be allowed for tension plus bending stresses than for uniaxial tension stress.



**Figure 2.23** Predicted membrane plus bending stress failure curves by the Weibull theory and design stress limits for core support graphite components [21].

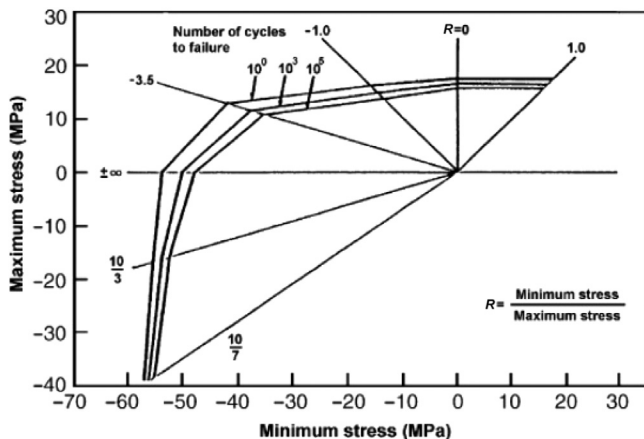


**Figure 2.24** Design fatigue life diagram of IG-110 graphite [21].

From the facts mentioned above, in the design criteria, the stress limits apply to the three stress components: membrane stress, point stress (membrane plus bending stress), and peak stress (total stress).

The design fatigue life diagram is expressed in terms of the ratio of minimum to maximum applied peak stresses on the basis of test data as shown in Fig. 2.24. Several kinds of R ratio show experimental data. For example,  $10/3$  means  $-10$  MPa compressive stress (minimum stress), and  $-3$  MPa compressive stress (maximum stress). The design life diagram is determined with a statistical basis of 99% survival probability with a 95% confidence level, which is consistent with the basis for the specified minimum ultimate strength. Additionally, in a fatigue evaluation, a linear cumulative damage law is assumed, and the usage factors are limited to  $1/3$ ,  $2/3$ , and  $1$  for operating conditions I and II, III and IV, respectively. Special limits of pure shear stress and buckling stress are also considered in the design criteria. The design stress limits (Hopper diagram) are presented for core support components and core components in Figs. 2.25 and 2.26, respectively.

#### 2.4.3.5 Buckling limit

Buckling tests simulating the load imposed on the support post have been conducted to obtain the empirical data for assessing the buckling limit of the support post, because the buckling behavior of the support post is generally difficult to predict only analytical approach. The test results give the formula of critical compressive stress ( $\sigma_{cri}$ ) [24], which is the Rankine–Gordon type, as shown in Fig. 2.27. The design critical stress ( $\sigma_d$ ) is determined conservatively from the critical compressive stress, and the design limits are specified in the design criteria. The design limits are determined such that the safety factor in each operational condition is in accordance with that of the design stress limits for membrane primary plus secondary stresses.

OPERATION CONDITION CATEGORY	PRIMARY PLUS SECONDARY STRESSES		PEAK STRESS	
	MEMBRANE $P_m, Q_m$	MEMBRANE PLUS BENDING OR POINT $P_b, Q_b, P_p, Q_p$	PEAK $F$	FATIGUE
I and II	$P_m + Q_m$	$P_m + Q_m + P_b + Q_b$ OR $P_p + Q_p$	$P_m + Q_m + P_b + Q_b + F$ OR $P_p + Q_p + F$	$0.9 S_u$ 1/3 <sup>2)</sup>
	$0.25 S_u$	$0.33 S_u$		$0.9 S_u$ 2/3
	$0.5 S_u$	$0.67 S_u$		$1.0 S_u$ 3/3
III				
IV	$0.6 S_u$	$0.8 S_u$		

1.  $S_u$  is the specified minimum ultimate strength of the material.

2. Allowable fatigue life usage fraction .

Figure 2.25 Design stress limit for core support graphite components [21].

OPERATION CONDITION CATEGORY	PRIMARY PLUS SECONDARY STRESSES		PEAK STRESS	
	MEMBRANE $P_m, Q_m$	MEMBRANE PLUS BENDING OR POINT $P_b, Q_b, P_p, Q_p$	PEAK $F$	FATIGUE
I and II	$P_m + Q_m$	$P_m + Q_m + P_b + Q_b$ OR $P_p + Q_p$	$P_m + Q_m + P_b + Q_b + F$ OR $P_p + Q_p + F$	$0.9 S_u$ 1/3 <sup>2)</sup>
	$0.33 S_u$	$0.5 S_u$		$0.9 S_u$ 2/3
	$0.5 S_u$	$0.75 S_u$		$1.0 S_u$ 3/3
III				
IV	$0.7 S_u$	$0.9 S_u$		

1.  $S_u$  is the specified minimum ultimate strength of the material.

2. Allowable fatigue life usage fraction .

Figure 2.26 Design stress limit for core graphite components [21].

#### 2.4.3.6 Stress analysis

Since the maximum principal stress failure theory, partially introducing the modified Coulomb–Mohr theory, is adopted, the maximum stress is calculated. An elastic analysis is basically carried out in order to estimate the higher stress. The basis for determining stress–strain field is linear elastic stress analysis for the core support graphite components and linear viscoelastic (irradiation-induced creep) stress analysis for the core graphite components.

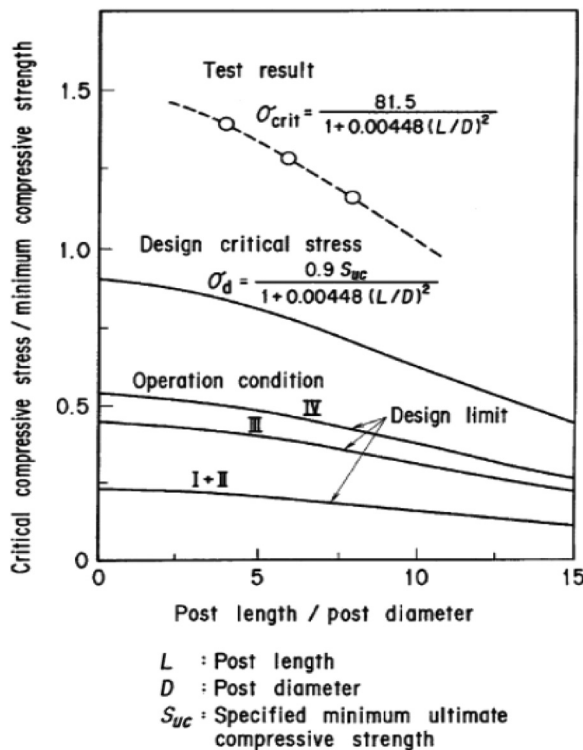


Figure 2.27 Buckling limit of core support post for each operating condition [21].

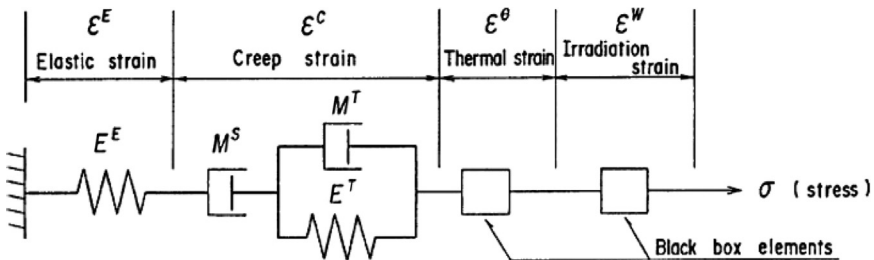


Figure 2.28 Viscoelastic stress analysis model [21].

Since the mechanical and physical properties of graphite change with temperature, irradiation, and oxidation, the design criteria specify that the design analysis shall be made in consideration of these changes. The analytical techniques are proposed in the design criteria for evaluation of irradiation and oxidation effects. A viscoelastic mechanical model, as shown in Fig. 2.28, is specified to use in the analysis of the thermal/irradiation environmental effects for the core graphite components [21].

### 2.4.3.7 Specified minimum ultimate strength

The specified minimum ultimate strength,  $S_u$ , is determined from statistical treatment of strength data such that the survival probability is 99% at a confidence level of 95% because the ultimate strength exhibits considerable statistical scatter. Table 2.7 shows the  $S_u$  values for graphites and carbon specified in the design criteria. As the environmental effect on the strength, both strength increase by neutron irradiation and strength decrease by oxidation are considered; however, strength increases by temperature and strain rate are not considered due to a conservative design viewpoint.

### 2.4.3.8 Oxidation effect

The graphite components in the HTTR are subjected to impurity reactants in the helium gas coolant during a normal operation and might react with O<sub>2</sub> or H<sub>2</sub>O in air or water ingress accidents. There are three kinds of reaction regimes, depending on temperature. At low temperature, in the “chemical regime,” the reactions are so low that the reactant can penetrate the graphite in depth, causing rather uniform attack and thus reducing the graphite strength without changing apparent geometries. At high temperature, in the “mass transfer regime,” the chemical reactivity is so high that thinning of component occurs because of successive surface oxidation. Between these two regimes, in the “in-pore diffusion-controlled regime,” the reactants diffuse in the pores of graphite with the gradient of concentration, resulting in the reduction of strength depending on the burnoff profile.

Since reaction rates depend on the temperature, the kind of reactants and graphite grade, oxidation analysis must be carried out in detail to estimate the burnoff

**Table 2.7** Specified minimum ultimate strength regulated by the graphite design criteria [21].

			Level A (MPa)	Level B (MPa)	Level C (MPa)
IG-110	Tensile strength		19.4	17.6	15.2
	Compressive strength		61.3	57.3	51.0
PGX	Tensile strength	L	6.4	5.9	5.4
		T	5.2	4.4	3.4
	Compressive strength	L	26.6	25.0	23.0
		T	26.1	25.0	23.0
ASR-ORB	Tensile strength	L	4.9	4.4	—
		T	4.8	4.2	—
	Compressive strength	L	46.9	43.6	—
		T	41.6	39.2	—

L, axial direction for original block; T, radial direction for original block; Level A, survival probability 99% with confidence level of 95%; Levels B and C, applicable to low stress components.

profiles of graphite structures. The strength of oxidized graphite is specified in the design criteria to be evaluated in the following manner:

1. Geometry reduction. The region where amount of oxidation exceeds the 80% burnoff shall be regarded as burned away completely from the structure.
2. Strength reduction. The tensile and compressive strength decreases of grade IG-110 are shown as a function of burnoff [25] in Fig. 2.29A and B, respectively [21]. Similar plots are shown in Fig. 2.30A and B for the PGX graphite [21,26,27]. The stress evaluation shall be made according to these figures.

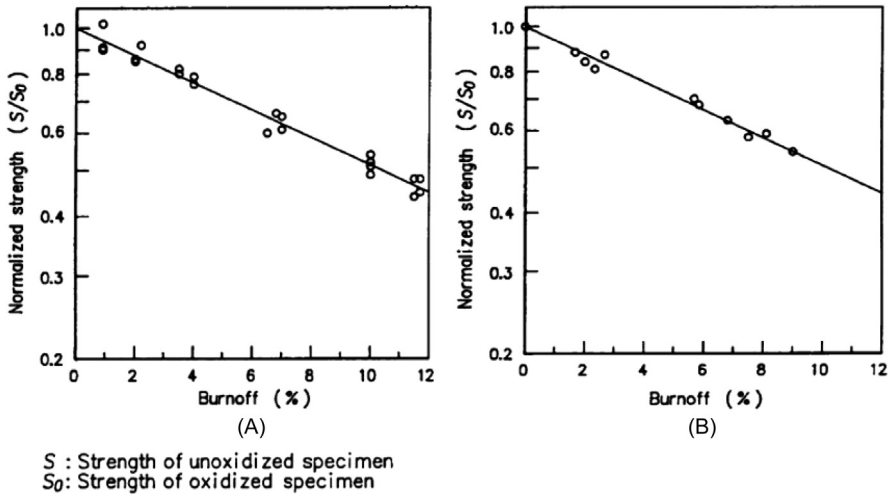


**Figure 2.29** Dependence of strength on burnoff in uniformly oxidized IG-110 graphite [21].  
(A) Tensile strength. (B) Compressive strength.

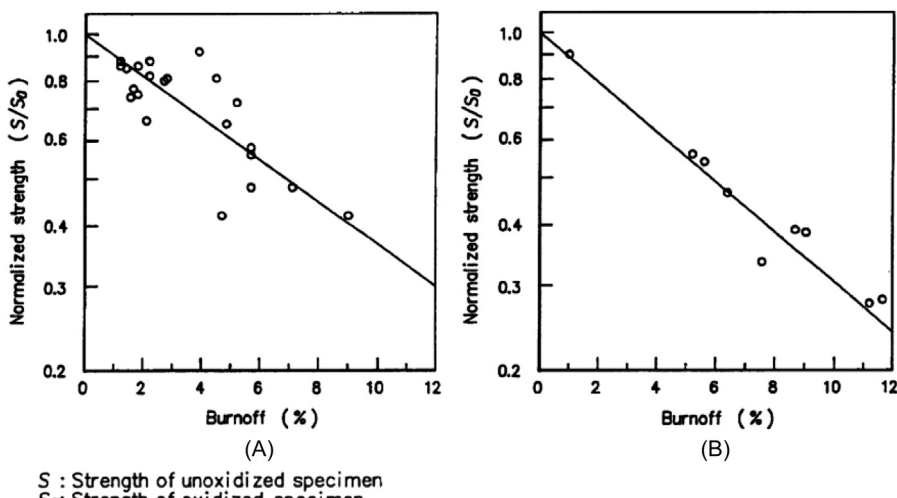


**Figure 2.30** Dependence of strength on burnoff in uniformly oxidized PGX graphite [21].  
(A) Tensile strength. (B) Compressive strength.

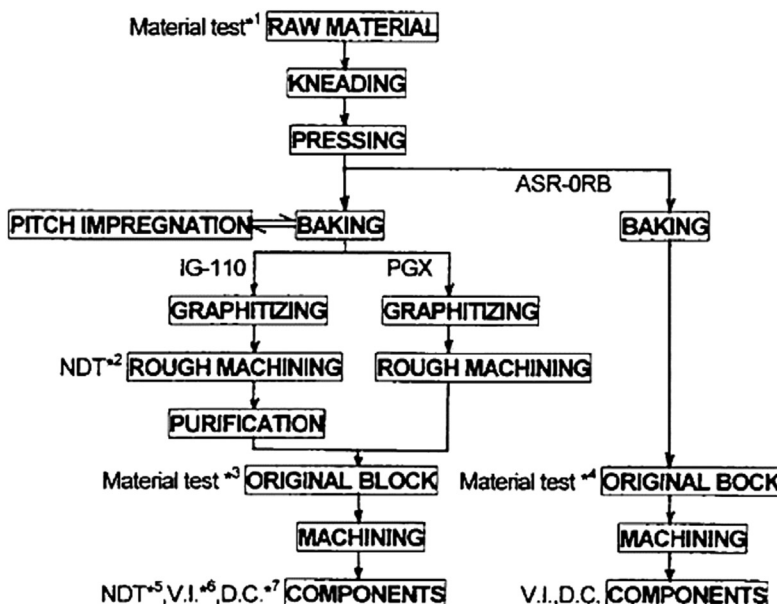
## 2.4.4 Quality control

Industry-wide standards for raw material formulations and processing of graphite and carbon have not been established. Therefore graphite and carbon must be selected on the basis of the appropriate required by reactor design. Their quality should be controlled during production and after machining with respect to their properties and specifications. Fig. 2.31 shows the flow diagram of acceptance test program with the manufacturing process of graphite's and carbon materials.

## 2.5 Metallic components

### 2.5.1 Introduction

The primary cooling system components and related components that serve as the reactor coolant pressure boundaries of the HTTR are used at high temperatures in



\*1: Kind of raw material, \*2: Ultrasonic test

\*3: Bulk density, Electric resistivity, Coefficient of thermal expansion, Anisotropic ratio, Bending strength, Microstructure, Ash contents, Impurity, Tensile strength, Compressive strength

\*4: Bulk density, Electric resistivity, Coefficient of thermal expansion, Thermal conductivity, Bending strength, Microstructure, Ash contents, Tensile strength, Compressive strength, High temperature dimensional stability

\*5: Eddy current test, \*6: Visual inspection, \*7: Dimensional check

Figure 2.31 Flow diagram of acceptance test program for graphite and carbon [21].

creep regime. In particular, the heat transfer tubes and hot header of the IHX are subjected to temperatures above 900°C. The RPV as well as the metallic core support structures are exposed to the reactor coolant at temperatures of around 400°C under an irradiation condition. High temperature structural materials are chosen for the high temperature components of the HTTR, taking into careful considerations the service conditions and safety functions of the components. The materials used are as follows:

- nickel-base corrosion and heat-resistant superalloy, Hastelloy XR;
- normalized and tempered (NT) 2½Cr–1Mo steel;
- two types of austenitic stainless steel, SUS321TB and SUS316; and
- 1Cr–0.5Mo–V steel, an alloy steel bolting material for high temperature service.

Components and their service conditions are listed up for these structural materials in [Table 2.8](#) [13]. Some of the high temperature materials and their service temperatures are beyond the well-established high temperature structural design codes such as the Elevated Temperature Structural Design Guide for the Prototype Fast Breeder Reactor “Monju” (abbreviated as FBR Code) and the ASME Boiler and Pressure Vessel Code Case N-47 [28]. Accordingly, development of a new high temperature structural design guideline was necessary for these materials at their service temperatures. Moreover, at the very high temperatures, where creep deformation is significant, component design based on elastic analysis is not possible. Thus extensive R&D was carried out not only in JAERI but also in national and private research organizations in Japan to establish a reliable high temperature structural design guideline.

### **2.5.2 Development of Hastelloy XR**

Taking into account service conditions of the IHX of the HTTR shown in [Table 2.8](#), a nickel-base Cr–Mo–Fe superalloy Hastelloy X, which has excellent accumulated experiences in jet engines, was selected for the heat transfer tubes and the hot header in the IHX. Hastelloy X is specified as SB-435, -572, -619, -622, and -626 for sheets and plates, bars, welded pipes, seamless pipes and tubes, and welded tubes, respectively, in the ASME Boiler and Pressure Vessel Code Section III Division 1. Since Hastelloy X does not have sufficient compatibility with the primary helium coolant at very high temperatures, Hastelloy XR was developed from Hastelloy X to improve the compatibility.

It was found that for Hastelloy X, tightening the contents of some elements even within the specification of the chemical compositions results in remarkable improvements in the compatibility. The following modification items (1) and (2) were done to Hastelloy X to improve the compatibility and further modification items (3) and (4) were given to improve the applicability to the HTTR.

1. Optimizing manganese and silicon contents: formation of stable and adherent oxidation films is essential for the very high temperature components. Such an oxidation film is formed on the base metal through optimizing the Mn and Si contents for Hastelloy X [29].
2. Lowering aluminum and titanium contents: internal oxidation and intergranular attack are suppressed through lowering the Al and Ti contents [29].

**Table 2.8** Material and service conditions of HTTR high temperature components [13].

Material	Product form	Components	Service conditions		Maximum allowable temperature (°C)
			Design temperature (°C)	Design pressure (MPa)	
9/4Cr–1Mo steel	Plate, forging, pipe	Reactor pressure vessel	440	4.8	550
		Shells of intermediate heat exchanger, primary pressurized water cooler, etc.	430	4.8	
		Outside pipe of concentric double pipe	430	4.8	
Hastelloy XR	Tube, plate forging	Intermediate heat exchanger heat transfer tubes	955	0.29	1000
		Intermediate heat exchanger hot header	940	0.29	
SUS321	Tube	Primary pressurized water cooler heat transfer tubes	380	4.8	650
SUS316	Bar	Core restraint mechanism	450	—	650
1Cr–0.5Mo–V steel	Forging	Core restraint mechanism	450	—	450

3. Lowering cobalt content: radioactive contamination in the primary cooling system by co-containing corrosion products decreases to negligible levels through lowering the Co content [29].
4. Optimizing boron content: addition of boron improves the creep strengths for Hastelloy XR [30] but causes contamination of the core and degradation in weldability. Optimization of the boron content is needed for a specific purpose. To a Tungsten-arc Inert-gas (TIG) welding wire, addition of boron within 40–60 ppm was made to improve the creep strengths of the welded joints.

The specifications of Hastelloy X and the improved version of Hastelloy X, called as the nuclear grade alloy Hastelloy XR, are shown in [Table 2.9](#). [Fig. 2.32](#) shows results of long-term corrosion tests under severe thermal cycles, wherein superiority of Hastelloy XR to Hastelloy X is demonstrated as expected from the protective oxide film formed on Hastelloy XR [31].

### **2.5.3 Identification of failure modes**

A high temperature structural design guideline provides design limits and rules for guarding high temperature components against failure modes. Development of a new high temperature structural design guideline, therefore, requires;

1. Identification of failure modes under exposure to service environments within the guideline application temperature range for each material and
2. development of design limits and rules for guarding against each failure mode with appropriate safety margins.

From reviewing material test results and information on failures at commercial plants and experimental facilities, the following failure modes were identified for the five structural materials mentioned above:

1. ductile rupture by short-term loading,
2. creep rupture by long-term loading,
3. buckling by short-term loading,
4. creep buckling by long-term loading,
5. creep–fatigue failure,
6. gross distortion by incremental collapse and ratcheting, and
7. loss of function by excessive deformation.

These failure modes are the same as those considered in well-established high-temperature structural design codes. It should be noted here that the long-term loading means loading at high temperatures that develops significant creep effect over a long period.

### **2.5.4 Developments of design limits and rules**

The fact that the failure modes for the new materials are the same as for those of the well-established codes suggests the possibility that fundamental philosophies on design limits and rules of the well-established codes can be applicable to the new materials. Among the well-established high temperature structural design codes, the

**Table 2.9** Specifications for chemical compositions of Hastelloy XR and X [31].

Material	Chemical components (wt.%)															
	Range	Elements														
		C	Mn	Si	P	S	Cr	Co	Mo	W	Fe	Ni	B	Al	Ti	Cu
Hastelloy XR	Maximum	0.15	1.00	0.50	0.040	0.030	23.00	2.50	10.00	1.00	20.00	Remainder	0.010	0.05	0.03	0.50
	Minimum	0.05	0.75	0.25	—	—	20.50	—	8.00	0.20	17.00	Remainder	—	—	—	—
Hastelloy X	Maximum	0.15	1.00	1.00	0.040	0.030	23.00	2.50	10.00	1.00	20.00	Remainder	0.010	0.50	0.15	0.50
	Minimum	0.05	—	—	—	—	20.50	0.50	8.00	0.20	17.00	Remainder	—	—	—	—

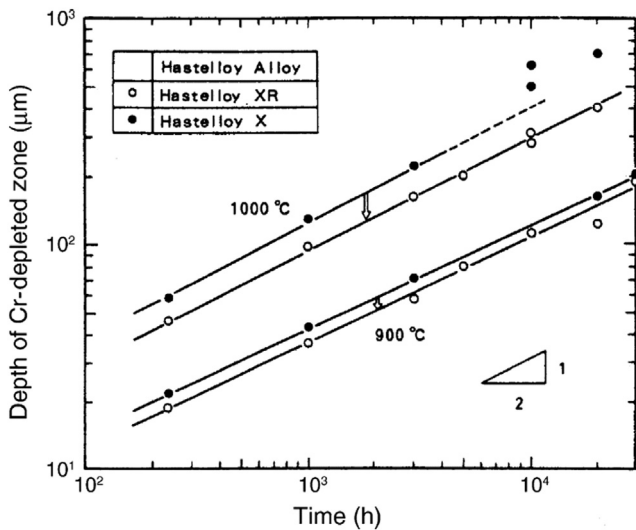


**Figure 2.32** Comparison of environmental effect (Cr-depleted zone depth) between Hastelloy XR and X [31].

FBR Code was the only one that had been authorized by the Japanese government, and so it was the most appropriate for discussion on applicability to new materials. We came to the conclusion that design limits and rules for the abovementioned seven failure modes and for the five materials can be developed on the basis of the fundamental philosophies of the FBR Code.

On this conclusion, the detailed design limits and rules were developed for each material, based on experimental data on material properties and structural mechanics behavior under multiaxial stress states, referring to those of the FBR Code, as described below.

### 2.5.4.1 Hastelloy XR

#### 2.5.4.1.1 Material characterization

The maximum metal temperature of Hastelloy XR in the HTTR reaches about 900°C even during the normal operation and is likely to exceed 950°C but less than 1000°C in events such as a loss of secondary cooling. Taking into account the service temperature conditions, material tests and structural mechanics tests for both base metals and TIG-weld joints were conducted at temperatures ranging from room temperature to 1050°C, mainly in JAEA but also in the National Research Institute for Metals and research laboratories of private nuclear power companies. Test conditions of major material property tests for the base metals are briefly listed in [Table 2.10](#). Test specimens were taken from product forms of tubes, plates, forging cylinders, and bars simulating application to the HTTR high temperature components. By carefully reviewing the experimental data, the following results were derived.

**Table 2.10** Mechanical properties data on Hastelloy XR obtained for high temperature structural design [29].

Test item	Test conditions
Tensile tests	Temperatures: room temperature to 1000°C, every 25°C
	Strain rates: 0.3–100 %/min
Creep tests	Temperatures: 500°C–1050°C, every 50°C
	Maximum test time: about 38,000 h
	Total number of tests: about 300
Fatigue and creep–fatigue interaction tests	Temperatures: room temperature to 1000°C, every 50°C at high temperatures
	Strain rates: $2 \times 10^{-5}$ to $1 \times 10^{-3} \text{ s}^{-1}$
	Hold times: 0–1 h
	Materials: as received and thermally aged
Fracture toughness tests	Thermal aging conditions
	Temperatures: 800°C–1000°C
	Maximum aging time: 2000 h
	Test items: V-notch charpy, fracture toughness, and fatigue crack propagation rate
Corrosion tests	Environment: HTTR coolant gas-simulated helium
	Temperatures: 900°C–1000°C
	Maximum test time: 30,000 h
Others	Poisson's ratio, thermal expansion, and so on

### 2.5.4.1.2 Tensile property

At low or intermediate temperatures up to 800°C, Hastelloy XR is work hardening under monotonic loadings at the strain rate of 0.3 %/min, which is specified for tensile tests by the Japanese Industrial Standards (JIS), and has hardening ratios of two or above, similarly to austenitic stainless steels (the hardening ratio is defined as a ratio of ultimate tensile strength to yield strength). On the other hand, at high temperatures above 850°C, an abrupt decrease in load or a wavy stress–strain curve under straining at this strain rate is observed due to dynamic recrystallization.

Taking into consideration that dynamic recrystallization is not observed at higher strain rates of about 100 %/min as shown in Fig. 2.33, the strain rate for the tensile tests is changed for Hastelloy XR from 0.3 to 100 %/min at high temperatures over

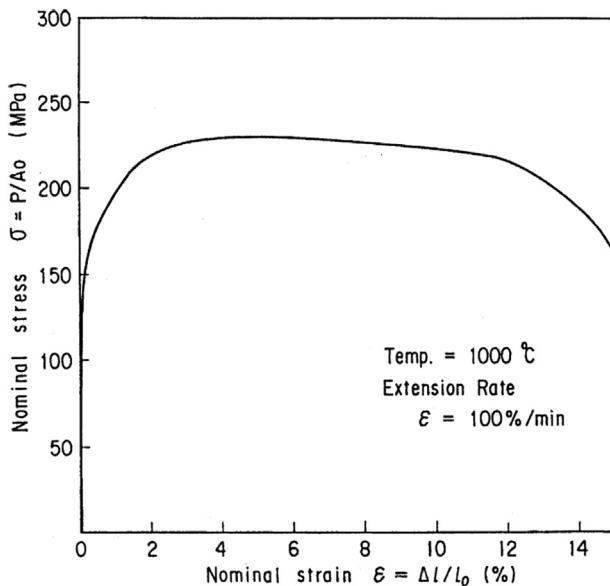


**Figure 2.33** Stress–strain curve for Hastelloy XR (1000°C, extension rate = 100 %/min) [31].

800°C. The time-independent allowable limits were generated from the tensile test data at this higher strain rate.

#### 2.5.4.1.3 Creep property

Since many commercial superalloys are known to lose their stability of mechanical strength at very high temperatures above 1000°C, the maximum temperature by which high temperature strengths, in particular creep rupture strength, are stable for Hastelloy XR is required to be identified. Fig. 2.34 shows that trends in stress dependence and data scattering of the creep rupture strength are quite similar at 1000°C to those at lower temperatures. Therefore it was concluded that Hastelloy XR is stable up to 1000°C.

Concerning the helium environmental effect on creep rupture strength, Fig. 2.35 shows creep rupture lives under a specific stress in various helium environments. Hastelloy XR suffers no degradation in creep rupture strength except in a decarburizing environment. In this figure, a helium environment is characterized fairly well in the stability diagram for Cr ( $a_{Cr} = 0.8$ ), which is expressed by a carbon activity  $a_C$  and oxygen partial pressure  $PO_2$ . Atmospheres denoted as the areas I and II lead to rapid decarburization with or without oxidation, while in the areas IV and V rapid carburization occurs. In area III, mild carburization occurs. In Fig. 2.35, a creep rupture life at a specified helium environment is scaled to lengths of the bar located on the stability diagram. A detailed description of this diagram is given in Kurata et al. [32]. The primary coolant of the HTTR shall be in the area III where any significant degradation in creep rupture life is not observed for Hastelloy XR. Then, it is not necessary to consider helium environment effects on design allowable limits for Hastelloy XR.

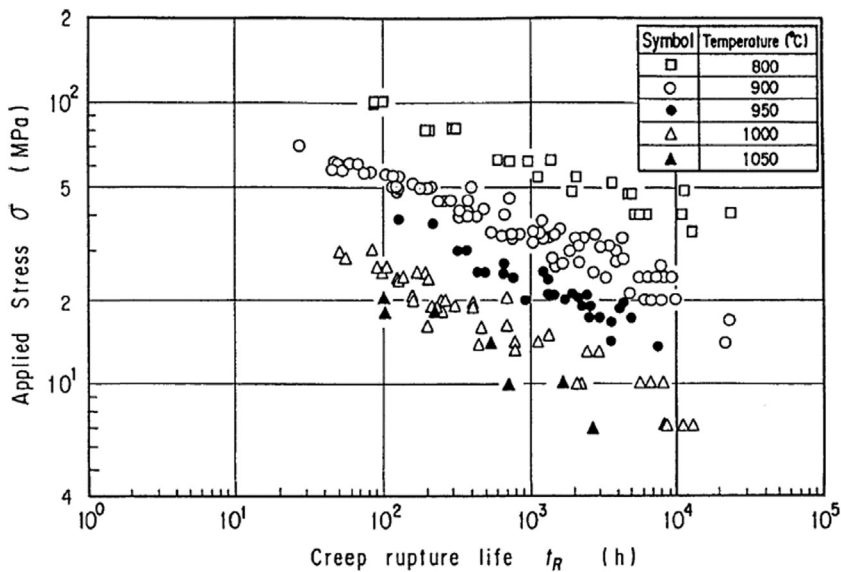


**Figure 2.34** Creep rupture life for Hastelloy XR [31].

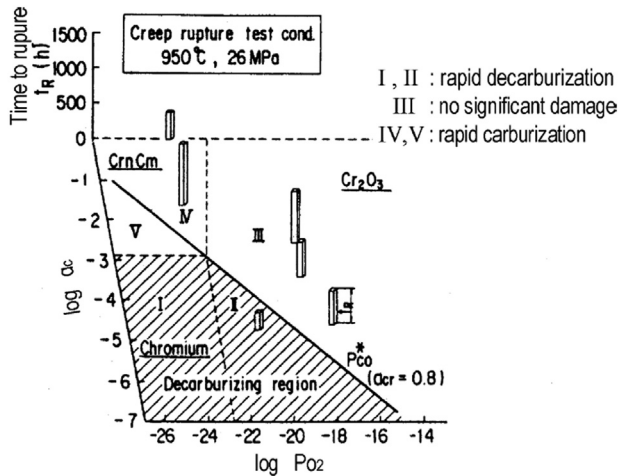


**Figure 2.35** Comparison of creep rupture lives for Hastelloy XR in several different helium environments on the stability diagram for Cr ( $a_{Cr} = 0.8$ ) at 950°C under 26 MPa [31].

#### 2.5.4.1.4 Creep–fatigue interaction

Creep–fatigue interaction for Hastelloy XR is quite similar to those for austenitic stainless steels such as SUS304 and 316. Degradations in lifetime are more pronounced due to holds in tension than those in compression. Fig. 2.36 shows the applicability of the well-known cycle and time fraction rule proposed by Robinson

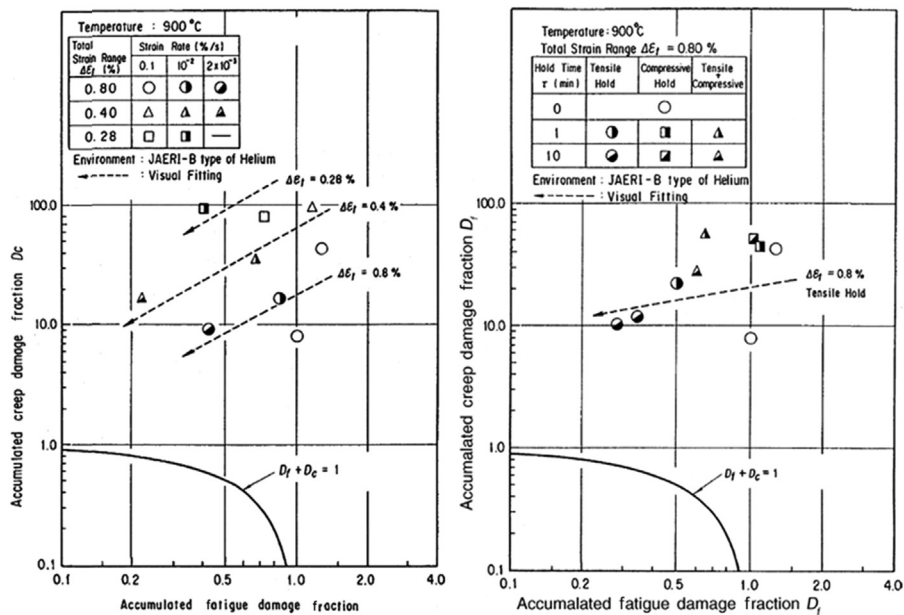


**Figure 2.36** Strain rate effect and hold time effect on creep–fatigue interaction for Hastelloy XR [31].

[33] and Taira [34], which is adopted in the FBR Code. It can be concluded from these figures that the linear summation rule of cycle and time fractions is applicable to Hastelloy XR with a great deal of safety margins even at very high temperatures.

#### 2.5.4.1.5 Applicability of the fast breeder reactor code

As discussed above, the material properties for Hastelloy XR were observed to be basically similar to those for austenitic stainless steels. These observations lead to the conclusion that the FBR Code is, in principle, applicable to Hastelloy XR at the temperatures ranging to 1000°C, with a modification to the tensile test procedure.

#### 2.5.4.1.6 Structural mechanics behavior

The high temperature structural design guideline for class 1 components of the HTTR was established on the basis of component-wise structural mechanics behavior data as well as material property data referring to the FBR Code. The emphasis of the structural mechanics research works was placed on the applicability of the FBR Code to Hastelloy XR under the service conditions of the very high-temperature components. Research works for Hastelloy XR include experiments on multiaxiality of creep rupture strength and creep–fatigue interaction, and on creep buckling. Further research works were carried out for establishment of creep analysis methods for Hastelloy XR.

#### 2.5.4.1.7 Multiaxiality of creep rupture strength and creep–fatigue damage

Since the very high temperature components are exposed to multiaxial loading conditions, multiaxial formulations are required for high temperature strengths of Hastelloy XR. In the FBR Code, the stress intensity criterion, that is, the maximum shear stress criterion, is adopted as the multiaxial formulation for primary stresses, while Von Mises' stress is that for the primary + secondary stresses in evaluating a creep damage. Experiments were carried out in such manners that a tubular test specimen was subjected to a combination of axial and torsional loads. From the experiments, it was concluded that the Von Mises' criterion predicts the creep rupture life on the safe side. Consequently, the multiaxial formulations, which were given in the FBR Code, were demonstrated to be applicable to Hastelloy XR.

#### 2.5.4.1.8 Creep buckling

Heat transfer tubes of the IHX shall not fail by a creep buckling at a piping rupture accident in the secondary cooling system. Component-wise experiments, therefore, were conducted at the HENDEL at JAEA so as to demonstrate the structural integrity of the tubes against the creep buckling and the applicability of a design rule given in the design code. The creep buckling data demonstrated the structural integrity with a great safety margin. A finite element calculation predicted the creep buckling time in good agreement with the experimental data, that is, within an accuracy of 50%.

#### 2.5.4.1.9 Creep analysis method

Key items for establishing an appropriate creep analysis method are as follows:

1. generation of an appropriate creep constitutive equation,
2. definition of correct safety margins for uncertainties in predicting creep behavior, and
3. a procedure to define loading sequences or combinations.

For the item (1), several research experiments were carried out to clarify a hardening rule and a flow rule under multiaxial stress states and also statistical analyses were made to formulate a creep equation, that is, a correlation of creep data from constant uniaxial load tests under isothermal conditions. The experimental data showed the applicability of strain hardening rule and Von Mises' flow rule to Hastelloy XR. The statistical analyses revealed that the time function proposed by Garofalo et al. [35] correlates the creep curve data in the superior agreement to the rational time function [36].

For the item (2), principles to define the safety margins for variations in creep behavior of a high temperature structure were established through sensitivity analysis of a creep constitutive equation [37]. The analytical results clarified that the variations might be covered with those in fundamental creep property such as creep strain curves. For the item (3), creep analyses of the very high temperature components were conducted, taking into account a unique feature of thermal transient behavior of the components. Finally, the design limits and rules for Hastelloy XR in the HTTR high temperature structural design guideline were developed referring to those of the FBR Code, with exceptions.

### 2.5.4.2 2½ Cr–1Mo steel

2½Cr–1Mo steel has a variety of applications to pressure-retaining components in service at elevated temperatures, in particular to boilers and liquid metal fast breeder nuclear reactors (LMFBRs), including the Japanese prototype LMFBR “Monju”. For this material, the FBR Code specifies that design rules and limits are applicable to class 1 components. The scope of the FBR Code for 2½Cr–1Mo steel is as follows:

- maximum application temperature: 550°C,
- product forms: tube and plate, and
- specified environment: sodium but no neutron irradiation.

In the HTTR, the NT material is applied to the RPV as well as the piping, shells of heat exchangers, etc. of class 1 components. During normal operation, the RPV attains a temperature of about 400°C; it is exposed to the highest temperature of about 530°C maximum during severe accidents such as a rupture of the primary concentric hot gas duct. The RPV is also exposed to neutron irradiation even during normal operation but the accumulated neutron flux is less than  $1 \times 10^{17}$  n/cm<sup>2</sup> ( $E > 1$  MeV), which is negligible. Product forms of this material are pipes, plates, and forgings in application to the HTTR class 1 components. Among these products, the plates and forgings are out of scope of the well-established Japanese structural design standards, entitled “Technical standards for LWR power plant components—MITI standards No. 501.”

The service conditions of high temperature and neutron irradiation require tightened specifications for chemical composition contents of impurities such as silicon and sulfur for guarding against brittle fractures due to thermal neutron irradiation embrittlement. This requirement is met by imposing additional requirements on the chemical composition specifications of the JIS.

Many mechanical strength tests as well as fracture toughness tests have been done to clarify the following fundamental characteristics for 2½Cr–1Mo steel of the HTTR specification:

1. mechanical strengths as compared to those of materials of the untightened JIS specifications,
2. mechanical strengths among the product forms of tubes, plates, pipes, and forgings,
3. thermal aging and/or neutron irradiation effects on mechanical strengths, and
4. simulated HTTR-helium gas environment effects on mechanical strengths.

Discussion on these mechanical strength data came to the following conclusions:

1. Mechanical strengths for the HTTR specification material are equivalent to those of the JIS specification material for creep rupture strength.
2. Among the product forms, the following relationships regarding mechanical strength exist:  
tube = pipe  
plate = forging.
3. Thermal aging and/or neutron irradiation do not cause any significant degradation in mechanical strengths in the service ranges of high temperatures up to 550°C and of a neutron flux up to  $1 \times 10^{19}$  n/cm<sup>2</sup>.
4. Simulated HTTR-helium also does not cause any degradation below a high temperature of 550°C.

Accordingly, design rules and limits for the HTTR specification material were generated in the HTTR high temperature structural design guideline from those for the JIS specification material, which are specified in the FBR Code.

#### **2.5.4.3 Austenitic stainless steels SUS321TB and SUS316**

SUS321TB and SUS316 are both well-experienced heat-resistant materials with superior mechanical strengths at temperatures up to about 700°C and are included in the FBR Code. In the HTTR, SUS321TB is applied to heat transfer tubes of helium-to-PWCs, that is, of the PPWC, the SPWC, and the auxiliary heat exchanger. The tube maximum temperature is about 400°C during normal operation. SUS316 is applied to reactor internal structures such as a core restraint mechanism, and control rod guide tubes. The maximum temperatures of these structures are also about 400°C during normal operation. Service conditions of the abovementioned structures are within the scope of the FBR Code with only one exception of the HTTR-helium gas environment effect. Such an effect is negligible at normal operating temperatures of the structures. Accordingly, design rules and limits for the both stainless steels were generated in the HTTR high temperature structural design guideline from those specified in the FBR Code.

#### **2.5.4.4 1Cr–0.5Mo–V steel**

1Cr–0.5Mo–V steel has widespread application for bolts for chemical plant vessels and is used as a bolting material in the MITI standard No. 501 for nuclear application below a maximum temperature of 425°C. For its application to high temperature components, design rules and limits have been specified up to 600°C in the JIS B 8243 “Construction of Pressure Vessels” but are not included in well-established nuclear high temperature structural design codes such as the FBR Code.

In the HTTR, 1Cr–0.5Mo–V steel (JIS SNB16) is applied to not only bolts for vessels such as the RPV and gas circulator castings but also for parts of the core restraint mechanism. A service temperature of 1Cr–0.5Mo–V steel is around 400°C, a little higher than its creep regime threshold temperature of about 380°C under which creep and relaxation effects are negligible. This means that 1Cr–0.5Mo–V steel is served under a “semicreep” condition.

Many mechanical strength tests were carried out to qualify the semicreep temperature condition. It has been clearly found from these tests that creep effects are not significant up to 450°C for creep rupture strength but are significant for higher temperature around 500°C for fatigue strength. Then, it was defined that the semi-creep temperature range for 1Cr–0.5Mo–V steel should be 375°C–450°C.

Taking into consideration such limited service temperatures of semicreep condition in the HTTR, structural design rules and limits for 1Cr–0.5Mo–V steel are developed through essentially extrapolating design rules and limits for application under low temperature condition, where creep deformation and damage are negligible.

## 2.6 Core components and reactor internals

### 2.6.1 Introduction

The reactor consists of core components, reactor internals, reactivity control equipment, and the RPV. One column is the row of prismatic hexagonal blocks piled up axially. The active core consists of 30 fuel columns and 7 control rod (CR) guide columns, and is surrounded by 12 replaceable reflector columns, 9 reflector region CR guide columns, and 3 irradiation test columns, as shown in Fig. 2.4 [13,38,39]. The permanent reflector blocks, surrounding replaceable reflector blocks, are fixed by the core restraint mechanism.

The reactor internals consist of graphite and metallic core support structures and shielding blocks as shown in Fig. 2.7. They support and arrange the core components, such as fuel elements and replaceable reflector blocks within the RPV. The graphite core support structures consist of permanent reflector blocks, hot plenum blocks, support posts, CBSs, etc. The metallic core support structures consist of support plates, a support grid, a core restraint mechanism, etc. This chapter describes the core components and reactor internals design of the HTTR and the program of in-service inspection (ISI) to confirm structural integrity of the reactor internals.

### 2.6.2 Fuel

The fuel element of the HTTR is a so-called pin-in-block-type fuel element, which is composed of fuel rods and a hexagonal graphite block. The fuel rod is classified into four types in the HTTR. One is A-type fuel rod, which is used as a driver fuel. The others are B-type fuel rods, namely, B-1, B-2, and B-3, which have different specification of coating layers of CFPs and are used in irradiation tests for advanced fuels.

The configuration of the fuel element is shown in Fig. 2.6. The CFP consists of a microsphere of low-enriched UO<sub>2</sub> with the TRISO coating. The CFPs are incorporated into fuel compacts with a graphite matrix. The fuel rod, which is composed of fuel compacts and a graphite sleeve, is contained within a vertical hole of a graphite block.

#### 2.6.2.1 Design requirement

In the fuel safety design of HTGR, it is important to retain FPs within the CFPs so that their release to the primary coolant may not exceed an acceptance level. From this point of view, the basic design criteria for the fuel are to minimize the failure fraction of as-fabricated fuel coating layers and to avoid significant additional fuel failures during operation. To meet the latter criterion, the fuel temperature is limited below 1495°C during normal operation conditions and below 1600°C during anticipated operational occurrences, and the fuel burnup is limited to 33,000 MWd/t based on the results of irradiation tests [40]. On these basic considerations, the safety requirements for the HTTR fuel, except for the graphite block, were settled as follows [41]:

1. The initial failure fraction of the as-fabricated coating layers of the CFPs shall be less than 0.2% in terms of the sum of heavy contamination and SiC defects, while the

- expected fraction is less than  $5 \times 10^{-4}$ . The value of 0.2% was determined from the viewpoint to limit off-site exposure during normal operation.
2. The CFPs shall not fail systematically under normal operating conditions.
    - a. The penetration depth of Pd–SiC interaction shall not exceed the thickness of the SiC layer of 25  $\mu\text{m}$ , because the fully penetrating Pd–SiC interaction will lead to a loss of the FP retention function of the SiC coating layer.
    - b. The kernel migration shall not exceed the thickness of 90  $\mu\text{m}$ , which is the sum of the first and second layers.
  3. The CFPs shall be designed so as to avoid failure considering irradiation-induced damage and chemical attack through the full-service period; namely, the additional failure fraction in the coating layers of the CFPs shall be less than 0.2% through the full-service period. The value of 0.2% was determined in the same manner as that for the initial failure fraction.
  4. The maximum fuel temperature shall not exceed 1600°C at any anticipated operational occurrence to avoid fuel failure. The temperature criterion is established to avoid any significant failure and remarkable degradation in the coating layers of the CFPs, taking into account the frequency of the anticipated operational occurrences and those continuous times at high temperature. The behavior of the irradiated CFPs was examined in a temperature range up to 2400°C, with a furnace installed in a hot cell in order to ensure fuel integrity at elevated temperature [42]. The temperature criterion of 1600°C was determined on the basis of these test results [13].
  5. In addition to above requirements, the following requirements were settled to guarantee mechanical integrity of the fuel compact and the graphite sleeve.
    - a. The fuel compact and the graphite sleeve shall not be broken or cracked considering thermal stress and irradiation-induced damage.
    - b. The fuel compact and the graphite sleeve shall not contact with each other to keep their mechanical integrity.

### 2.6.2.2 Design details

The specification of the CFPs is shown in Table 2.11. Table 2.12 shows the specification of the fuel compact, the graphite sleeve, and the fuel block. The CFP consists of spherical fuel kernel of low-enriched UO<sub>2</sub> (12 kinds of enriched UO<sub>2</sub> from 3.4% to 9.9% and about 6% on the average) with the TRISO coating. The TRISO coatings consist of a low-density, porous PyC buffer layer (60  $\mu\text{m}$ ) adjacent to the fuel kernel (600  $\mu\text{m}$  in diameter) followed by high-density isotropic pyrolytic carbon layer, an SiC layer (25  $\mu\text{m}$ ) and a final outer PyC coating.

The CFPs are incorporated with graphite matrix into the fuel compact, which is 10 mm in inner diameter, 26 mm in outer diameter, and 39 mm in height. The fuel rod, which is composed of fuel compacts and the graphite sleeve, is contained within a vertical hole of a graphite block. Helium gas flows downward through the 3.5 mm annular gap between the vertical hole and the fuel rod to remove heat produced by fission and gamma heating.

### 2.6.2.3 Evaluation

The fabrication of the first-core fuel started in June 1995 and took in total 33 months. A total of 66,780 fuel compacts in 126 fabrication lots were produced corresponding to 4770 fuel rods, using a total of 900 kg of uranium. The fabrication data show the low

**Table 2.11** Specification of coated fuel particles [38].

Item	A-type	B-1/B-2 type	B-3 type
Fuel type	Rod	Rod	Rod
Fuel coating type	TRISO	TRISO	TRISO
Diameter of particle ( $\mu\text{m}$ )	920	940	830
Fuel kernel			
Material	$\text{UO}_2$	$\text{UO}_2$	$(\text{U}, \text{Th})\text{O}_2(\text{Th}/\text{U} = 4)$
Density (% of T.D.)	95	95	95
Diameter ( $\mu\text{m}$ )	600	570	500
Material and thickness ( $\mu\text{m}$ )			
First layer	Low-density PyC 60	Low-density PyC 80	Low-density PyC 60
Second layer	High-density PyC 30	High-density PyC 30	High-density PyC 30
Third layer	SiC 25	$(\text{SiC } (\text{B}-1))/(\text{ZrC } (\text{B}-2))$ 35	SiC 30
Fourth layer	High-density PyC 45	High-density PyC 40	High-density PyC 45
Enrichment of $^{235}\text{U}$ (wt.%)	3–10 (average 6)	5	20

initial failure fraction of the order of  $10^{-5}$  as compared with the requirement of 0.2% [43]. For the Pd–SiC interaction in the HTTR fuel, a relationship between the maximum penetration depth and the amount of Pd released from the kernel was expected by cubic root [44], from which the maximum penetration depth of the HTTR fuel through the full-service period is estimated. About 11  $\mu\text{m}$  of the penetration depth for the maximum is obtained, which is far less than the safety design limit of the total SiC layer thickness of 25  $\mu\text{m}$  [45]. The distance of the kernel migration in the HTTR fuel was calculated based on the R&D results. The maximum kernel migration length is 55  $\mu\text{m}$ , which is far less than the safety design limit of 90  $\mu\text{m}$ .

From the tests on fuel behavior under accidental conditions, it was found that the coating layers of the HTTR-CFPs would maintain their intactness below 1600°C within the range of HTTR design condition, such as burnup [13,40]. The requirements of mechanical integrity of the fuel rods were verified by irradiation tests, in which neither crack nor break of the fuel rods was observed in the irradiation range. It is also verified through extensive R&D that the B-type fuel elements will meet the design requirements and fulfill their function at normal operation as well as anticipated operational occurrences.

**Table 2.12** Specification of fuel compact, graphite sleeve, and fuel block [38].

Item	Properties
Fuel compact	
Type	Hollow cylinder
Material	Coated fuel particle, binder, and graphite
Packing fraction of coated fuel particle	30 vol.% (A and B-3); 35vol.% (B-1 and B-2)
Dimension	
Outer/inner diameter (mm)	26/10
Height of a compact (mm)	39
Effective length of a fuel rod (mm)	546 (14 fuel compacts)
Graphite sleeve	
Type	Cylinder
Material	Graphite
Dimensions	
Outer diameter (mm)	34
Thickness (mm)	3.75
Length (mm)	580
Gap width between fuel compact	0.25 and graphite sleeve (mm)
Fuel block	
Type	Pin-in-block
Configuration	Hexagonal
Dimensions	
Width across the flats (mm)	360
Height (mm)	580
Fuel hole diameter (mm)	41
Material	Graphite
Number of fuel rods in a block	33 or 31

### 2.6.3 Hexagonal graphite blocks

The core is an array of hexagonal graphite blocks made up of fuel blocks, control rod guide blocks and replaceable reflector blocks. These blocks provide the structure for the arrangement and confinement of the fuel material; neutron moderation, heat

transfer, and positioning of control/shielding absorber materials. The core consists of vertical columns of hexagonal blocks arranged on a uniform triangular pitch. Within the array of the vertical columns, 30 columns contain fuel. The vertical structure of the column is composed of nine hexagonal graphite blocks. The triangular pitch of the columns on each support block is 362 mm at cold condition. The hexagonal fuel block is 360 mm in width across the flats and 580 mm in height. The core is approximately 2.3 m in equivalent diameter and 2.9 m in height.

### **2.6.3.1 Design requirement**

The design requirements for the hexagonal graphite blocks are as follows:

1. The fuel and BP rods are retained within the core at all the operational conditions.
2. Coolant channels remain free of obstructions and offset displacement, which would impair the core cooling capability.
3. Control rod insertion holes remain free of obstructions and offset displacements, which would impair the insertion of control rods.
4. Reserved shutdown system pellet insertion holes remain free of obstructions and offset displacement, which would disturb the insertion of B<sub>4</sub>C/C pellets or would cause a loss of absorber pellets from the core.
5. The blocks support the structure located above.
6. The capability to handle blocks using the fuel handling machine is not impaired.
7. The integrity of the fuel and BP rods or shield pins is not impaired.

A loss of structural integrity is defined as any damage to the blocks or dowel/socket connections, which would prevent any of the above requirements from being met. The structural integrity of the graphite blocks is assured by limiting the maximum stress to the value given in the Graphite Structural Design Guideline of core components [10]. The calculated stresses should include the effects of dead weight, pressure and seismic loads, and thermal and irradiation-induced strains. Creep and changes in physical properties as a function of temperature and fast neutron fluency should be considered as well as the effect of chemical reactions with oxidizing impurities contained in the coolant.

### **2.6.3.2 Design details**

The primary objective of the mechanical core design is to provide a structurally stable core array, which satisfies the nuclear, thermal/hydraulics, seismic design, and refueling operation requirements. The location and structural restraint for the columns in the core are provided by the core support structures. The core columns have structural features to maintain the alignment of the coolant channels and control rod insertion holes, to ensure a proper coolant flow distribution, and also to ensure that the control absorbers can be inserted as required. All graphite blocks are designed to support the weight of blocks above, loads created by coolant flow pressure differences, seismic loads, loads induced by core restraint, and fuel handling forces. Internal stresses due to dimensional changes induced by thermal and irradiation gradients are considered in the block structural design.

The fuel blocks are graphite hexagonal prisms, which are 360 mm in width across the flats and 580 mm in height, with arrays of coolant channels and BP insertion holes as shown in Fig. 2.6. Thirty-one or thirty-three fuel channels of 41 mm in diameter extend through the block and are aligned with coolant channels in the blocks above and below. The fuel rod is supported in each channel and is cooled by helium flowing through the annular gap. Three threaded dowels are installed on the top face coupled with sockets in the bottom face of the block located above. A hole at the center of each fuel block is provided for fuel handling. The hole profile is shaped so that a lifting ledge is machined at the lower end. Additional holes are provided in the corners of the blocks for the insertion of the BP rods.

Control rod guide blocks with control rod and reserved shutdown system pellet insertion holes are of the same external shape and envelope dimensions as the fuel blocks and use the same dowel/socket connections as shown in Fig. 2.37. These blocks have two control rod insertion and one reserved shutdown system pellet insertion holes of 123 mm in diameter. Envelope dimensions and dowel pattern of the block are the same as the fuel block. The bottom block of the control rod guide column contains B<sub>4</sub>C/C pins for the thermal neutron shield.

The top and bottom replaceable reflector blocks have the same basic configuration as the fuel blocks but do not contain fuel rods. These reflector blocks, above and below the active core, have the same arrangement of coolant channels as the fuel blocks within the same columns. The side replaceable reflector blocks adjacent to the core have the same envelope dimensions as fuel blocks but are solid graphite and contain only a central handling hole for removal and insertion. The bottom replaceable reflector block below each fuel block column provides a transition of the many coolant channels to a single large channel, which mates with the coolant

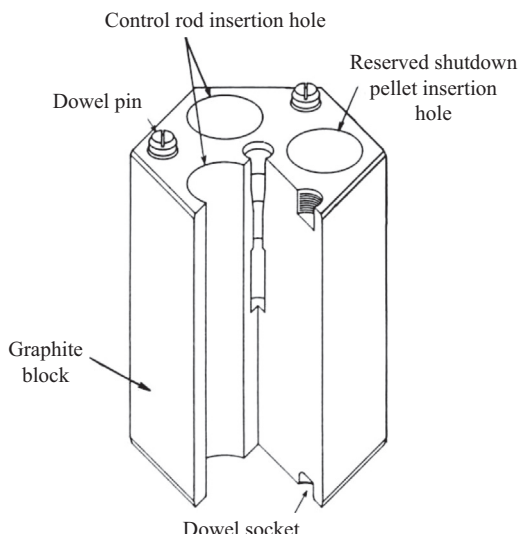


**Figure 2.37** Schematic view of control rod guide block [38].

channels within the hot plenum blocks. The alignment of the fuel, control rod guide, and replaceable reflector columns with the hot plenum blocks is maintained by dowel/socket connections in the bottom reflector blocks, which fit into the hot plenum blocks. The bottom layer of reflector blocks contains  $B_4C/C$  pins for the thermal neutron shield.

### 2.6.3.3 Evaluation

The structural integrity of the graphite components is ascertained by limiting the calculated maximum principal stress to the value defined in the graphite structural design criteria [22]. The characteristics of the design criteria are presented in this issue [46]. The basis for determining stress-strain fields is linear viscoelastic (irradiation-induced creep) stress analysis for core graphite components. The stress analysis, thus, is carried out by a specially developed viscoelastic stress analysis code VIENUS [47].

The fuel blocks are categorized into three column regions, taking into account of the similarity of the thermal and boundary conditions, as shown in Fig. 2.38. The critical stress condition is the combined residual stress, caused by both irradiation-induced creep and dimensional change, and transient thermal stress. With increasing the neutron irradiation, tensile residual stress increases at the central region of the fuel blocks, while compressive at the periphery region. When inner coolant channels are suddenly cooled down in the transient condition, tensile thermal stress arises at the center region and compressive thermal stress periphery region. This transient event is a severe condition for the fuel blocks, and the lifetime of the fuel block is limited from it.

The maximum residual stresses and transient stresses, occurred in the fuel blocks as shown in Fig. 2.38, are shown in previous study [48]. The maximum transient stress appears at the third-layer C column block, while the maximum residual stress appears at the fourth-layer C-column block. This is due to the different temperature boundary conditions for each fuel block position; the cold gas flows downward at the top part with increasing its temperature. The operational stress and residual stress at third-layer C-column are plotted in Fig. 2.39. The operational stresses are reduced by the creep deformation; on the other hand, the residual stresses are increased due to the accumulation of residual strain by the irradiation-induced creep deformation and dimensional

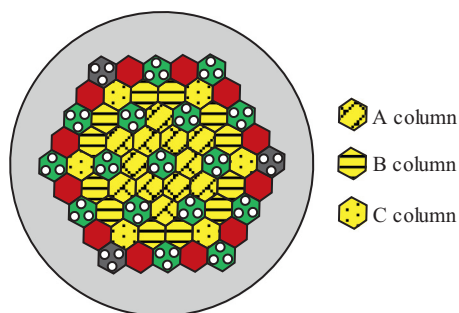


**Figure 2.38** Arrangement of fuel blocks in HTTR.

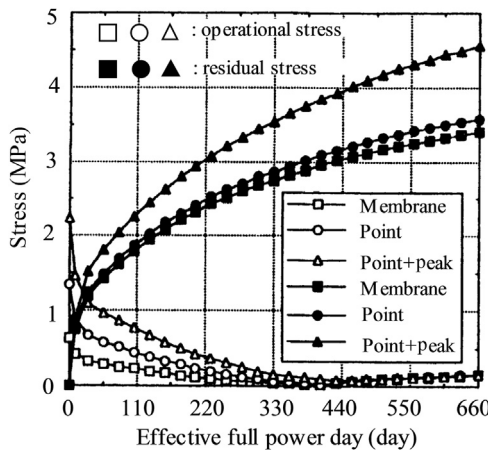


**Figure 2.39** Operational stress and residual stress at the third-layer C column [38].

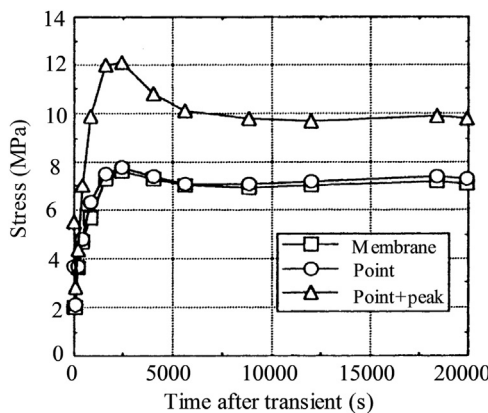


**Figure 2.40** History of calculated maximum stress in the fuel block [38].

change. The combined stresses are plotted in Fig. 2.40. The transient stresses increase at the first stage until about 2400 s from the beginning of the transient, and then these stresses reduce gradually. The maximum point plus peak stress component is about 12 MPa, which is about a half of the limiting stress.

The stress analysis for the control rod guide blocks is performed using the VIENUS code under the same condition as the fuel blocks. Table 2.13 shows estimated stress based on the graphite structural design criteria for the control rod guide block. The maximum tensile stress of the membrane component is about 81% of the stress limit as seen in Table 2.13. The stress analysis for the replaceable reflector blocks is also performed under the same conditions as for the fuel blocks. The bottom replaceable reflector block just below the active core gives the highest stress among

**Table 2.13** Stress evaluation of control rod guide block [38].

Operation condition	Stress	Stress component <sup>a</sup>		
		Membrane	Point	Peak
I and II	Estimated <sup>b</sup>	6.0, -5.3	6.2, -5.8	6.4, -6.4
III	Limited	7.4, -20.3	11.1, -30.4	20.1, -54.7
	Estimated	6.0, -5.3	6.2, -5.8	6.4, -6.4
IV	Limited	11.3, -30.7	16.7, -45.6	20.1, -54.7
	Estimated	6.0, -5.3	6.2, -5.8	6.4, -6.4
	Limited	15.8, -43.0	20.1, -54.7	22.3, -60.7

<sup>a</sup>Positive and negative values mean tensile and compressive stresses, respectively.

<sup>b</sup>Stresses are calculated conservatively during over cooling, which leads to the maximum estimated stress components in plant condition I.

the replaceable reflector blocks. The maximum tensile stress of the membrane stress component is about 78% of the stress limit for the bottom replaceable reflector block.

## 2.6.4 Core support structures

The core support graphite structures mainly consist of permanent reflector blocks, hot plenum blocks, support posts, and bottom structures as shown in Fig. 2.37. The permanent reflector blocks surrounding the replaceable reflectors are made up of large polygonal graphite blocks fixed by key elements and a core restraint mechanism. The support posts located between the hot plenum blocks and CBSs provide a hot plenum space where the hot core outlet helium gas can be mixed uniformly.

To design these graphite core support structures, the graphite structural design code was developed on the basis of graphite test data. During an earthquake, key/key-way structures and support posts are the important components to maintain the core array. In order to obtain design data such as design load to verify the seismic response and to develop the seismic analysis code, seismic tests, therefore, were performed using two kinds of scaled models, a 1/5-scale model simulating a horizontal two-dimensional array of the hot plenum blocks and a 1/3-model simulating a horizontal two-dimensional array of CBSs including the support post structures [49].

### 2.6.4.1 Design requirement

The design requirements for the graphite core support structures are summarized as follows:

1. To have sufficient strength to maintain the structural integrity during normal operation and anticipated operational occurrences, and to maintain the structural functions during an earthquake or accidents.

2. To ensure the core cooling capacity by the restriction of leakage flow through the permanent reflector blocks and hot plenum blocks.
3. To support the core array during an earthquake and to control the mechanical interaction of the core components so that these will not fail.
4. To ensure the coolability of the metallic core support structures.

#### 2.6.4.2 Design details

The hexagonal hot plenum block array is made up of two axial layers. The upper layer consists of sealed plenum blocks, in which leakage flow between these blocks is sealed by the triangular seal elements, and the lower layer is composed of keyed plenum blocks, which provide lateral and vertical positioning and support of the core array. The hot plenum block assembly contains passages for the primary coolant flow from the columns in the core to the hot plenum. These blocks are fabricated from grade PGX graphite, a medium-to-fine grained, molded structural graphite. Severe load is applied to the hot plenum block during an earthquake. The design seismic load is determined by the vibration test of core support structures as mentioned in the following section. The stress analysis for the hot plenum block is carried out by the finite element stress analysis code. The estimated stresses based on the graphite structural design code are shown in [Table 2.14](#). The maximum tensile peak stress is about 79% of the limited peak stress at the S<sub>2</sub> earthquake, an extreme design earthquake.

The support posts and seats are so designed as to support the core and hot plenum block array while providing the hot plenum for the primary coolant flow. The support posts and seats are made of grade IG-110 graphite. The maximum stress for the support post and seat component arises at the spherical contact area. The evaluated stresses at this point during an earthquake are summarized in [Table 2.15](#). The maximum compressive peak stress component becomes about 83% of the limited peak stress during the S<sub>1</sub> earthquake, the maximum design earthquake.

**Table 2.14** Estimated earthquake stresses based on the graphite structural design code for the hot plenum block [39].

Operation condition	Stress	Stress component <sup>a</sup> (MPa)					
		Membrane		Point		Peak	
I, II, and III and S <sub>1</sub>	Estimated	1.0	-0.9	1.8	-1.9	2.6	-2.1
	Limited	2.2	-8.8	2.9	-11.8	4.0	-15.9
I, II, and III and S <sub>1</sub>	Estimated	1.2	-1.3	2.3	-2.7	3.5	-2.9
	Limited	2.7	-10.6	3.5	-14.1	4.4	-17.6

<sup>a</sup>Positive and negative values mean tensile and compressive stresses, respectively.

**Table 2.15** Estimated earthquake stresses based on the graphite structural design code for the support post [39].

Operation condition	Stress	Stress component <sup>a</sup> (MPa)					
		Membrane		Point		Peak	
I, II, and III and S <sub>1</sub>	Estimated	1.6	- 18.8	4.6	- 34	12.4	- 45.8
	Limited	9.7	- 30.7	12.9	- 40.9	17.5	- 55.2
I, II, and III and S <sub>1</sub>	Estimated	1.6	- 19.4	4.6	- 34.2	12.4	- 45.8
	Limited	11.6	- 36.8	15.5	- 49.1	19.4	- 61.4

<sup>a</sup>Positive and negative values mean tensile and compressive stresses, respectively.

**Table 2.16** Estimated earthquake stresses based on the graphite structural design code for the permanent reflector [39].

Operation condition	Stress	Stress component <sup>a</sup> (MPa)					
		Membrane		Point		Peak	
I, II, and III and S <sub>1</sub>	Estimated	0.7	- 2.2	1.4	- 3.4	2.5	- 5.5
	Limited	1.7	- 8.8	2.3	- 11.8	3.1	- 15.9
I, II, and III and S <sub>1</sub>	Estimated	0.9	- 2.1	1.9	- 3.5	3.1	- 5.6
	Limited	2.3	- 10.6	2.7	- 14.1	3.4	- 17.6

<sup>a</sup>Positive and negative values mean tensile and compressive stresses, respectively.

The CBSs consist of three blocks: lower plenum blocks, carbon blocks, and bottom blocks. These blocks have a function of thermal insulation between the hot plenum and metallic core support structures.

The permanent reflector is a graphite structure immediately surrounding the replaceable reflector and control rod guide columns. It is an assembly of graphite blocks consisting of 12 circumferential segments in 8 axial layers fabricated from grade PGX graphite. The severe stress of the permanent reflector is created by the earthquake load at the connecting keyway position. The evaluated stresses based on the graphite structural design code are summarized in **Table 2.16**. The maximum tensile peak stress reaches about 90% of the limited value for the S<sub>2</sub> earthquake.

The typical properties of graphite and carbon are listed in **Table 2.17**. These components are so designed as to maintain the structural integrity during accidents and earthquakes in accordance with the graphite structural design code considering the brittle nature of graphite material.

**Table 2.17** Typical material characteristic values for graphite and carbon (unirradiated material) [39].

Item	IG-110 graphite	PGX graphite	ASR-0RB carbon
Bulk density ( $\text{mg}/\text{m}^3$ ) <sup>a</sup>	1.78	1.73	1.65
Mean tensile strength (MPa) <sup>a</sup>	25.3	8.1	6.8
Mean compressive strength (MPa) <sup>a</sup>	76.8	30.6	50.4
Young's modulus (GPa) <sup>a</sup> ( $(\pm 1/3)S_u$ ) <sup>b</sup>	7.9	6.5	8.7
Mean thermal expansion coefficient (293–673 K) ( $10^{-6}$ K)	4.06	2.34	4.40
Thermal conductivity (W/(m K)) (673 K)	80	75	10
Ash (ppm)	Max. 100	Max. 7000	Max. 5000
Grain size ( $\mu\text{m}$ )	Mean: 20	Max. 800	Max. 2000

<sup>a</sup>At room temperature.

<sup>b</sup>Determined from the cord joining two points (one point is the one-third of the specified minimum tensile strength and the other is the one-third of the specified minimum compressive strength) on the stress–strain curve.

### 2.6.4.3 In-service inspection and surveillance test

In order to confirm structural integrity of the core support graphite structures, visual inspection will be performed using a TV camera as ISI and measurement of material characteristics using Surveillance Test specimen (Surveillance Test). Fuel replacing and ISI will be carried out at the same period, and the surveillance test will be carried out at the second and fourth refueling time and at the end of the plant lifetime.

#### 2.6.4.3.1 In-service inspection using TV camera

To conduct the visual inspection, the ISI system was developed. Fig. 2.41 shows the structure of the ISI system. In the visual inspection, surface flaws as well as an array of core support graphite structures will be visually examined.

The required flaw size in the visual inspection is determined on the basis of the fracture mechanics approach taking into consideration of the fracture toughness and stress profiles in the graphite structures. Possible visual inspection areas by a TV camera are inner surfaces of the permanent reflector blocks, upper surfaces of the sealed plenum blocks, side surfaces of core support posts, and upper surfaces of the lower plenum blocks. The important positions of core support graphite structures in the visual inspection are as follows:

- Permanent reflector blocks
  - surface flaws on the permanent reflector blocks
  - gaps between the permanent reflector blocks

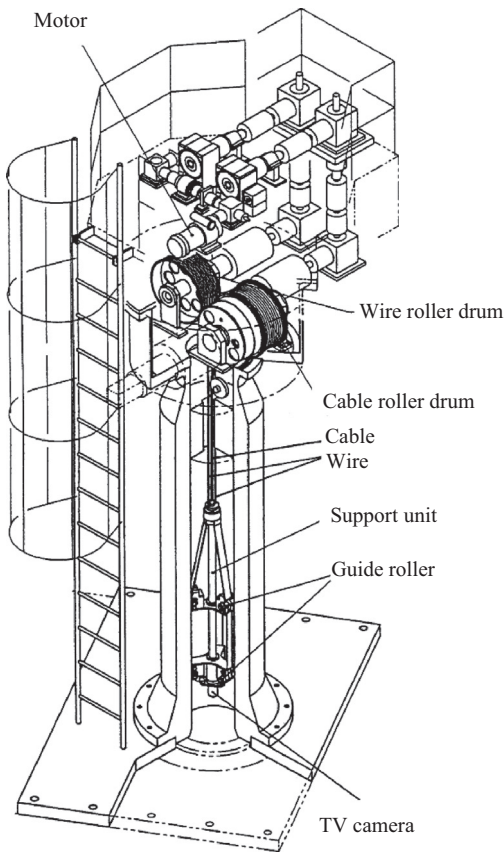


**Figure 2.41** Schematic view of ISI system [39].

- Hot plenum blocks
  - gaps between the permanent reflector blocks and hot plenum blocks
  - surface flaws on the hot plenum blocks
- Hot plenum region
  - inclination of the support posts
  - surface flaws on the lower plenum blocks
  - gaps between the lower plenum blocks

#### 2.6.4.3.2 Results of preservice inspection

In order to obtain the reference data of ISI, a preservice inspection (PSI) of core support graphite structures was carried out using the developed ISI system. Fig. 2.42 shows one of the results of the PSI, the surface of permanent reflector blocks, and the axial gap between permanent reflector blocks. No harmful flaw and abnormal array were observed in the PSI. In the visual inspection, structural integrity of the core support graphite structures will be evaluated by comparing the results of PSI.

### 2.6.4.3.3 Surveillance test

Measurement of material properties using surveillance test specimens will be carried out to evaluate the irradiation effect on mechanical and thermal properties of graphite and carbon. [Table 2.18](#) shows the measured properties in the surveillance test. Bending and compressive strengths, Young's modulus, etc. will be measured at regular intervals. An oxidation weight loss will be also measured to examine the oxidation-induced damage.

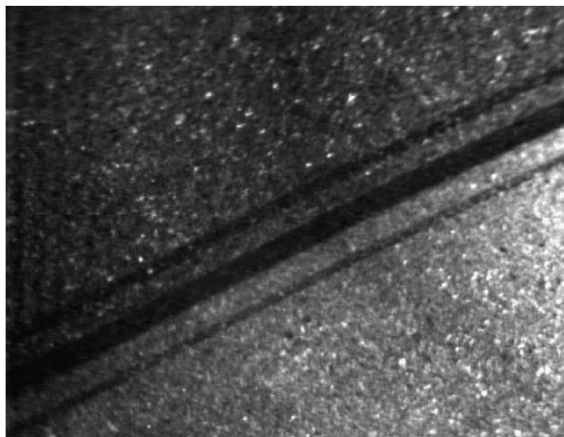


**Figure 2.42** Surface of permanent reflector blocks and axial gap between permanent reflector blocks [39].

**Table 2.18** Measured properties in the surveillance test [39].

	Test items	Material
Permanent reflector block	Dimension change	PGX
	Bending strength	
Hot plenum block	Bending strength	PGX
	Oxidation weight loss	
Support post	Young's modulus	IG-110
	Bending strength	
	Compressive strength	
	Oxidation weight loss	

## 2.6.5 Core support metallic structures

The core support metallic structures are composed of the support plate, the core support grid, the core restraint mechanism, etc. as shown in Fig. 2.7. The support plate and core support grid are located under the core bottom insulation layer. The core restraint mechanism surrounds the permanent reflector blocks.

### 2.6.5.1 Design requirement

The support plate and core support grid is so designed as to form a statically stable foundation for the core components and reactor internals under the highest postulated temperatures and under seismic loads. The core restraint mechanism has to fulfill the following functions:

1. To provide a stable lateral support not only during normal operation condition in the anticipated operational occurrences but also during accident conditions and the seismic conditions for the full core height.
2. To prevent radial outward movement of the permanent reflector blocks in order to avoid forming excessive bypass gaps between blocks.
3. To reduce impact loads on core components, reactor internals during a seismic event.
4. To maintain sufficient annular space for the primary coolant flow between the permanent reflector blocks and the RPV.

### 2.6.5.2 Design details

The support plate forms a plain foundation surface for the core components and reactor internals, and is composed of steel plates with a thickness of 89 mm. The support plates are set on steel support posts, guiding the core weight to the core support grid below.

The core support grid transfers the total weight of the core to the RPV through the support ribs welded on the inner surface of the hemispherical bottom head closure. The grid is reinforced with welded diamond shaped plate structures. The support plate and the core support grid are cooled by the primary coolant flowing into the RPV.

The core restraint mechanism surrounds and stresses the permanent reflector blocks with 10 axially distributed units. Each unit consists of 12 restraint bands, 12 band supports, 2 restraint rings, and radial keys as shown in Fig. 2.43. The restraint bands are stressed to produce radial force on the band supports that is transmitted to the permanent reflector blocks via the side shield blocks and support legs.

The restraint rings, located above and below the restraint bands, are normally stress-free. They limit the radial displacement of the bands during a seismic event and restrain the lateral load of the core directly in case the restraint bands fail. In such a case, the restraint rings transfer the load to the RPV through the radial keys. Normally, there is no contact between the restraint rings and the radial keys. The radial keys are individually adjusted before being attached to the RPV and are provided to compensate for circumferential fabrication tolerances.

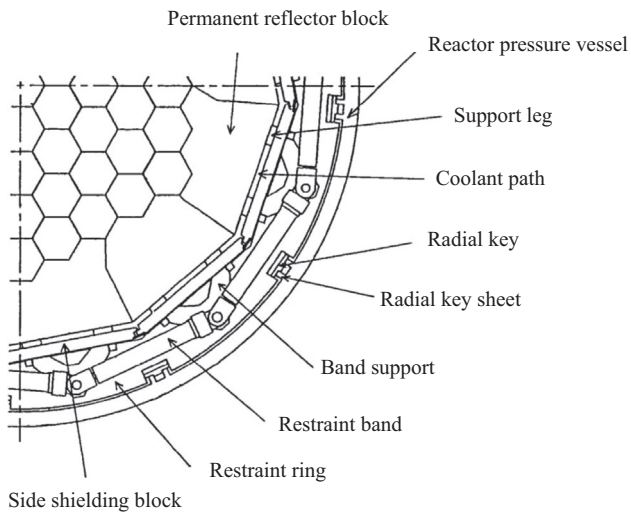


**Figure 2.43** Arrangement of core restraint mechanism [39].

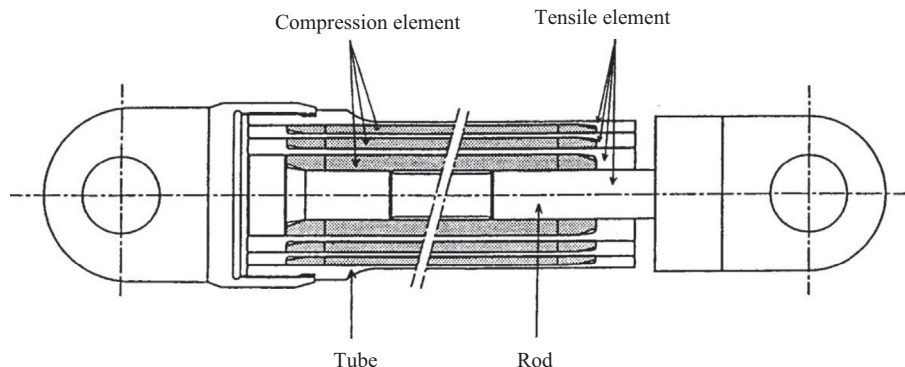


**Figure 2.44** Schematic view of core restraint band [39].

The restraint bands are composed of a central rod and six concentric pipes as shown in Fig. 2.44 except for the 9th and 10th units. The 9th and 10th units have eight concentric pipes. The pipes are connected in series with the pipes mutually acting as compression and tensile elements. With the bolt eyes connected to the central bar on one end and to the outer pipe on the other end of the band, the whole arrangement forms a sort of tensile spring.

The component materials of the restraint band are SNB16 steel for the tensile element and SUS316 for the compression element. Even though the thermal expansion coefficients of both steels are different from those of graphite and core structural materials, the coefficient of the band itself is adjusted to be equal to that of

graphite. Therefore the restraint of the permanent reflector blocks is maintained in spite of change in temperature.

The restraint mechanism is used during plant lifetime without repair. Relaxation of SNB16, used for the tensile element, under high temperature creep conditions causes reduction of the restraint force that could even lead to coolant leakages through gaps between the permanent reflector blocks. For the bottom layer of the band, at the end of plant lifetime, approximately 60% of restraint force is reduced by the relaxation of SNB16 with a conservative estimation. This result satisfies design requirement of the restraint band. Therefore mechanical properties of SNB16 are important and were accumulated for the design of the restraint mechanism.

### ***2.6.5.3 In-service inspection and surveillance test***

The restraint mechanism is used during plant lifetime without repair. By the relaxation of SNB16, used for the tensile element, under high temperature creep conditions, the restraint force will decrease, and then coolant leakages through gaps between the permanent reflector blocks will increase. Therefore deformation characteristics of SNB16 are important, and the relaxation as well as Charpy impact tests of the SNB16 are programmed during HTTR operation as surveillance tests. These tests will both be carried out after 5 and 10 years of operation and at the end of the plant lifetime.

## ***2.6.6 Shielding blocks***

Shielding blocks consist of top and side shielding blocks and are composed of a neutron-absorbing material and casing. The top shielding block is installed at the top of each column and has coolant channels matching the channels in the column below. The side shielding blocks are installed outside of the permanent reflector blocks and compressed inward by the core restraint mechanism.

### ***2.6.6.1 Design requirement***

Requirements for the design of the shielding blocks are as follows:

1. The shielding blocks have the function to limit the thermal neutron fluence in the metallic core support structures and the RPV.
2. The top shielding blocks for the fuel column have coolant channels of adequate diameter to adjust coolant flow rate distribution.
3. The side shielding blocks shall have sufficient strength to transfer compression force by the core restraint mechanism to the permanent reflector blocks.

### ***2.6.6.2 Design details***

The top shielding block is a hexagonal block, which is composed of a neutron-absorbing material of sintered B<sub>4</sub>C/C, a casing of SUS316 and dowel pins. The top shielding blocks for the fuel and control rod guide columns have coolant channels matching the channels in the succeeding blocks. The top shielding block for the fuel

column has an internal cavity for coolant in order to prevent neutron streaming. [Fig. 2.45](#) shows a schematic structure of the top shielding block for the fuel column. Dowel pins on the top are used for positioning of the handling head of fuel handling machine.

The side shielding block is also composed of sintered  $B_4C/C$  and a SUS316 casing as shown in [Fig. 2.46](#). The compressive force by the restraint band is transferred to the side shielding blocks through the band supports as shown in [Fig. 2.43](#). Four support legs are connected directly to the thick SUS316 plate, which locates RPV side of the block, and transfer the compressive forces to the permanent reflector blocks.

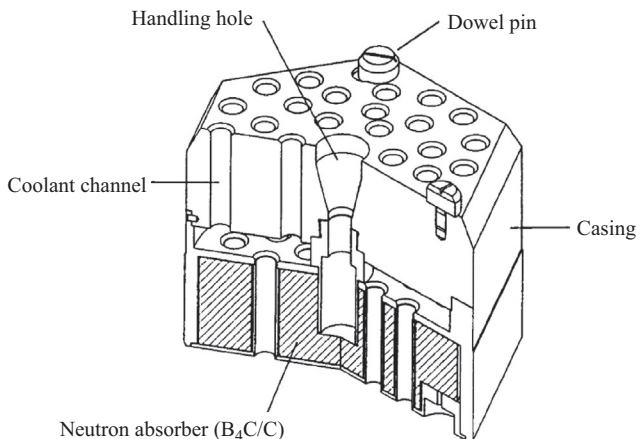


**Figure 2.45** Schematic view of top shielding block [39].

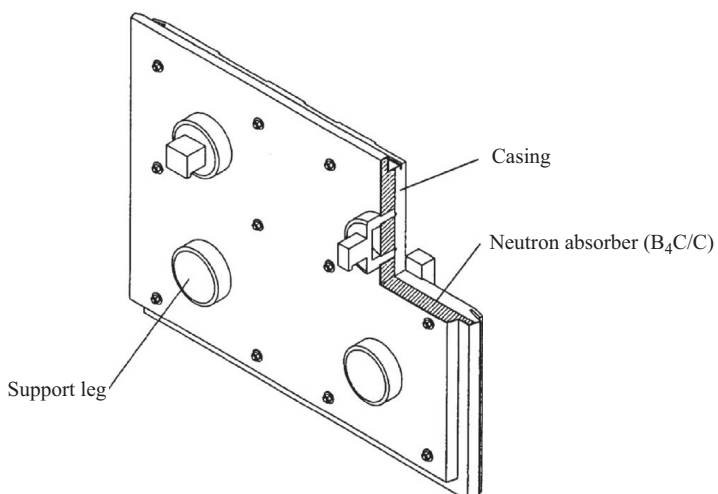


**Figure 2.46** Schematic view of side shielding block [39].

## 2.7 Seismic design

### 2.7.1 Introduction

The seismic design for the HTTR facilities was based on “Guidelines for Aseismic Design of Nuclear Power Plants (GAD)” [50]. It is stated in the guidelines that important buildings and structures must be supported on base rock. The reactor building of the HTTR, however, has been planned to be supported on a sand layer formed during the Quaternary era. For this reason, various seismic safety evaluations for the HTTR facility were investigated for construction of the HTTR building [51]. After the HTTR was constructed, seismometers were installed in the surrounding foundation and in the reactor building for confirmation of the vibration behavior of the HTTR. The seismic response analysis was performed using a seismic observation record and basic earthquake motion [51].

Fig. 2.47 shows a vertical view of the core, the CBS, and RPV. Permanent disarray of, or damage to, the core components induced by an earthquake would prevent insertion of control rods. Aseismic design of the core, thus, is one of the major concerns in the safety evaluation of the HTTR. In the earthquake, the HTTR core requires

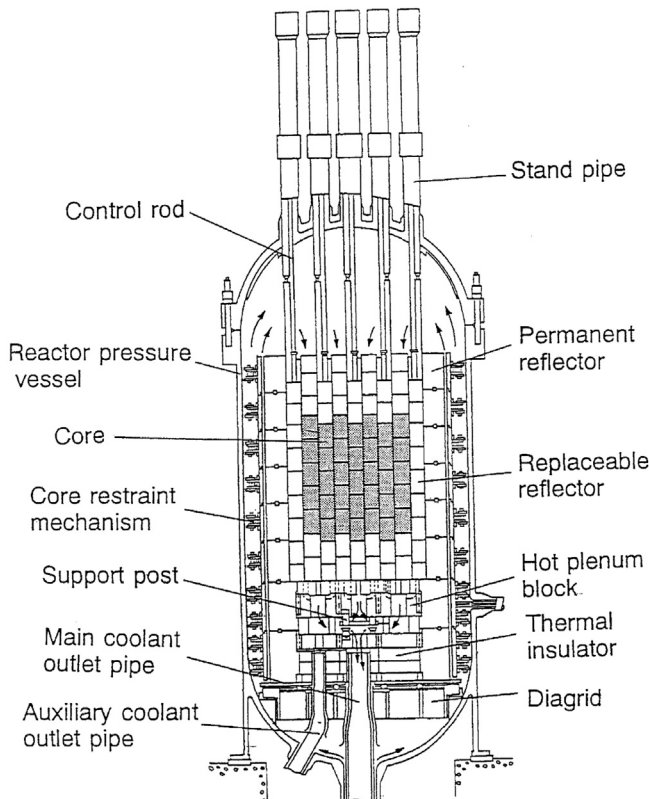


**Figure 2.47** Vertical view of reactor internals and vessel [52].

structural integrity to maintain the safety functions of reactor shutdown and decay heat removal. Since the core is composed of piled graphite blocks with their associated clearances on the CBS, the vibration response of the blocks is highly nonlinear with multiple impacts occurring between adjacent blocks [52]. Aseismic studies of the core were carried out through experimental and analytical approach to clear the singularity of vibrational behavior due to impact phenomena [48,53].

The basic guidelines of seismic design, geological composition, R&D results on aseismic studies, and the typical integrity evaluation result of graphite components of the HTTR [3,4] are described.

## **2.7.2 Seismic design**

### **2.7.2.1 Basic guideline of seismic design**

The nuclear power plant is so designed that all anticipated earthquakes may not cause a severe accident. Then the structures are considered to possess seismic safety on the basis of following provision.

1. The core, which is a multilayered structure of graphite blocks, is supported on the metallic core support structure. Buildings, structures, systems, and equipment except for the core should be made rigid as a rule. Moreover, important buildings and structures should be supported on a foundation, which is safe enough against any postulated earthquake.
2. The degree of importance of facilities is classified into classes A, B, and C from viewpoint of effect of radiation release to the environment. The seismic design should be done according to this degree of importance.
3. Abovementioned facilities of classes A, B, and C should be designed so as to resist against a seismic force, which is obtained from the story shear coefficient according to the degree of importance.
4. Facilities of class A should be so designed that they may resist seismic forces determined by use of a dynamic analysis with the basic earthquake motion  $S_1$  defined according to GAD.
5. Especially, important facilities among those of class A are classified into "class As." They must maintain a safety function basic earthquake motion  $S_2$  defined according to GAD. Moreover, a dynamics analysis is done for equipment and piping of class B, which might vibrate in resonance.
6. Seismic forces to facilities of the class A act on a disadvantageous direction, which is a combination of a horizontal force obtained from basic earthquake motion with a vertical force obtained from a vertical seismic coefficient which is half of the maximum amplitude acceleration of seismic earthquake motion. It is assumed that the vertical earthquake coefficient is constant in the direction of height.
7. If there is a possibility that components and piping resonate with the structure, dynamic analysis should be carried out.

### **2.7.2.2 Seismic classification**

The classification of facilities is shown in [Table 2.19](#).

1. Class A: Facilities storing radioactive material, or relating directly to the facilities which stores radioactive material and may release radioactive material to the environment by the loss of function, and/or one to prevent these situations and one to mitigate the effect of released radioactive material.

**Table 2.19** Classification of HTTR facilities [51].

Class	Facilities belonging to each class	Main facilities	Seismic classification
A	(1) Equipment and pipings composing a reactor coolant pressure boundary	Reactor pressure vessel	As
		Vessels, pipings, gas circulators, and valves belonging to reactor coolant pressure boundary	As
	(2) Facilities to store spent fuel	Spent fuel storage pool	As
		Spent fuel storage rack	As
	(3) Facilities to add negative reactivity for the emergency shutdown of a reactor and to maintain the subcritical condition	Control rod and control rod drive mechanism (as for scramability)	As
	(4) Facilities to remove decay heat from a core after the emergency of a reactor	Auxiliary cooling system (except an inner piping of concentric hot gas duct)	As
	(5) Facilities to remove decay heat from a core after a failure of reactor coolant pressure boundary	Reactor vessel cooling system	As
	(6) Facilities act as pressure barrier in case of failure of a reactor coolant pressure boundary and to prevent directly the release of radioactive material	Reactor containment vessel	As
		Pipings and valves belonging to the reactor containment vessel boundary	As
	(7) Facilities to control the release of radioactive material to environment in case of the accident with such possibility except facilities belonging to "6"	Emergency air purification system	A
(8) The other		Core internal structure (except facilities of class As)	A
		Reserved shutdown system	A
		Primary helium purification system (except facilities of classes B and C)	A
		Fuel failure detection system (except facilities of classes B and C)	A
		Primary helium sampling system (except facilities of classes B and C)	A

*(Continued)*

**Table 2.19** (Continued)

<b>Class</b>	<b>Facilities belonging to each class</b>	<b>Main facilities</b>	<b>Seismic classification</b>
B	(1) Equipment connecting directly to reactor coolant pressure boundary which are storing primary coolant or capable to store it	Primary helium purification system (except facilities of classes A and C)	B
		Fuel failure detection system (except facilities of classes A and C)	B
		Primary helium sampling system (except facilities of classes A and C)	B
	(2) Facilities storing radioactive waste except facilities, which have a little storage or less effect of radiation to public by the failure than the limitation of dose equivalent at outside of surrounding observed area	Radioactive waste disposal system (except facilities of class C)	B
		Fuel handling machine	B
		Ceiling crane	B
		Shield with much reduction of radiation	B
		Reactor pressure vessel leak detection system	B
		Ceiling crane in the spent-fuel storage building	B
	(4) Facilities to cool spent fuel	Pool water purification system for spent pool (a part related to cooling water pool)	B
	(5) Facilities to control a release of radioactive material in case of an accident and not belonging class A	A part of ventilation and air conditioning system in the spent fuel storage building	B

*(Continued)*

**Table 2.19** (Continued)

Class	Facilities belonging to each class	Main facilities	Seismic classification
C	(1) Equipment not belonging to classes A and B	Control rod drive mechanism (except a part related scramability)	C
		Secondary helium sampling system	C
		Fresh fuel storage system	C
		Secondary helium cooling system	C
		Pressurized water-cooling system	C
		Primary helium purification system, primary helium sampling system, fuel failure detection system not related to high radioactive material	C
		Secondary helium purification system	C
		Primary helium storage and supply system	C
		Secondary helium storage and supply system	C
		Waste disposal system not related to high radioactive material	C
		Pool water-cooling and purification system (related to the supply of pool water)	C
		Fire extinguishing system	C
		Ventilation and air conditioning system	C
		Air compressioning system for nonsafety use	C
		Cooling water system for nonsafety use	C
		The others	C

2. Class B: Above-mentioned facilities, the facilities of which the effect and the influence are comparatively small.
3. Class C: Facilities for which the safety equal to the conventional industrial facilities is required.

### 2.7.2.3 Basic design earthquake ground motion

Basic design earthquake ground motions are defined at the free field of the base stratum surface in the HTTR site. The base stratum is a firm base, which was formed in the tertiary or earlier geological era and, which is not weathered significantly with shear wave velocity of more than 700 m/s. At the HTTR sites, the level is set up to be the upper surface of the Neogene-Tertiary Miocene based on the survey results.

The basic earthquake motions were defined, as shown in Fig. 2.48, by means of Ohsaki spectra. At this time, the maximum design earthquake  $S_1$  and the extreme design earthquake  $S_2$  are supposed based on the investigation on the historical earthquakes, the active faults, and the seismotectonic structure.

The maximum accelerations of  $S_1$  and  $S_2$ , which are envelop curves of these earthquakes, are  $1.8 \text{ m/s}^2$  (180 gal) and  $3.5 \text{ m/s}^2$  (350 gal), respectively.

## 2.7.3 Geological composition and seismometry

### 2.7.3.1 Geological composition

To grasp the geological composition at the HTTR site and obtain samples for laboratory tests, a boring survey was performed at the positions as shown in Fig. 2.49. The geological sections obtained from the survey are shown in Fig. 2.50. The supporting foundation at the HTTR site is formed by horizontal layers with continuity.

### 2.7.3.2 Seismometry

A seismometry system was installed in the HTTR facility to confirm the behavior of a seismic event, and earthquake observation was started in October 1997. Seismometers were installed in the surrounding foundation at the positions of underground 250, 94, 30, and 1 m, and in the reactor building at the position of BF3, BF1 1F and 2F. Figs. 2.51 and 2.52 show the points of seismometers in the surrounding foundation and in the reactor building, respectively.

## 2.7.4 Structure of core components

The reactor core is an array of graphite blocks composed of fuel elements, a control rod guide, and replaceable reflector, which provide neutron moderation and heat transfer, and serves for positioning of control and shielding absorber materials. One column is the row of prismatic hexagonal blocks piled up axially. The active core consists of 30 fuel columns and 7 control rod guide columns and is surrounded by 12 replaceable reflector columns, 9 reflector region control rod guide columns, and

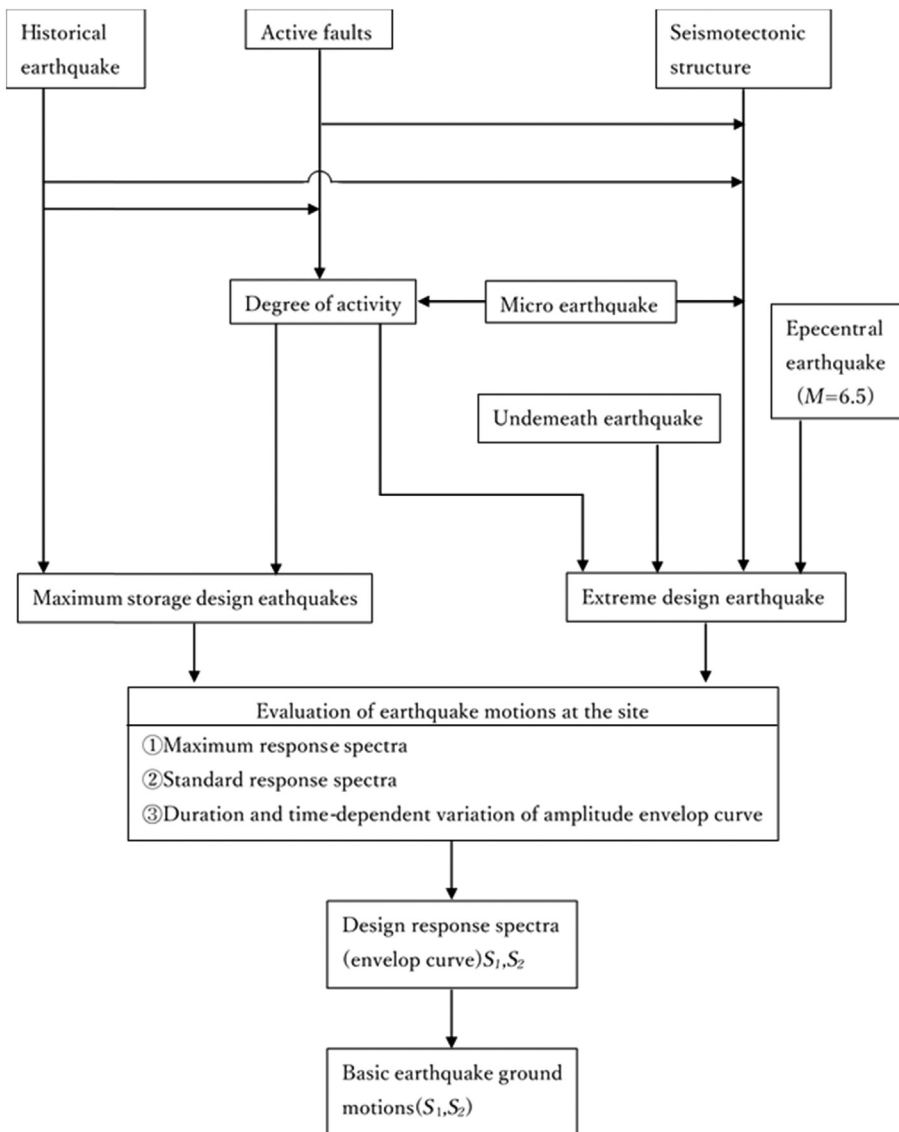


**Figure 2.48** Flow diagram of definition of basic earthquake ground motion [51].

3 irradiation test columns. Each column consists of nine piled graphite blocks and one top shielding block. The top shielding block is a hexagonal block, which is composed a neutron-absorbing material of sintered B<sub>4</sub>C/C, a casing of SUS316. The permanent reflector blocks are fixed by the core restraint mechanism.

The graphite block of the fuel elements is a hexagonal right prism with an array of fuel element holes, as shown in Fig. 2.23. The block is 0.36 m across the flats

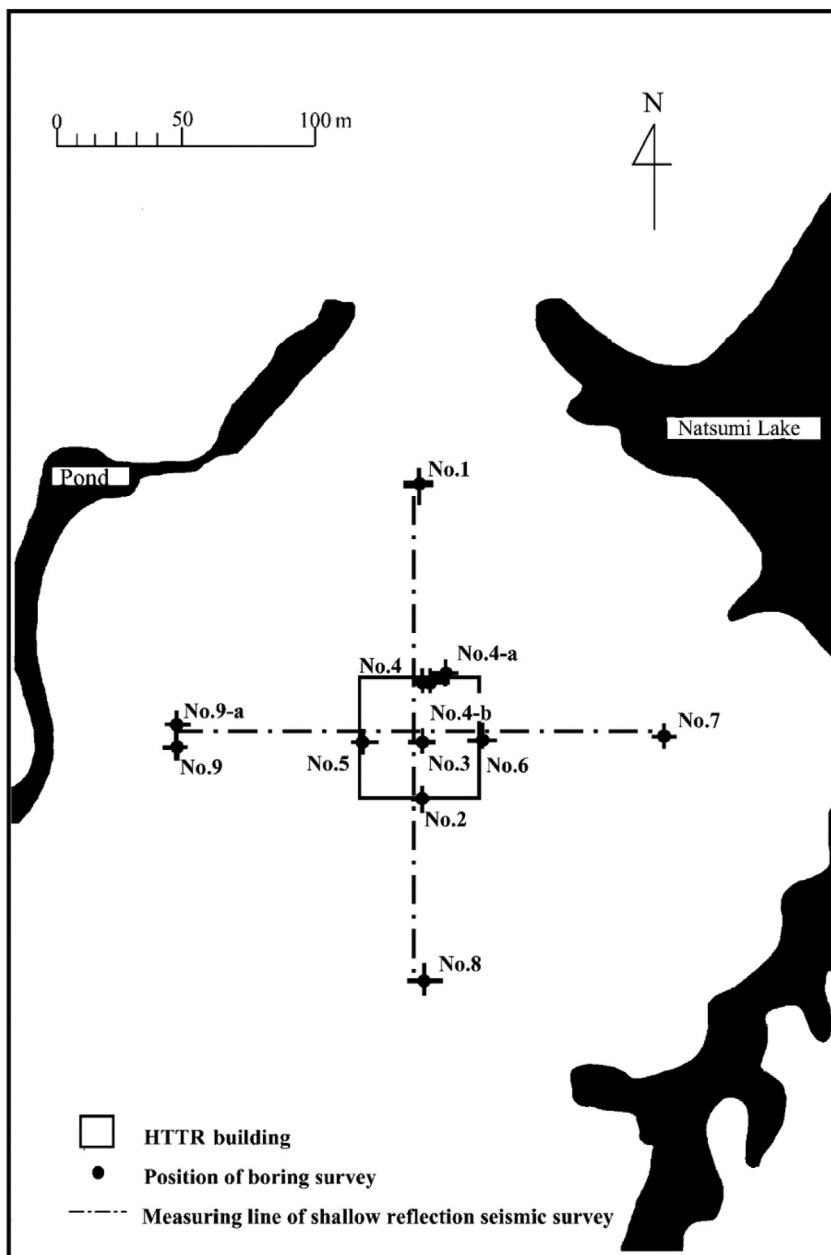


**Figure 2.49** Position of geological survey [51].

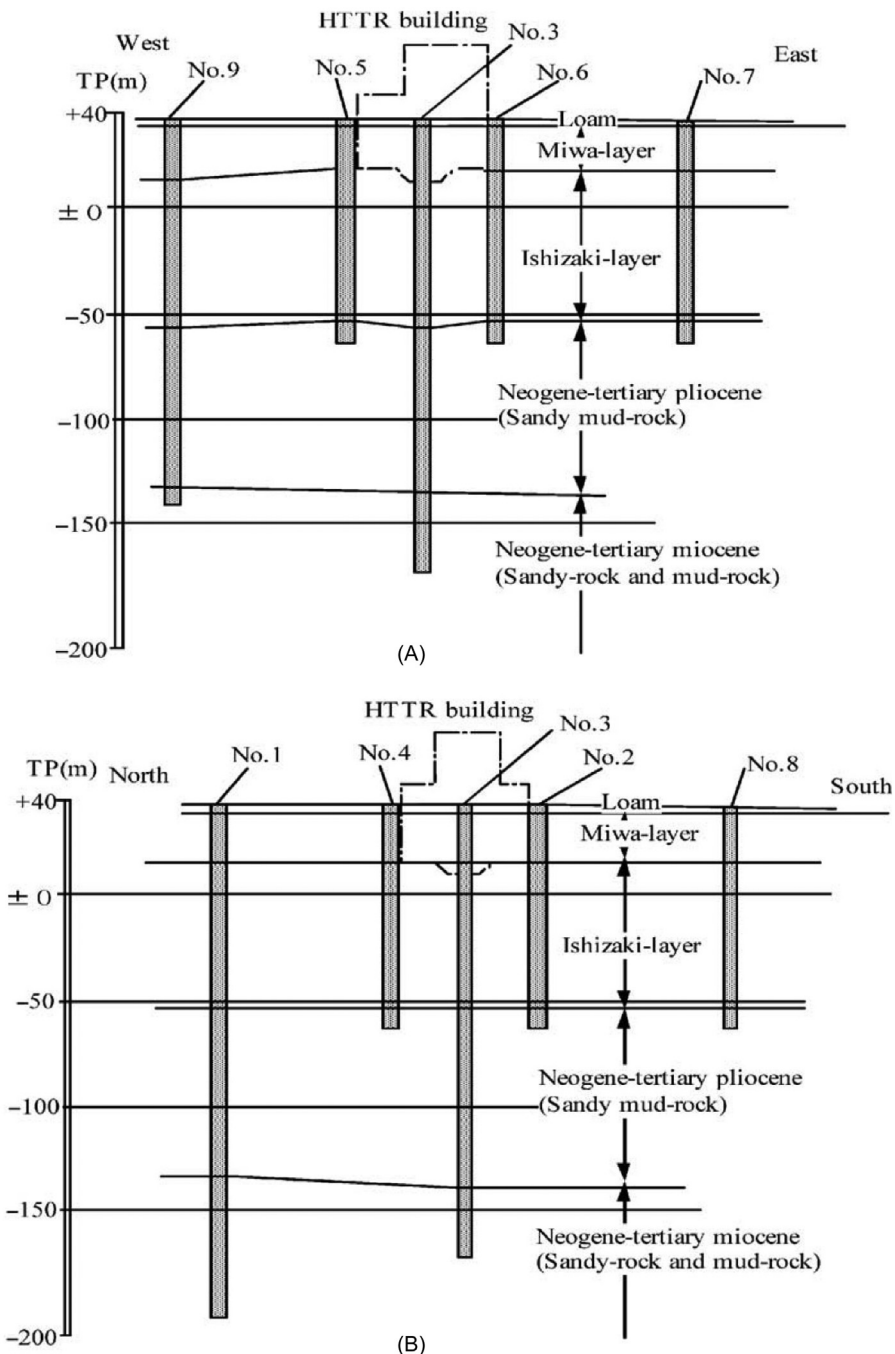
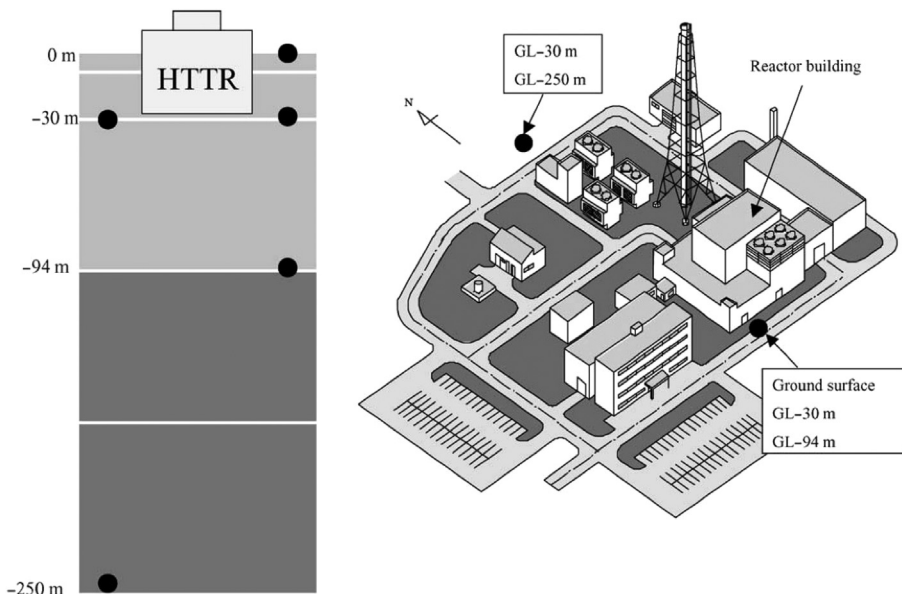
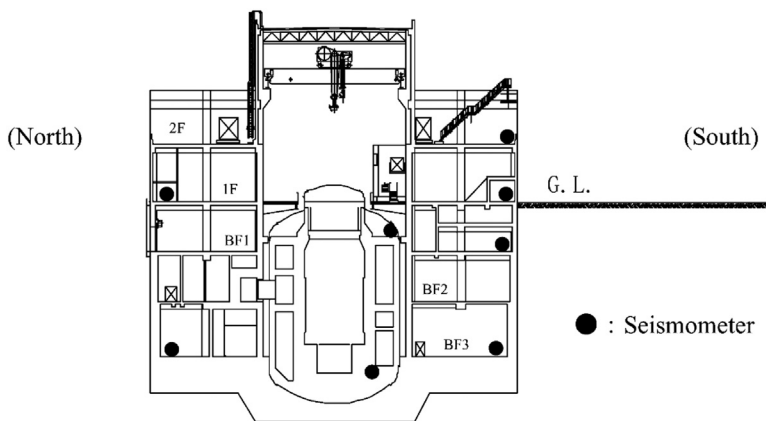


Figure 2.50 Geological section [51]. (A) East-West. (B) North-South.



**Figure 2.51** Position and depth of seismometers in surrounding foundation [51].



**Figure 2.52** Position of seismometers in reactor building [51].

and 0.58 m high. Three dowel pins are installed on the top face, coupled with sockets in the bottom face of the block above. The dowel-socket system ensures the correct orientation of the blocks within the column with respect to each other. The control rod guide block shown in Fig. 2.38 and the replaceable reflector block have the same external dimensions as the fuel element block.

## 2.7.5 Development of evaluation method

Aseismic studies have been performed to clarify the vibration characteristics and assess the structural integrity for the core components and the CBS. These studies have been done independently through experimental and analytical methods.

### 2.7.5.1 Vibration characteristics of core components

A core seismic computer code is required for determination of the overall core response and the displacement characteristics of the core and design loads for the core components. A comprehensive R&D program was conducted to develop a means to analyze the block-type core for a seismic design. However, no general-purpose codes met the above requirements. This was due to a number of limitations, especially the inability to efficiently treat impacts and highly nonlinear characteristics in large numbers. We, therefore, developed the SONATINA-2V code [54]. This code is used to predict the impact phenomena between graphite blocks and to provide information on impact forces, displacements, etc. that is required for the safety evaluation of the structural integrity of the core. To evaluate the validity of the SONATINA-2V code and to confirm the structural integrity of the core graphite blocks, many seismic tests were conducted.

### 2.7.5.2 Validation of SONATINA-2V code

The impact of the graphite block, particularly the dowel and socket system, and the displacements of blocks were the most important items from the viewpoint of the core seismic design. Therefore the code was verified in terms of these response values [53]. Fig. 2.53 shows the typical overall core response characteristics at  $2.5 \text{ m/s}^2$ . The analytical results were in good agreement with the test.

Since the SONATINA-2V code applied to a two-dimensional analytical model, it is necessary to confirm that the code can predict the seismic response of the three-dimensional full core. Fig. 2.54 presents the relative displacements of the core graphite blocks as a function of excitation frequency at  $1.0 \text{ m/s}^2$ , comparing the test results using the full-scale seven-column model with the analytical one. In a low-frequency range, where the first vibration mode of the column is dominant, the columns vibrate together. When the frequency exceeds the resonance frequency, the columns exhibit different response modes where the relative displacement response is small. As the code models a two-dimensional vertical slice core (three degrees of freedom), the equivalent column stiffness becomes harder than that of a three-dimensional core (six degrees of freedom). As a result, the calculated frequency response shifts to a slightly higher frequency region in comparison with the experimental result. It can be, thus, seen that the analytical results showed good agreement with the test.

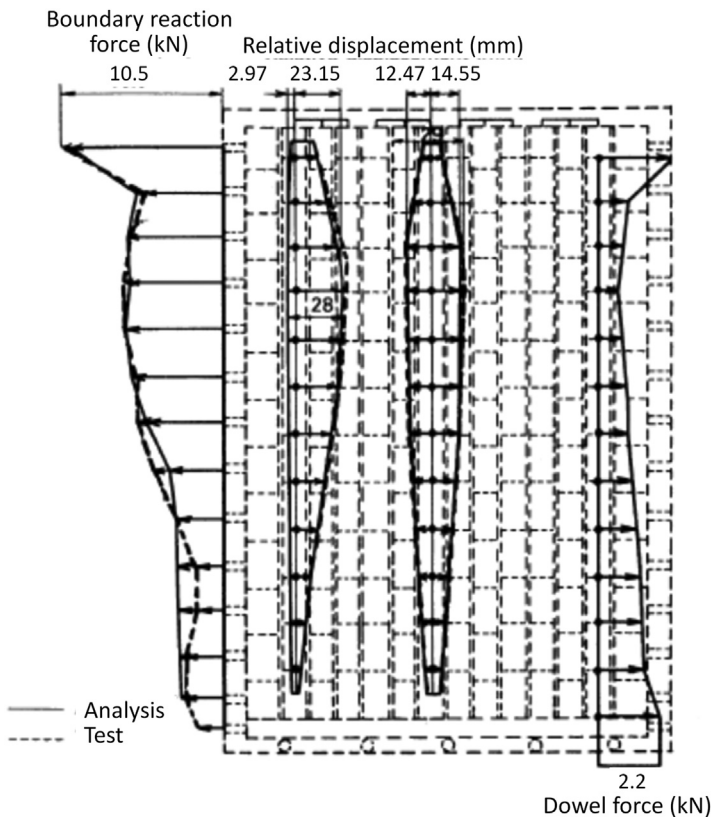


**Figure 2.53** Typical core overall response characteristics at resonance [52].

## 2.7.6 Structural integrity of graphite components

The dowel socket and key–keyway systems are designed such as to transfer the shear force between connected blocks during earthquake [55]. The core support posts are subjected to vertical loads induced by the vertical and rocking motions of the hot plenum block [56]. Consequently, the excessive load concentrates on these connecting elements such as dowel sockets, key–keyway, and support post seat. The assessment of structural integrity for the connecting elements is one of the major concerns in the aseismic design because their fracture may lead to the serious damage to the reactor core. Thus the evaluation results for their structural integrity will be described in the following subsection.

### 2.7.6.1 Core components

The design load acting on three dowel-socket systems in a fuel block was 7.4 kN in the postulated maximum design earthquake denoted by S<sub>2</sub> using the SONATINA-2V

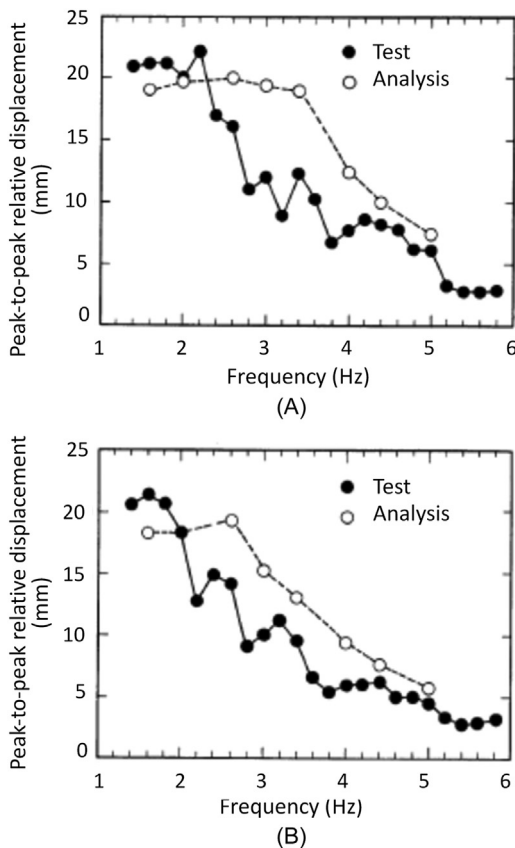


**Figure 2.54** Comparison between test and analytical results of relative block displacement (full-scale seven-column test) [52]. (A) Secondary block from top. (B) Fourth block from top.

code. Based on the fracture tests for a dowel-socket system, the safety load factor (fracture load divided by the design load) becomes about 4.6 for the final failure [55]. It can be seen that the dowel-socket system withstands more than three times as much as the seismic load in an S<sub>2</sub> earthquake. After the seismic tests using the full-scale seven-column model, including excitation over the S<sub>2</sub> level, the graphite blocks were visually inspected, and there had never been any damage in these components.

### 2.7.6.2 Core bottom structure

The CBS is designed to withstand earthquakes such as S<sub>1</sub> and S<sub>2</sub>. The maximum stress on the keyway corner was estimated to be 1.7 MPa from the measured strain under S<sub>2</sub>. This stress is sufficiently lower than the fracture stress (about 10 MPa) obtained from the full-scale fracture test of the key-keying system. The seismic loads on the core support posts were evaluated from the 1/3-scale model test. The

design load using the test results gets to be 130 kN and results in an estimate of 7 MPa for the axial compressive membrane stress in the core support post [56]. This stress is sufficiently lower than the strength of the core support post (about 55 MPa). After  $\sim 60$  excitation in the 1/3-scale model test, including excitation over the  $S_2$  level, the hot plenum blocks and the core support posts were visually inspected. There was no damage in these graphite components.

## 2.8 Cooling system

### 2.8.1 Introduction

The reactor cooling system consists of the primary cooling system, the secondary helium cooling system, the pressurized water-cooling system, the auxiliary cooling system, and the VCS as schematically shown in Fig. 2.55. The main cooling system consists of the primary cooling, the secondary helium cooling, and the pressurized water-cooling systems [57].

The primary cooling system has two heat exchangers of the IHX and the PPWC. The primary helium gas is transported from the reactor core to the IHX and to the PPWC through the primary concentric hot gas duct. The secondary helium cooling system, mainly consisting of the SPWC, removes the heat from the primary helium gas through the IHX. The pressurized water-cooling system consists of an air cooler and water pumps. The air cooler cools the pressurized water in both the PPWC and the SPWC and transfers the heat from the reactor core to the atmosphere as final heat sink. The auxiliary cooling system is in stand-by during normal operation and starts up to remove the residual heat after reactor shutdown. The VCS runs at rated flow rate during normal operation to cool the biological concrete shield. It cools the

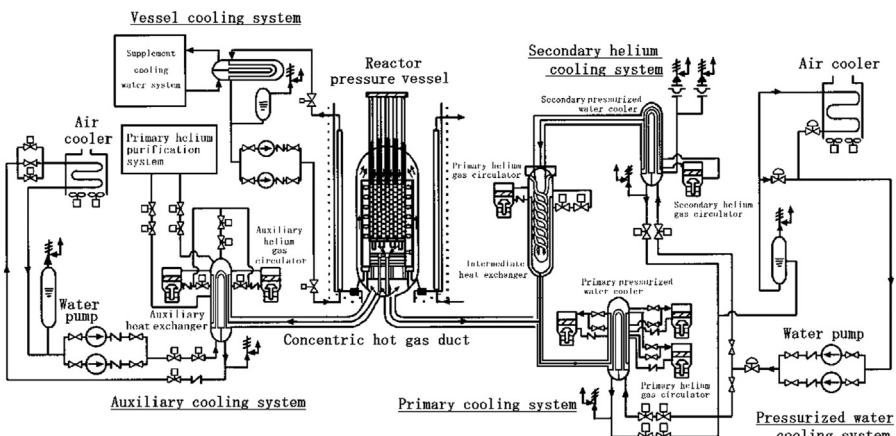


**Figure 2.55** Schematic diagram of cooling system for HTTR [57].

reactor core at accident such as a primary-pipe rupture when the auxiliary cooling system is no longer able to cool the core effectively.

The HTTR has two operation modes. One is the single-loaded operation using only the PPWC, and the other is the parallel-loaded operation using both the PPWC and the IHX to cool the primary helium gas from the reactor. In the single-loaded operation, the PPWC removes the heat of 30 MW. In the parallel-loaded operation, the PPWC and the IHX remove the heat of 20 and 10 MW, respectively.

The pressure boundary of the main components such as the IHX, the PPWC, the SPWC, the auxiliary heat exchanger, and the primary concentric hot gas duct are served at temperatures slightly above 400°C. The pressure boundary between the primary and secondary helium gases, such as the heat transfer tubes of the IHX, reaches approximately 900°C during the high temperature test operation.

To assure the structural integrity of these high temperature components, the following rules are applied:

1. To use several kinds of heat-resistant metallic materials, taking into account the service conditions of components.
2. To establish a reliable high temperature structural design guideline.
3. To apply countermeasures for overcoming the severity of the service conditions.

As for item (1), two commercial materials and a superalloy, which was developed for the HTTR, are used as follows:

- a. 2½Cr–1Mo steel for the reactor coolant pressure boundary in-service at temperatures of approximately 400°C;
- b. austenitic stainless steels (SUS321TB and SUS316) for the heat transfer tubes of the PPWC, the SPWC, and the auxiliary heat exchanger;
- c. Ni-base corrosion and heat-resistant superalloy Hastelloy XR [58] for the heat transfer tubes of the IHX and other reactor coolant pressure boundaries reaching very high temperature of approximately 900°C.

## 2.8.2 Primary cooling system

### 2.8.2.1 Primary pressurized water cooler

The PPWC is a vertical U-tube type heat exchanger. Fig. 2.56 shows a schematic view of the PPWC and Table 2.20 shows its major specifications.

The hot primary helium gas from the inlet nozzle flows horizontally between the baffle plates and cools the outside surface of the heat transfer tubes, flowing upward and turns backward several times. It flows out via the upper or lower outlet nozzles to the primary gas circulators and flows back to the annular space between the inner and outer shells to cool them. The pressurized water of 3.5 MPa is led to each heat transfer tube and heated up by the primary helium gas. The thermal insulation is installed inside the inner shell so as to maintain its temperature lower than 440°C. A tube sheet supports the heat transfer tubes. The heat capacity of the PPWC can be changed from 30 to 20 MW and vice versa by changing helium gas flow paths according to the loop operational modes. The

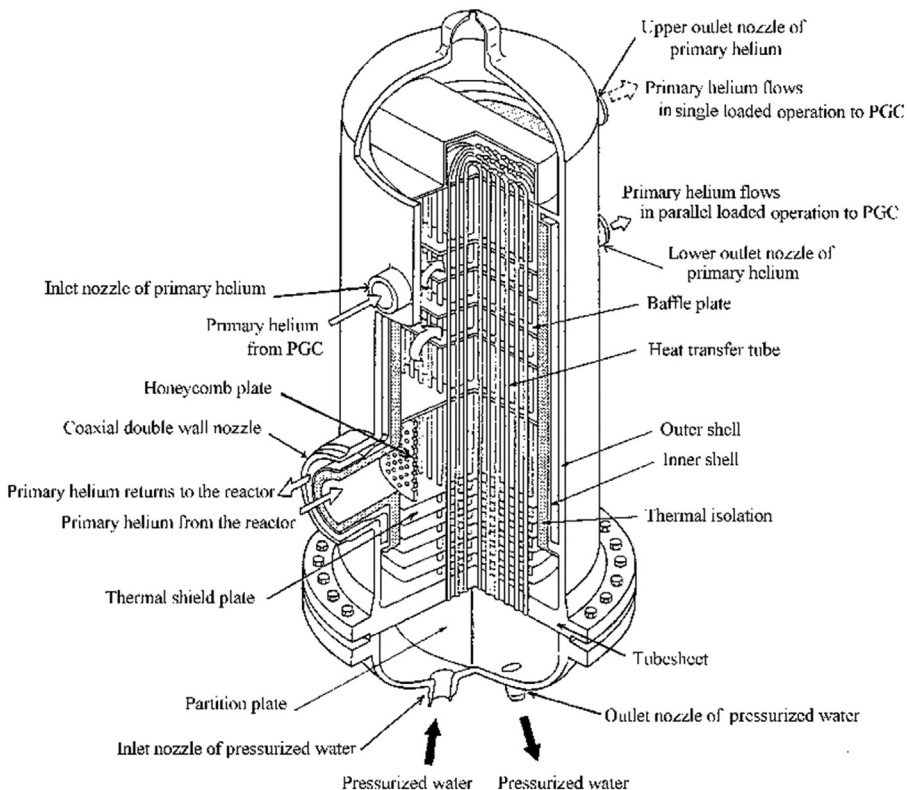


**Figure 2.56** Schematic view of primary pressurized water cooler [57].

primary helium gas flows out through three lower outlet nozzles during the parallel-loaded operation, while three upper nozzles during the single-loaded operation. The inner and outer shells are made of 2½Cr–1Mo steel. The austenitic stainless steel (SUS321TB), which is superior not only in strength at high temperatures but also anticorrosion, is used for the heat transfer tubes. Material of the baffle plates is Hastelloy XR because they are exposed to the primary helium gas of approximately 950°C for a long time.

Burnout of the pressurized water was the major problem to be solved because the maximum temperature difference between the primary helium gas and pressurized water is approximately 800°C, which is higher than that of existing PWCs. To prevent burnout, the flow velocity of the primary helium gas in high temperature region is maintained lower than the average flow velocity in the PPWC. The flow velocity in the low temperature region is maintained higher than the average to promote heat transfer. The size of the PPWC remains compact by the above design method.

**Table 2.20** Major specifications of primary pressurized water cooler [57].

Type	Vertical U-bent tube type	
Design pressure		
Outer shell	4.7 MPa	
Heat transfer tube	4.7 MPa	
Design temperature		
Outer shell	430°C	
Heat transfer tube	380°C	
Operating condition	Rated operation	High temperature test operation
Flow rate of primary helium gas (max.)		
Single-loaded operation	45.2 t/h	37.0 t/h
Parallel-loaded operation	29.7 t/h	24.3 t/h
Inlet temperature of primary helium gas	890°C	950°C
Outlet temperature of primary helium gas	395°C	395°C
Flow rate of pressurized water		
Single-loaded operation	625 t/h	618 t/h
Parallel-loaded operation	413 t/h	410 t/h
Inlet temperature of pressurized water	135°C	134°C
Outlet temperature of pressurized water	175°C	174°C
Heat capacity		
Single-loaded operation	30 MW	
Parallel-loaded operation	20 MW	
Heat transfer tube		
Number	136	
Outer diameter	25.4 mm	
Thickness	2.6 mm	
Length	10 m	
Outer diameter of shell	2.1 m	
Total height	7.5 m	
Material		
Outer and inner shell	SCMV4-2NT (2½Cr-1Mo steel)	
Heat transfer tube	SUS321TB	
Tube sheet	SFVA F22B (2½Cr-1Mo steel)	

### 2.8.2.2 Intermediate heat exchanger

The IHX is a vertical helically coiled counter flow-type heat exchanger in which primary helium gas flows on the shell side and secondary helium gas in the tube side as shown in Fig. 2.57. Table 2.21 shows the major specifications of the IHX.

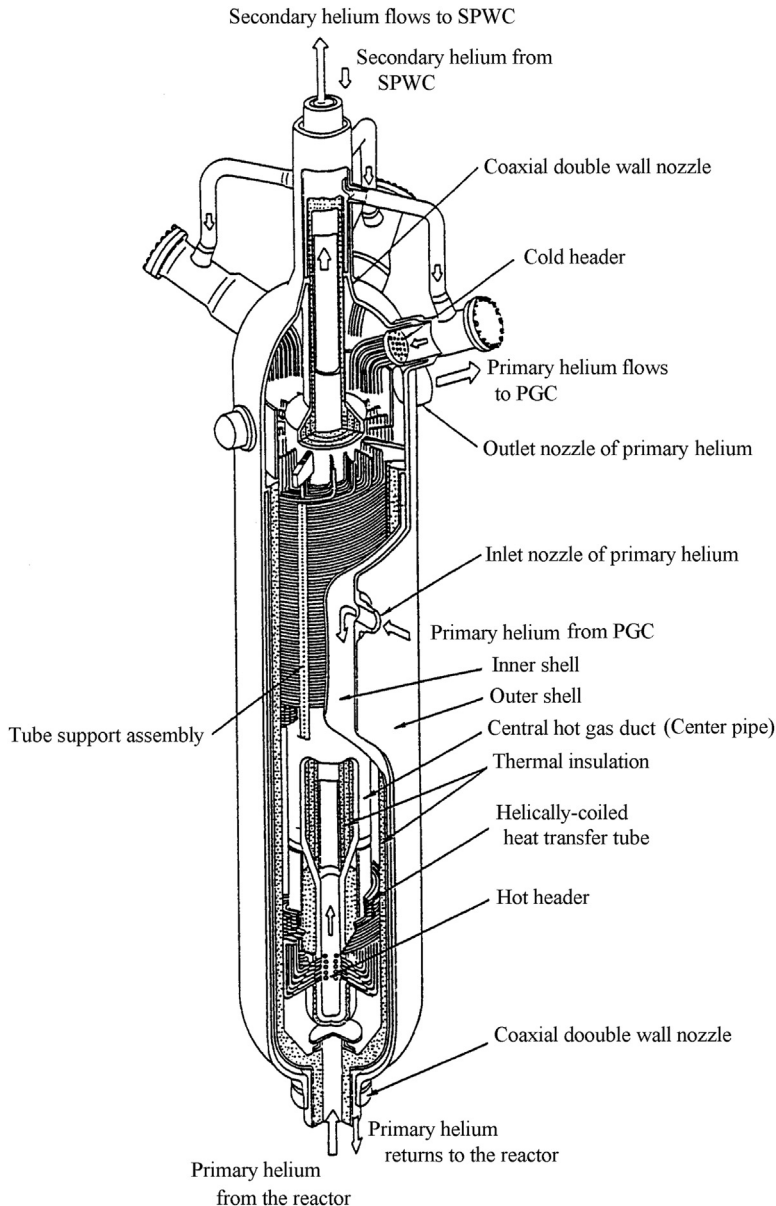


**Figure 2.57** Schematic view of intermediate heat exchanger [57].

**Table 2.21** Major specifications of intermediate heat exchanger [57].

Type	Vertical helically coiled counter flow	
Design pressure		
Outer shell	4.7 MPa	
Heat transfer tube	0.29 MPa (differential pressure)	
Design temperature		
Outer shell	430°C	
Heat transfer tube	955°C	
Operating condition	Rated operation	High temperature test operation
Flow rate of primary helium gas (max.)	14.9 t/h	12.2 t/h
Inlet temperature of primary helium gas	850°C	950°C
Outlet temperature of primary helium gas	395°C	395°C
Flow rate of secondary helium gas	12.8 t/h	10.8 t/h
Inlet temperature of secondary helium gas	244°C	237°C
Outlet temperature of secondary helium gas	175°C	174°C
Heat capacity	10 MW	
Heat transfer tube		
Number	96	
Outer diameter	31.8 mm	
Thickness	3.5 mm	
Length	30 m	
Outer diameter of shell	1.9 m	
Total height	10 m	
Material		
Outer and inner shell	SCMV4-2NT (2½Cr–1Mo steel)	
Heat transfer tube	Hastelloy XR	
Hot header and center pipe	Hastelloy XR	

The primary helium gas enters into the IHX through the inner pipe of the primary concentric hot gas duct. It is deflected under a hot header and discharged around the heat transfer tubes to transfer the heat to the secondary helium cooling system. It flows to the primary gas circulator via the upper outlet nozzle and flows back to the annular space between the inner and outer shells.

The secondary helium gas flows downward in the heat transfer tubes and upward in the central hot gas duct through the hot header. The inner insulation is installed inside the inner shell to maintain its temperature below 440°C. The insulations outside and inside the central hot gas duct restrain the heat transfer so that high efficiency can be obtained. In addition, it also keeps the temperature of the central duct below 940°C. The primary helium gas is contained only in the primary cooling system because the pressure in the secondary helium cooling system is adjusted somewhat higher than that in the primary cooling system. The tube support assemblies hold the heat transfer tubes. Both the central hot gas duct and the heat transfer tube support assemblies are hung from the vessel top so that the thermal expansion is not constrained. The material of the heat transfer tubes and the hot header is Hastelloy XR, and the inner and outer shells are made of 2½Cr–1Mo steel.

The IHX has a bypass line, which prevents natural circulation from the reactor core to the IHX during the single-loaded operation. The forced circulation from the PPWC through the bypass line occurs and keeps the temperature of the outer shell below 430°C. The primary helium gas flows from the PPWC and enters into annulus space between the inner and outer shells and then flows inside the inner shell through the bypass line. It returns to the PPWC through the IHX and the primary concentric hot gas duct. The shutoff valve stops this forced circulation during the parallel-loaded operation and in case of a scram when the auxiliary cooling system is activated.

The inner structures such as the heat transfer tubes, the central hot gas duct, and the hot header are operated beyond 900°C. A design method based on the elastic analysis cannot meet the criteria of the high temperature structural design code for the HTGR class 1 components. Therefore the design method based on a creep analysis is used for evaluation of their structural integrity. The creep–fatigue damage was properly evaluated and is capable of meeting the criteria.

### 2.8.2.3 Primary gas circulator

The primary gas circulator is a centrifugal, dynamic gas bearing type circulator. [Table 2.22](#) shows the major specifications of the circulator. Three circulators for the PPWC and one for the IHX are installed in the primary cooling system. The former circulators are operated during both the parallel-loaded operation and single-loaded operation, and the latter during the parallel-loaded operation.

During operation, the rotating assembly is fully floating on sets of a dynamic gas bearing system. [Fig. 2.58](#) shows a schematic view of the circulator. The circulator consists of the following components: (1) electric stator and rotor assembly, (2) internal structure supports, (3) thrust bearings and journal bearings, (4) impeller unit, and (5) filter unit. These internal structures are contained in a casing which is cooled by a water jacket. The casing prevents primary helium gas from leaking into

**Table 2.22** Major specifications of primary gas circulator [57].

	<b>For the IHX</b>	<b>For the PPWC</b>
Type	Centrifugal gas bearing	Centrifugal gas bearing
Flow rate (max.)	14.9 t/h	15.1 t/h
Head (max.)	79.4 kPa	107.9 kPa
Design pressure	4.7 MPa	4.7 MPa
Design temperature	430°C	430°C
Casing material	SCMV4-2NT SFVA 22B (2½Cr–1Mo steel)	SCMV4-2NT SFVA 22B (2½Cr–1Mo steel)
Motor		
Type	Cage-type induction motor	Cage-type induction motor
Power	260 kW	260 kW
Revolution speed	3000–12,000 rpm	3000–12,000 rpm
Type of frequency converter	Thyristor convertor	Thyristor convertor
Filter		
Type	Sintering metal	Sintering metal
Material	SUS316	SUS316

the atmosphere. The flow rate of primary helium gas is controlled by a variable speed motor using a frequency converter. The filter unit, which is on the top of the circulator, protects the impeller and rotating shaft from dust. The material of the casing is 2½Cr–1Mo steel.

#### 2.8.2.4 Primary concentric hot gas duct

The primary concentric hot gas duct consists of an outer pipe, an inner pipe, and a thermal insulator as shown in Fig. 2.59. Table 2.23 shows the major specifications. The cold helium gas of 400°C flows in an annular path, inside the inner pipe the temperature is 950°C. The outer pipe can contain high-pressure helium gas of 4.0 MPa. The inner pipe, which separates the high and low temperature helium gas paths, supports the pressure difference between the high and low temperature helium gas. The pressure difference is about 0.1 MPa. The liner forms a high temperature helium gas boundary and reinforces the ceramic fiber insulator. The internal insulator between the liner and inner pipe minimizes heat loss from the high to low temperature helium gases and maintains the temperature of the inner pipe below 440°C.

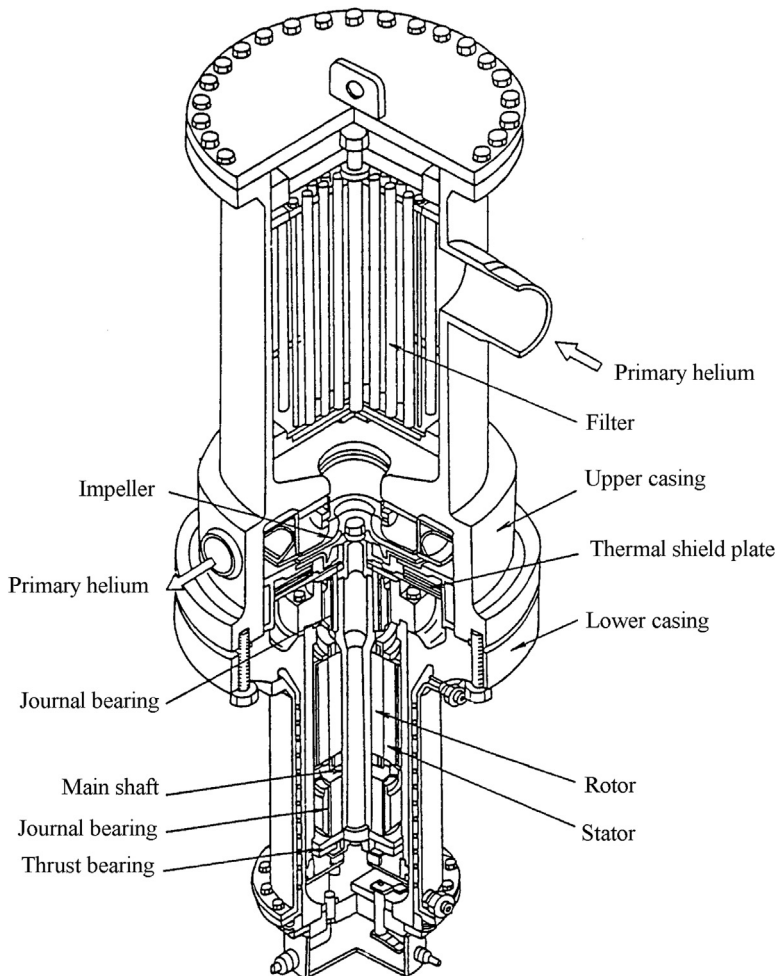


**Figure 2.58** Schematic view of primary gas circulator [57].

The outer pipe and the inner pipe are made of  $2\frac{1}{4}\text{Cr}-1\text{Mo}$  steel, the material of the liner is Hastelloy XR, and the insulation material is a ceramic fiber composed of  $\text{SiO}_2$  and  $\text{Al}_2\text{O}_3$ .

### 2.8.3 Secondary helium cooling system

The secondary helium cooling system consists of a secondary gas circulator, the SPWC, and a secondary helium piping. This system is operated during the parallel-loaded operation. The heat is transferred from the primary to the secondary helium gas through the IHX. This transported heat is sent to the pressurized water-cooling system through the SPWC. In the future, the hydrogen production system will be connected to the secondary helium cooling system [59].

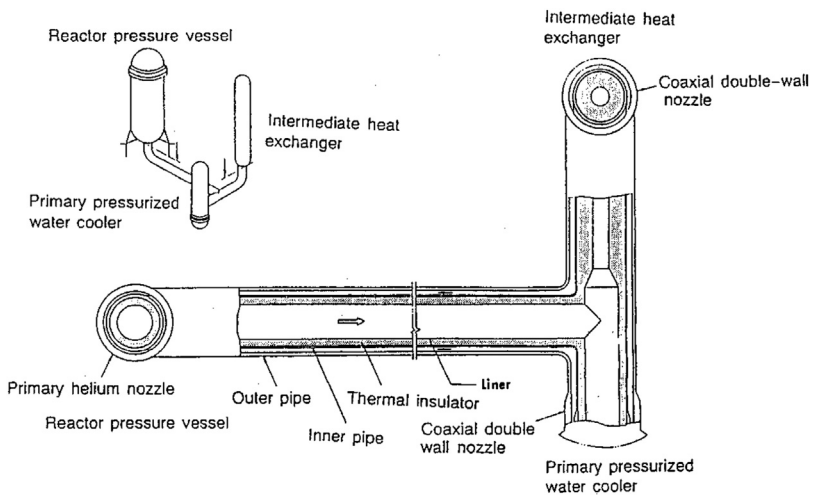


**Figure 2.59** Cross-sectional view of primary concentric hot gas duct [57].

**Table 2.23** Major specifications of primary concentric hot gas duct [57].

Design pressure	
Outer pipe	4.7 MPa
Design temperature	
Outer pipe	430°C
Dimension of outer pipe	
Outer diameter	863.6 mm
Thickness	42 mm
Dimension of inner pipe	
Outer diameter	660.4 mm
Thickness	15 mm
Thickness of thermal insulator	90 mm
Material	
Outer pipe	SCMV4-2NT SFVA 22B (2½Cr–1Mo steel)
Inner pipe	SCMV4-2NT (2½Cr–1Mo steel)
Liner	Hastelloy XR

### ***2.8.3.1 Secondary pressurized water cooler***

The structure of the SPWC is fundamentally the same as that of the PPWC. The SPWC is a vertical U-bent type heat exchanger and has double shells. Inside of the inner shell, it is thermally insulated. 2½Cr–1Mo steel of SCMV4-2NT is used for the inner and outer shells, SUS321TB is used for heat transfer tubes, and Hastelloy XR is used for the baffle plates and the liner.

### ***2.8.3.2 Secondary gas circulator***

The structure of the secondary gas circulator is nearly the same as that of the primary gas circulator. The secondary gas circulator has one gas circulator, which is vertical centrifugal type. The circulator is composed of the casing, an impeller, a rotor, bearings, and a motor. The speed of the circulator is changed by a frequency converter to control the helium flow rate.

### ***2.8.3.3 Secondary helium piping***

The secondary helium piping consists of a concentric hot gas duct connecting the IHX and the SPWC, and a single wall piping connecting the SPWC and the secondary gas circulator. Thermal insulator is attached on the inside of the inner pipe of the concentric hot gas duct. The hot helium gas from the IHX flows inside the inner pipe. The helium gas, pressurized by the circulator, flows in the annular space between the inner and outer pipes. The 2½Cr–1Mo steel is used in the inner and outer pipes, and Hastelloy XR is used as the liner.

## ***2.8.4 Pressurized water-cooling system***

The pressurized water-cooling system is installed to cool primary and secondary helium gas in the PPWC and the SPWC, respectively. The heat is finally released to the atmosphere via the air cooler. This system consists of a pressurized water pump, an air cooler, and piping. The pressure of water is controlled to be lower than that of the primary cooling system in order to minimize the amount of water ingress into the primary cooling system in case of a heat transfer tube rupture accident but still high enough to prevent boiling.

### ***2.8.4.1 Pressurized water pump***

Two pressurized water pumps (including a spare) of horizontal centrifugal type are installed. They have a capacity of 640 t/h flow rate at 90 m delivery head.

### ***2.8.4.2 Air cooler***

The air cooler consists of finned heat transfer tubes and blowers. It has a 30 MW cooling capacity. Its air flow rate is 2600 t/h.

## **2.8.5 Residual heat removal system**

The main cooling system is also used to remove the decay heat of the core at normal reactor shutdown conditions. Besides the main cooling system, the HTTR has two other residual heat removal systems, which are the auxiliary cooling system and the VCS. The auxiliary cooling system removes the residual heat during anticipated operational occurrences and for accidents as reactivity insertion or pipe rupture in the secondary cooling system. The VCS removes the residual heat during the loss of coolant accident in the primary cooling system.

### **2.8.5.1 Auxiliary cooling system**

The auxiliary cooling system consists mainly of an auxiliary heat exchanger, an auxiliary gas circulator, and an auxiliary water-cooling system including an air cooler. The auxiliary cooling system has a capacity of about 3.5 MW. The system starts up automatically when the reactor is scrammed in case of an accident if the core cooling by a forced circulation is still possible, while the main cooling system is stopped. The auxiliary cooling system has engineered safety features with redundant dynamic components such as gas circulators, water pumps, and valves, which are also backed up with an emergency power supply. The residual heat of the core can be removed even by the VCS without the auxiliary cooling system. The auxiliary cooling system, however, is needed from the viewpoint of operation flexibility because it takes a very long time for cooling down the core only with the VCS.

### **2.8.5.2 Vessel cooling system**

The VCS consists of upper, lower, and side cooling panels around the RPV and cooling water circulation systems. The amount of the heat removal is less than 0.6 MW to accomplish the outlet gas temperature of 950°C because the heat removal of the VCS means heat loss from the RPV. Besides, the VCS is required to remove more than 0.3 MW since the temperatures of the fuel and the RPV did not exceed their limit temperature of 1600°C and 550°C, respectively, to keep their structural integrity. The system is used as a residual heat removal system when the forced circulation in the primary cooling system cannot be maintained due to the rupture of the inner pipe or both pipes in the concentric hot gas duct. The VCS has engineered safety features, that is, it is equipped with two independent sets, which are backed up with an emergency power supply. It is operated even in normal operation in order to cool the biological concrete wall shield.

## **2.9 Reactivity control system**

### **2.9.1 Introduction**

The reactivity control system of the HTTR is comprised of a control rod system and a reserve shutdown system. Reactivity is controlled by 16 pairs of control rods, which are individually moved by control rod drive mechanisms located in stand pipes connected to

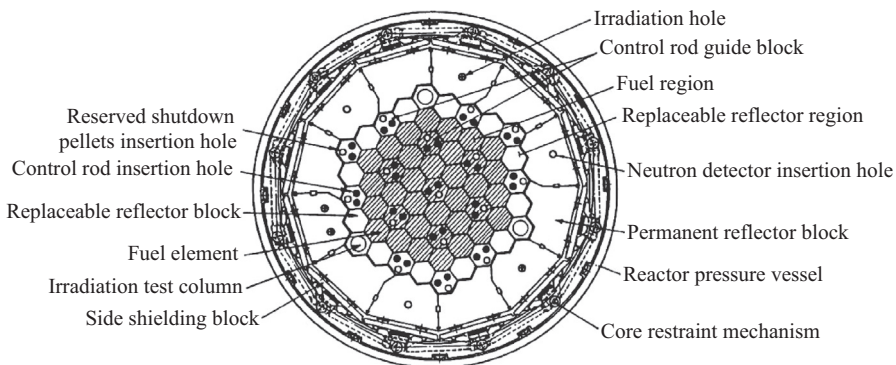


**Figure 2.60** Horizontal arrangement of HTTR core [60].

the hemispherical top head closure of the RPV. The control rods are inserted into appropriate holes in the core and the replaceable reflector regions as shown in Fig. 2.60 [60].

The control rod drive mechanism inserts and withdraws a pair of control rods using an AC motor. In the event of a scram, which needs to separate the clutch gear teeth, the control rods are inserted into the core by gravity.

Ferritic superalloy Alloy 800H is selected for a material of metallic parts of the control rod. The maximum allowable temperature for the control rod to be used repeatedly after scrams is 900°C, that is, the control rod must be replaced when the temperature exceeds 900°C [13]. Since the maximum temperature of the graphite blocks in the fuel region reaches about 1100°C at “high temperature test operation of 950°C reactor outlet gas temperature,” a two-step control rod insertion method for reactor scram must be adopted for the HTTR. The outer nine pairs of control rods in the reflector region are inserted into the core immediately at a scram, and the other inner seven pairs in the fuel region are inserted 40 min later or when the outlet coolant temperature becomes less than 750°C. Preliminary temperature analysis revealed that in most events that cause scrams, the maximum temperature of the control rods is lower than 900°C [61].

The reserve shutdown system is located in stand pipes accompanied by the control rod system. In case the control rods cannot be inserted, the reserve shutdown system drops B<sub>4</sub>C/C pellets into the core to shut down the reactor.

## 2.9.2 Control rod system

### 2.9.2.1 Design requirement

The following criteria are established for design of the control rod system:

1. The control rod system shall be designed to shut down the reactor reliably and safely when required during normal operation conditions and accidents including earthquakes as well as at the lowest shutdown temperature of 27°C (300 K).
2. The control rod system shall be capable of controlling the reactivity changes due to temperature and Xenon density, fuel burnup, experimental samples, etc.
3. The control rod system shall be designed to be failsafe.

4. The reactivity worth and reactivity insertion rate by a control rod shall be restrained to the level that break of reactor internals preventing the core cooling should not occur in a postulated reactivity insertion accident. Even if a stand pipe break should occur, control rod ejection shall be limited by the stand pipe fixing device.

### 2.9.2.2 Design details

The specifications of the control rod system are shown in [Table 2.24](#).

**Table 2.24** Specifications of HTTR control rod [60].

Items	Properties
Control rod	
Type	Double circular cylinders with lid and vent
Number	16 pairs (32 rods) (15 pairs in irradiation tests using the center column)
Total length (m)	3.1
Outside diameter (mm)	113
Inside diameter (mm)	65
Sleeve	
Thickness (mm)	3.5
Material	Alloy 800H
Neutron absorber	
Outside diameter (mm)	105
Inside diameter (mm)	75
Material	Sintered compact of $B_4C/C$
Spine	
Diameter (mm)	10
Material	Alloy 800H
Control rod drive mechanism	
Drive method	
Normal operations	Rolled up and down by AC motor through control rod support cable
Scram	Separate electromagnetic clutch and the control rod fall by gravity
Number	16 (15 in irradiation tests using center column)
Drive speed (mm/s)	From about 1–10 (variable)
Insertion time (s)	<12 (after being triggered)

### 2.9.2.2.1 Control rod

The control rod system of the HTTR is shown in Fig. 2.61. To reduce thermal stresses in the sleeves, the neutron absorber sections and spine are separated from each other and each section is sustained by a support ring. For the same purpose, the absorber section is assembled from parts with gaps between them and all parts are mechanically connected without welds. Each absorber section contains a guide ring to restrain them from rolling too much. The lower end of the spine is attached to a tubular-type shock absorber. At the bottom of the core are graphite dishes, also called shock absorber, which absorb impact of a control rod, when the control rod support cable breaks.

During normal operation, the temperature of the clad material is about 600°C maximum, whereas at the time of a scram, the temperature will attain nearly 900°C and a significant thermal stress will occur, which causes severe creep–fatigue damage if this occurrence is repeated. It is noted that the primary loads can be disregarded due to no differential pressure since the sleeves are equipped with ventilation gaps and the weight of the neutron absorber is small.

The annular space of each absorber section contains a neutron absorber, which is made up of five sintered compacts of B<sub>4</sub>C/C. The density of the neutron absorber is 1.9 g/cm<sup>3</sup>.

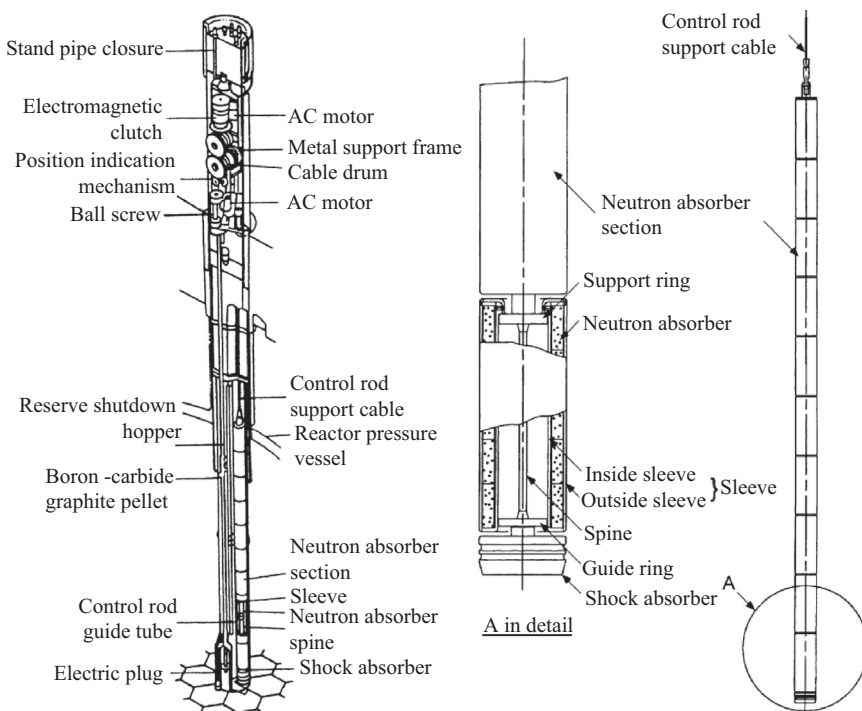


**Figure 2.61** Schematic view of control rod system of HTTR [60].

### 2.9.2.2.2 Control rod drive mechanism

The control rod drive mechanism consists of an AC motor, a decelerator, an electromagnetic clutch, a velocity-limiting brake, a shock-absorbing mechanism, position indicators, manual control mechanisms, gears, a control rod support cable, etc. as shown in Fig. 2.61.

The drive motor is coupled to the cable drum through the decelerator, the electromagnetic clutch, and the gears. During normal operation, the position of the control rod is sustained by the torque of the motor. The maximum withdrawal velocity is limited to a value below 70 mm/s by the decelerator even when the motor is running at the maximum speed even if the motor is uncontrollable.

When the electric current through the electromagnetic clutch is cut off by a scram signal, the clutch is separated to insert the control rod into the core by gravity as mentioned before. To protect the control rod support cable from overloading, the velocity-limiting brake maintains the insertion speed constant during a reactor scram by applying the braking torque in proportion to the speed. The shock-absorbing mechanism reduces the speed of the control rods at the last stage of the insertion by using a gas damper to absorb any impact when the control rods are inserted for more than 80% of their full stroke. The position indicator has three independent systems using synchro-mesh transmitters as a built-in safety factor.

### 2.9.2.3 High temperature structural design guideline of control rod

Fig. 2.62 shows the flow diagram for the elevated temperature design of the HTTR control rod [62]. The high temperature design is based on the ASME Boiler and

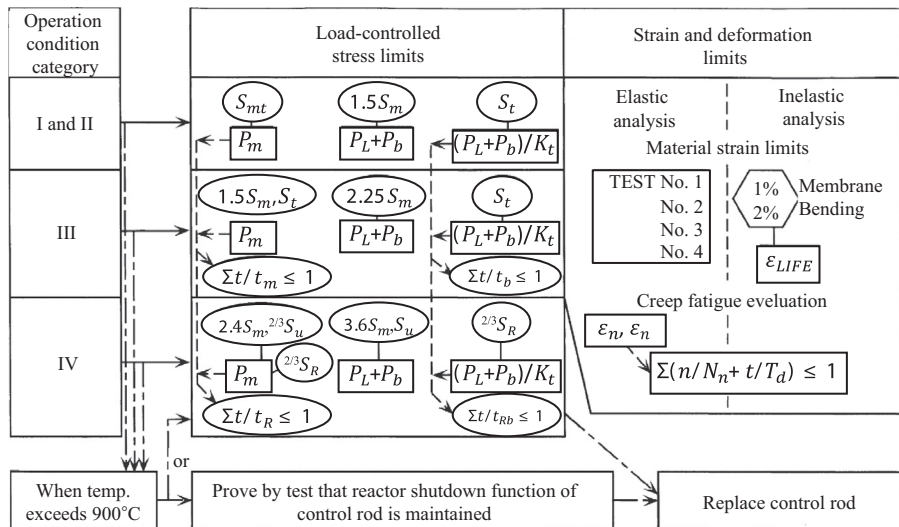


Figure 2.62 Schematic flow diagram for high temperature design of HTTR control rod [60].

Pressure Vessel Code Case N-47-21 [28] because the failure modes assumed in the code case are most generic and their integrity evaluation methods are applicable to the design of HTTR control rods. With respect to the factors of the stress limits on  $S_m$ : the allowable stress intensity values, laid down in the Japanese structural guideline for core support structures of LWRs are adopted.

One notable merit of the HTTR control rod design is that the control rods are replaceable, which makes the structural design easier and lessens the requirements for a database on material properties at the same time.

As also shown in Fig. 2.62, the design code for the control rod requires that the control rod be replaced when it has been subjected to temperatures above 900°C. The threshold temperature of 900°C is provided not only to reduce the need for very high temperature material data but also to have a reasonably long life for the control rods [13]. Damage such as cracks to the structural metal is essentially acceptable as far as the reactor shutdown function is secured. In some events of Japanese operation condition categories II–IV (corresponding to levels B–D in N-47, respectively), the temperature of the control rod can exceed 900°C. In these cases, it must be proved by analysis or test that the reactor shutdown function of the control rods is maintained and the control rods need to be replaced. The analytical approach is possible up to 1000°C. For the design by test, verification tests using a full-size model of the neutron absorber section were carried out above 900°C (at 1100°C maximum), which will be described in Section 2.9.2.5. Significant deformation or cracks were not observed, which allow the control rod to function properly. Thus design of the control rod below 900°C and above 900°C is conducted by “design by analysis” and “design by analysis or test,” respectively.

Alloy 800H is selected for the metal parts of the control rod mainly because iron base alloys are superior to nickel-rich alloys in both postirradiation tensile and creep properties [63]. Design material data on Alloy 800H were determined in this study, which covers temperatures of up to 900°C for  $S_{mt}$ ,  $S_t$  and design fatigue curves, and up to temperature of 1000°C for  $S_m$ ,  $S_u$ , and  $S_R$ , which will be presented in the following section.

During normal operation of the high temperature test operation mode, that is, when the control rods are withdrawn from the core, the maximum temperature of the sleeve at the bottom neutron absorber section is approximately 550°C by preliminary temperature analysis [61]. Since the maximum temperature of graphite blocks in the fuel region is calculated to be around 1100°C, temperatures of the control rods in the fuel region exceed 900°C when all the control rods are inserted into the core at the same time at a scram. Then, the inner seven pairs of control rods in the fuel region must be replaced under the design guideline. Thus it is indispensable for the HTTR to employ a two-step control rod insertion method to avoid a control rod replacement.

The outer nine pairs of control rods in the replaceable reflector region are inserted into the core first. The maximum temperature of the outer control rods then attains a temperature somewhat lower than 900°C, which will be shown in Section 2.9.2.6. The other inner seven pairs in the fuel region are inserted 40 min later or when the outlet coolant temperature becomes less than 750°C so that the maximum temperature of the inner control rods stays lower than the temperatures of the outer control rods. Out of

these outer nine pairs of control rods, six pairs, which are positioned nearer to the center of the core than the other three, are subjected to the severest thermal conditions. Stress analysis of one of these six pairs of control rods in the replaceable reflector region was conducted and will be shown in [Section 2.9.2.7](#).

#### 2.9.2.4 Design material data on Alloy 800H

The high temperature design of the HTTR control rod is based on the ASME Boiler and Pressure Vessel Code Case N-47-21 as shown in the previous section; however, design material data on Alloy 800H available in the Code Case are below 1400°F (760°C). Allowable stresses and design curves on Alloy 800H, which are needed for the design of control rods, were determined up to temperature of 1000°C in this study based on existing data. Material data in the previous papers [64–67] are used for the determination.

In the following, design curves of allowable stress intensity values:  $S_m$ ,  $S_u$ ,  $S_t$ , expected minimum stress-rupture values, denoted  $S_R$  in this paper, and design fatigue strain range  $\varepsilon_t$  are shown. Definitions of the values are the same as those in the Code Case N-47-21.

[Fig. 2.63A–C](#) shows design curves of  $S_m$  and  $S_u$ ,  $S_t$ , and  $S_R$ , respectively. In [Fig. 2.63D](#), relation between shifted curves of test results by Furukawa et al. [68] and design fatigue strain range  $\varepsilon_t$  of Alloy 800H at 1400°F (760°C) in the Code Case N-47-21 is depicted. In the figure, the original regression curve in Furukawa

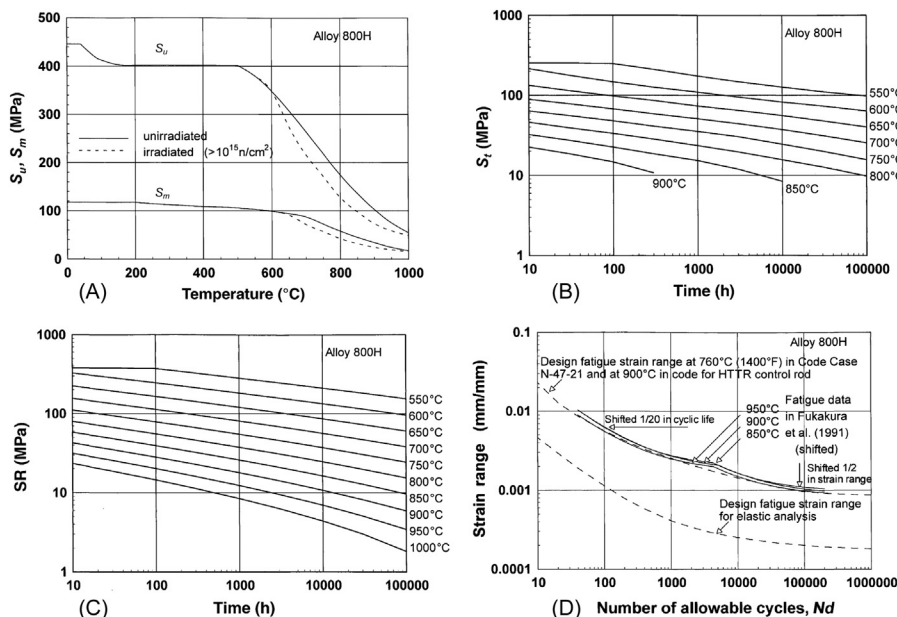


**Figure 2.63** Design properties of Alloy 800H: (A)  $S_m$  and  $S_u$ ; (B)  $S_t$ ; (C) stress-to-rupture; (D) design fatigue strain range [60].

et al. [67] is shifted by less than 1/20 in cyclic life and  $\frac{1}{2}$  in total strain range to derive the design fatigue curve.

The test results between 850°C and 950°C in Fig. 2.63D indicate very small temperature dependence. The shifted curves at 850°C and 900°C locate at a region of longer life than the design curve of N-47-21 at 1400°F (760°C). At 950°C, the shifted curve and the design curve lie at almost the same position. Thus it is concluded that design fatigue strain range  $\varepsilon_t$  of Alloy 800H at 1400°F (760°C) in the Code Case N-47-21 is applicable to the design of the HTTR control rod at 900°C.

### 2.9.2.5 Results of R&D

Various tests were performed to evaluate the reliability of the control rod system. It is assumed in design of the HTTR that the number of scrams during plant lifetime is 211 including ten and one times for service loadings of levels III (C in ASME) and IV (D in ASME), respectively.

#### 2.9.2.5.1 Scram tests of the control rod system under seismic conditions

Fig. 2.64 shows the scram test equipment, which consists of a control rod drive mechanism, a pair of control rods, and a control rod guide column at the center of a vibrating table. The whole arrangement is supported by a rigid concrete test tank.

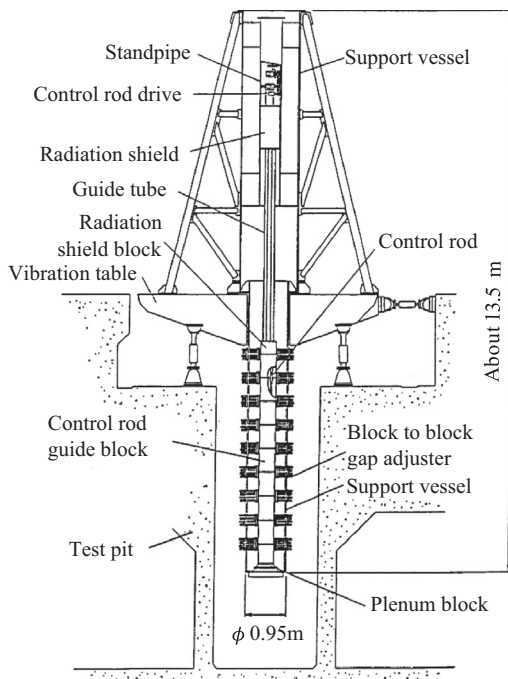


**Figure 2.64** Schematic view of scram test equipment under seismic condition [60].

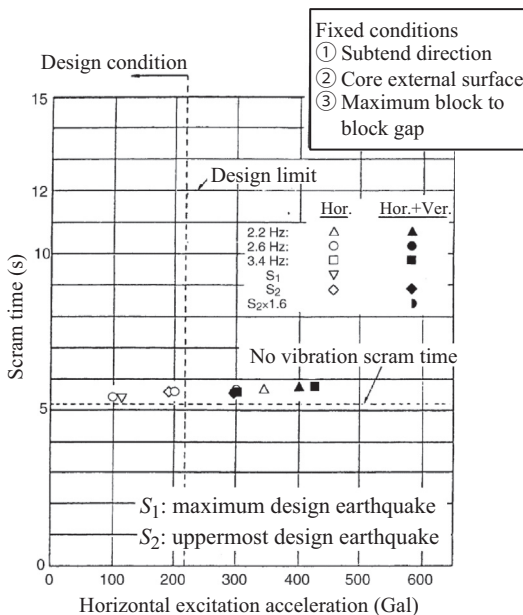


**Figure 2.65** Typical results for scram time [60].

Block misalignment and contact of a control rod with the boring wall surface of the block during earthquakes were considered as major causes of disturbance during a scram. The following parameters, therefore, were chosen in the tests: the excitation direction, which is a combination of horizontal and vertical excitations, acceleration, and frequency and block-to-block gaps.

Fig. 2.65 shows the typical scram time under seismic conditions. Generally, compared with the design specifications or the scram time during normal operation conditions, the amount of disturbance during a scram was found to be negligible for all test results. Therefore it was concluded that the seismic effect on the ability of scrambling the reactor is not significant.

### 2.9.2.5.2 Reliability test of control rods in the HENDEL loop

Tests on the control rod system were performed to verify its reliability with single-channel test rig of the fuel stack test section in the HENDEL loop under the same operation conditions as anticipated for the HTTR. The control rod drive mechanism was operated reliably far more than the total driving numbers considered for a 20-year HTTR operation. No failure of a scram was observed, that is, the phenomena which make it impossible to insert or withdraw a control rod did not occur, and the control rod drive mechanism could move the control rod to given positions without error.

Overruns during a scram were small, ranging from 63 to 71 mm. A pressure drop change in the channel due to the movement of the control rod was found to be so small that it did not affect the flow rate distribution of the coolant in the fuel

stacks. After the test, parts of the control rod system were disassembled and examined with no damage being observed [68].

#### 2.9.2.5.3 Verification tests of the control rods

In addition to the above tests, verification tests using a full-size model of the neutron absorber section were carried out. In the tests, postulated accident conditions and cyclic thermal stress were induced in accelerated conditions by heaters around the test model. The effect of inelastic deformation and creep–fatigue damage, induced by the thermal stress, was investigated. As a result, little deformation was seen. In other tests of postulated severe accident conditions, the model was subjected to its own load and to severe temperatures as high as 1100°C. After the tests, the shape of the model was investigated. Its deformation was found to be within the limits that will allow the control rod to function properly.

#### 2.9.2.6 Temperature analysis

Preliminary temperature analyses revealed that in several events of operation categories II and III, which induce reactor scrams, the maximum temperature of the control rod can exceed 900°C [61]. The severe events include “Failure in the start-up of one of two auxiliary gas circulators,” “Failure in the start-up of one of two auxiliary gas circulators and loss of off-site electric power,” “Leakage from the inner pipe of primary concentric hot gas duct,” and “Leakage from the inner pipe of auxiliary concentric hot gas duct.” At normal operation conditions, the main cooling system of the HTTR removes heat of the reactor. At a scram, the primary gas circulators stop and the auxiliary cooling system starts cooling the reactor core instead. So, trouble of the auxiliary cooling system increases temperature of the control rod.

Detailed temperature analyses were performed, which took into consideration improvement of the design of the HTTR control rod such as alteration in dimensions. Among the events of operation categories II and III, the representative event in which temperature of the control rod is predicted to become close to 900°C is “loss of off-site electric power.”

This event is due to a failure of the power transmission line for the HTTR electrical equipment. The loss of electric power supply causes all of the gas circulators and pumps to stop. Then the reactor scrams, emergency power feeder starts up, and the auxiliary cooling system starts automatically in less than 60 s after the scram because the emergency electric generator takes 60 s, at the maximum, to supply sufficient electricity. Procedure and result of temperature analysis at normal operation and “loss of off-site electric power” are shown below.

The temperature analysis consists of two steps: analysis of the core and analysis of the control rod. Calculations of the two steps were performed using the flow analysis code “TRUMP” [69], which solves problems involving flow in temperature fields, pressure fields, etc. In the first step, 1/12 sector of the HTTR core is three-dimensionally modeled. More detailed control rod model is used in the second step as shown in Fig. 2.66. It should be noted that difference of elevation of 100 mm exists between the fuel elements and control rod guide blocks.

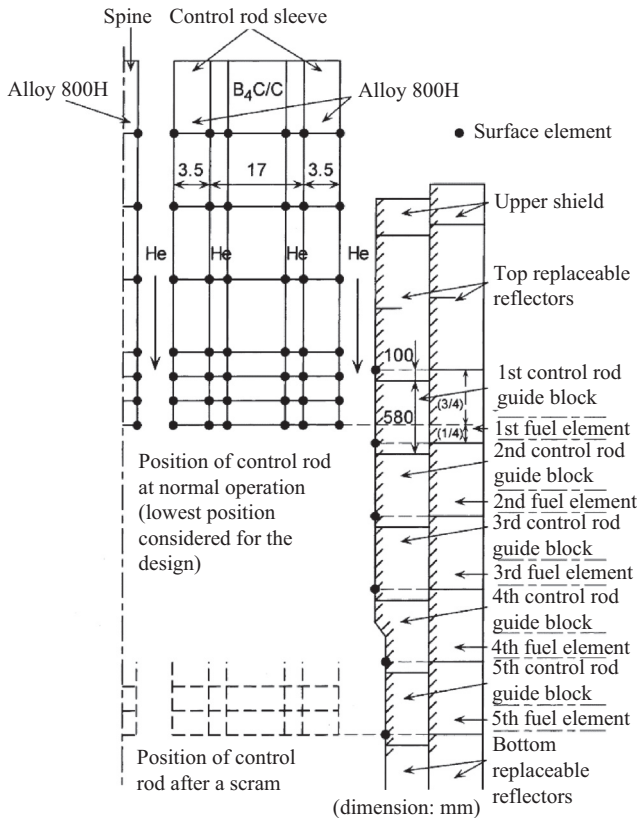


**Figure 2.66** Model of control rod for flow network analysis [60].

In the thermal design of the HTTR control rod, systematic and random factors are considered to account for various uncertainties [13]. The systematic factors, which are a direct accumulation of conservatism, include total reactor power, primary coolant flow rate, and reactor inlet coolant temperature. The random factors, statistically treated, consist of manufacturing tolerances, uncertainties on physical properties, etc. In temperature analysis for the control rods, systematic factors are multiplied to input data, while temperature increases due to the random factors are added to the calculated result.

During normal high temperature test operation, inlet and outlet coolant temperatures of the reactor are controlled within  $395^{\circ}\text{C} \pm 2^{\circ}\text{C}$  and  $950^{\circ}\text{C} \pm 17^{\circ}\text{C}$ , respectively. The position of the control rod considered in the design at the normal operation is shown in Fig. 2.66, which is the lowest position during the life of the control rod. As it can be easily seen, temperature of the control rod becomes highest at the bottom end of the center control rod, which is nearest to the center of the core. Fig. 2.67 shows results of temperature analyses of the center control rod at the

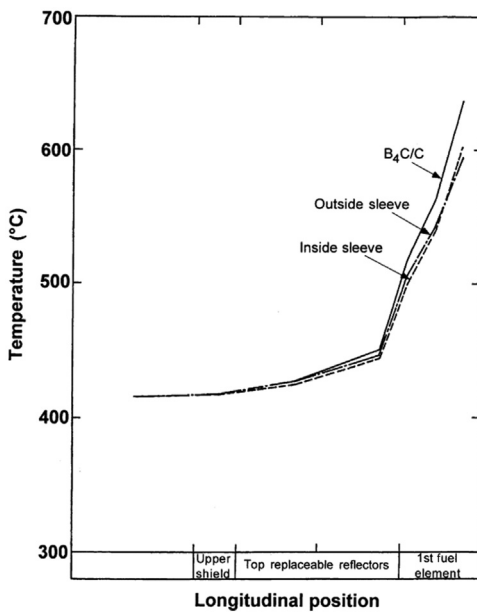


**Figure 2.67** Temperature of the center control rod at high temperature test operation [60].

normal high temperature test operation. The maximum temperature of the control rod sleeve reaches 600°C. Temperature of the neutron absorber B<sub>4</sub>C/C is higher than that of the sleeve because of  $\gamma$ -heating of the absorber.

In the event of “loss of off-site electric power,” when the scram signal triggers the rods, the outer nine pairs of the control rods in the replaceable reflector region are inserted into the core first. The two-step control rod insertion method is employed. Then the auxiliary cooling system starts up in 60 s to remove residual heat, and flow rate of the reactor inlet/outlet coolant becomes twelve percent of that at normal operation. Fig. 2.68 shows the transient temperature of the reactor inlet and outlet coolant in the event, which was derived from simulations using a model of the whole HTTR system with the THYDE-HTGR code [70]. It is 2400 s (40 min) after the scram that the inner six pairs of control rods in the fuel region are inserted, which allows a further decrease in reactor inlet coolant temperature.

Fig. 2.69 shows how temperatures of the control rod sleeve and spine in the replaceable reflector regions change as time elapses in the event of “loss of off-site electric power.” Because the control rod is inserted into the hot well at a scram, the temperature increases rapidly at first, reaches 884°C maximum for the outside sleeve, and then decreases slowly. The systematic factors described above are included in the calculations shown in Fig. 2.69. Considering the random factors, the maximum temperature of the sleeve becomes 898°C, which is less than the design limit of 900°C.

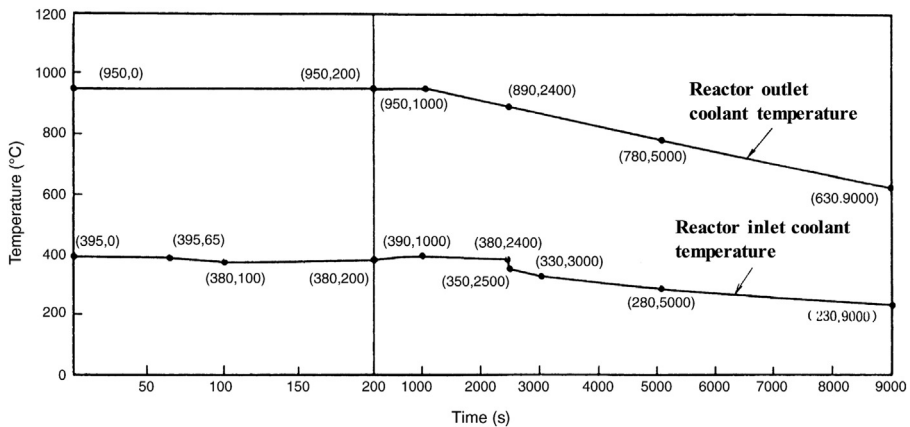


Figure 2.68 Transient behavior at “loss of off-site electric power” [60].

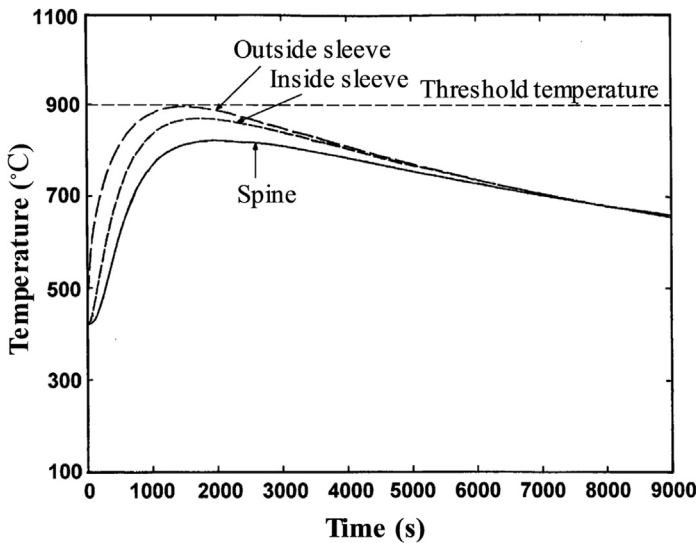


Figure 2.69 Temperature change of control rod in replaceable reflector region at “loss of off-site electric power” [60].

### 2.9.2.7 Stress analysis

Elastic stress analyses were performed utilizing the well-known FEM code ABAQUS. Primary stress is the largest at the top of the spine, nevertheless, the value is quite small (about 13 MPa). Because temperature change of the sleeve is rapid and repeated, evaluation of its secondary stress, and therefore, creep–fatigue damage, is the most important in the design of the control rod. The secondary stress range,  $Q_R$  in the event of “loss of off-site electric power” is calculated to be a maximum of 140 MPa. Fatigue

damage,  $D_f$  per event is about 0.008 and creep damage,  $D_c$  is 0.002, that is, creep–fatigue damage per scram is about 0.01. Because the number of scrams postulated in the HTTR is about 50 for 5 years, which is the target life of the HTTR control rod, cumulated creep–fatigue damage is about 0.5. Since the design limit is 1.0, the target life of the control rods of 5 years can be readily achieved [71].

### 2.9.3 Reserve shutdown system

#### 2.9.3.1 Design

**Fig. 2.70** and **Table 2.25** show an outline and specification of the reserve shutdown system. The reserve shutdown system consists of  $B_4C/C$  pellets, hoppers that

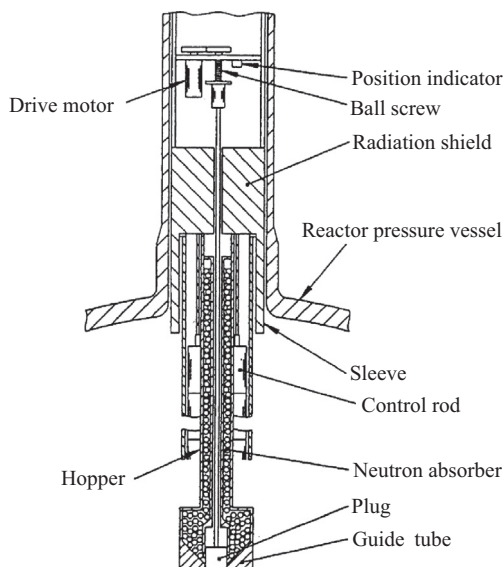


**Figure 2.70** Schematic view of reserved shutdown system [60].

**Table 2.25** Specifications of reserve shutdown system [60].

Items	Properties
Driver method	Drop $B_4C/C$ pellets by gravity
Number	16 (15 in irradiation tests using the center column)
$B_4C/C$ pellets	
Diameter (mm)	13
Length (mm)	13
Material	Sintered pellets of $B_4C/C$

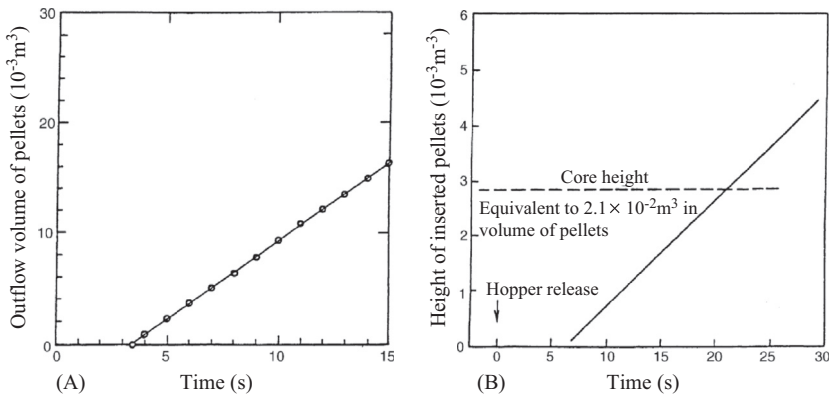


**Figure 2.71** Outflow property of pellets (A) Change of outflow of dummy pellets after pulling out the electric plug; (B) Change of stack height of inserted pellets [60].

contain the pellets, driving mechanisms, guide tubes, etc. In accidents when the control rods cannot be inserted, the electric plug is pulled out by the drive motor, and the neutron-absorbing pellets fall into the core by gravity. The reserve shutdown system shall be designed so that the reactor should be made and held subcriticality from any operation condition at temperatures from 27°C (300 K) to 950°C by dropping the pellets in.

### 2.9.3.2 Results of R&D

R&D was carried out to investigate the reliability of the reserve shutdown system, especially its mechanism. Fig. 2.71A shows the relation between the outflow volume of the dummy pellets and the time after an operator begins pulling out the electric plug. The pellets fall at a constant rate after the flow has become stable. Fig. 2.71B shows the stack height of the inserted pellets versus time, calculated from the results of Fig. 2.71A. The pellet stack reaches the height of the core in about 22 s. It was not observed that any of the pellets stuck preventing them from falling into the core. Thus it was confirmed that the reserve shutdown system is able to insert pellets reliably and stably.

## 2.10 Instrumentation and control system

### 2.10.1 Introduction

The instrumentation and control system consists of the instrumentation, control equipment, and safety protection system. There are not many differences in the instrumentation and control equipment design between the HTTR and light water reactors except some features. Various R&D for reactor instrumentation were performed taking into account the HTTR operational conditions. For the HTTR, some

detectors were developed in order to measure the neutron flux and the in-core temperature because these detectors have to operate in a high temperature environment in comparison with light water reactors. A detection system of fuel failure was developed because the FP from the failed fuel to the primary cooling system are far smaller than in light water reactors during normal operation [13].

In the HTTR, the temperature of the moderator and the coolant changes slowly with reactor power since the heat capacity of the core is very large. A plant dynamic analysis was carried out considering the operational conditions of the HTTR in order to design the control system of the HTTR [72].

## 2.10.2 *Instrumentation system*

The instrumentation system consists of reactor and process instrumentations to provide information for operation and reactor protection.

### 2.10.2.1 *Reactor instrumentation*

The reactor instrumentation monitors the major parameters in the operation condition of the HTTR, such as the neutron flux, the position of control rods, the differential pressure in the core, the coolant temperature at the hot plenum, and FPs from failed fuel.

#### 2.10.2.1.1 *Nuclear instrumentation*

Two types of neutron detectors were developed for the HTTR: One is a fission counter, which is prepared for the wide range monitoring system and is used under a high temperature environment at the top of the permanent reflector; the other is an uncompensated ionization chamber, which is prepared for the power range monitoring system and can detect a low neutron flux level outside the RPV. The wide range monitoring system and power range monitoring system are used in the power range from  $10^{-8}\%$  to 30% and 0.1% to 120%, respectively. The temperature around the wide range detector becomes about  $600^{\circ}\text{C}$  and the neutron flux level around the power range detector becomes about  $10^7 \text{ n/cm}^2$  during rated power operation of 30 MW. Fig. 2.72 shows the arrangement of neutron detector for the wide range monitoring system and power range monitoring system.

The neutron detector for the wide range monitoring system is required to be able to detect the neutron flux at  $400^{\circ}\text{C}$  and  $600^{\circ}\text{C}$  for normal operation and design basis accident, respectively. A neutron detector, which can be used at high temperature environment of  $600^{\circ}\text{C}$ , was developed. Though an accelerated irradiation test at  $600^{\circ}\text{C}$ , a long-term in-core operation test at  $600^{\circ}\text{C}$  for 1000 days, and an overheating test at  $800^{\circ}\text{C}$  for about 500 h in simulating the condition of an accident, it was found that this detector could withstand the test.

The neutron detector for the power range monitoring system is required to have high sensitivity because the neutron detector is arranged outside the RPV and the neutron flux is about  $10^7 \text{ n/cm}^2\text{s}$ , which is lower than that of light water reactors by the magnitude of two orders. The high sensitivity neutron detector, in which  ${}^3\text{He}$  gas is charged, was developed. The sensitivity of the neutron detector for the power

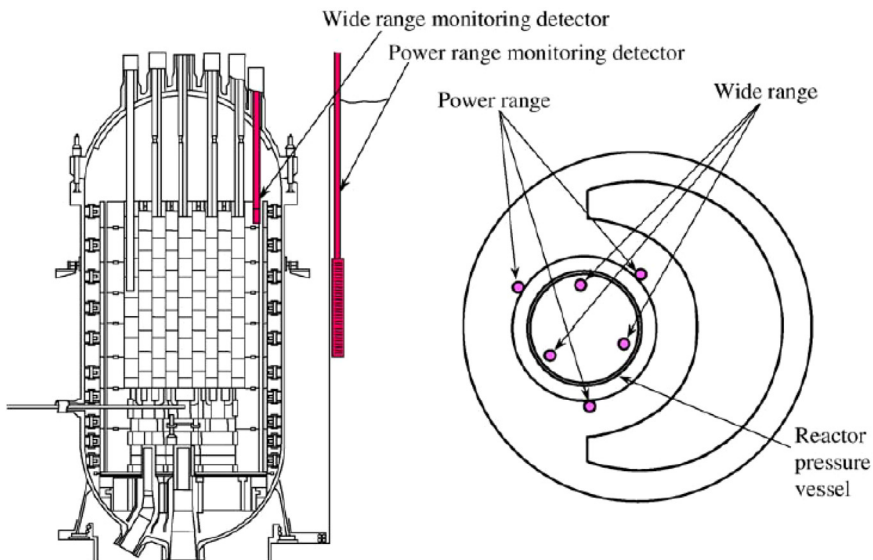


**Figure 2.72** Neutron detector arrangement [13].

range monitoring system was  $4.7 \times 10^{-12}$  A/nv and no noticeable change of the output linearity is observed after the irradiation test. The results satisfied the requirement for the nuclear instrumentation of the HTTR.

#### 2.10.2.1.2 Control rods position instrumentation

The control rods position instrumentation monitors the position of 16 pairs of control rods. The position of control rods is measured by the encoder sensor in the control rod drive mechanism and the signal from this instrumentation is used for the reactor control system and the safety protection system.

#### 2.10.2.1.3 Three core differential pressure instrumentation

The core differential pressure instrumentation detects a decrease in primary coolant flow in the reactor core. The core differential pressure instrumentation measures the differential pressure between the inlet and outlet of the core, and the signal from this instrumentation is used for the safety protection system and is transferred to the central control room.

#### 2.10.2.1.4 Fuel failure detection system

It is very important to prevent FPs from being released abnormally into the primary cooling system during the normal operation. The fuel failure detection system detects the failure of CFPs by detecting short-life FPs, such as  $^{88}\text{Kr}$  and  $^{138}\text{Xe}$ . The conceptual block diagram is shown in Fig. 2.73. The fuel failure detection system is composed of two precipitators, a preamp and a compressor. The schematic drawing of precipitator is shown in Fig. 2.74 [73]. The helium gas of primary cooling system from the seven regions in the hot plenum is transferred to the precipitator chambers.

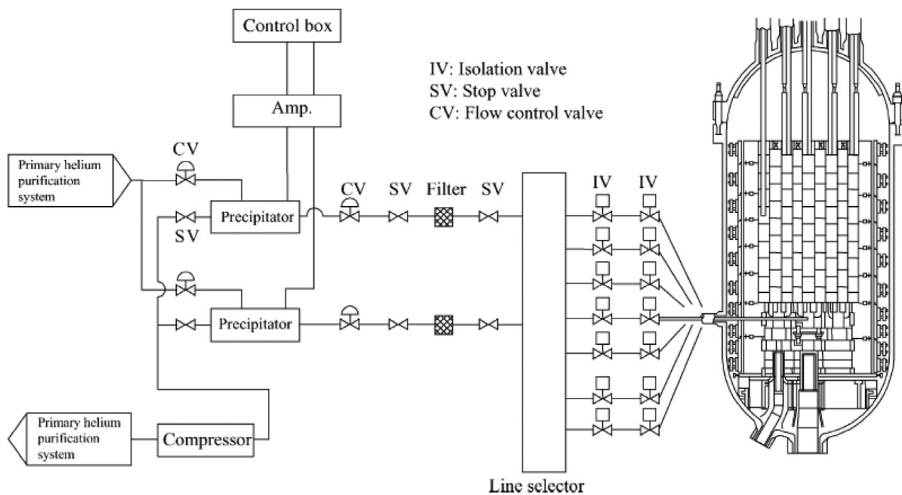


**Figure 2.73** Schematic view of fuel failure detection system [13].

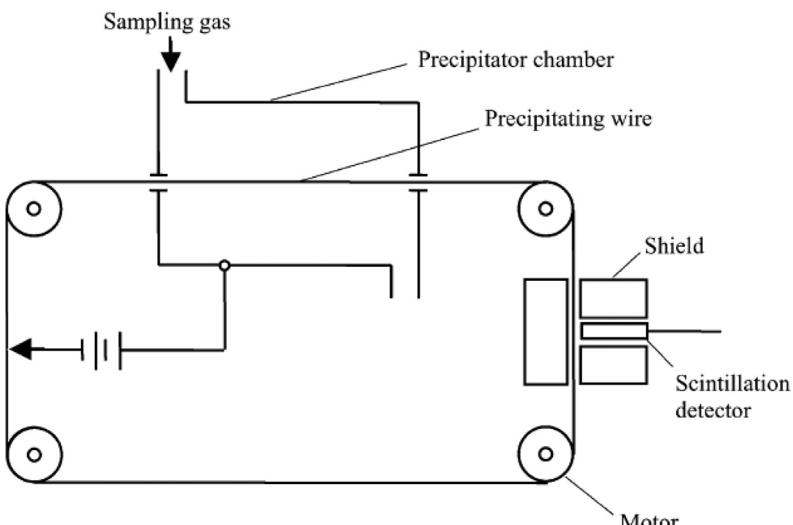


**Figure 2.74** Schematic drawing of precipitator [73].

And FPs in the helium gas are collected by precipitating wire in the precipitator chambers. Collected FPs are transferred to the front of the scintillation detector by wire. Then a scintillation detector detects  $\beta$ -rays radiated from short-life gaseous FPs.

In the HTTR, the initial failure shall be less than 0.2% in terms of the sum of heavy metal contamination and SiC defects. The value of 0.2% was determined from the viewpoint of limit of off-site exposure during normal operation. The fuel failure detection system is able to detect 0.002% fuel failure.

The detection of fuel failure is difficult in comparison with that for conventional metal cladding fuel. A CFP consists of a microsphere of low enrichment UO<sub>2</sub> with the TRISO (TRi-ISOtropic) coating. The CFPs are incorporated into fuel compacts with a graphite matrix. If the CFP is failed, the FPs from the failed fuel to the primary cooling system are very small. Furthermore, the radiation background changes depending on the condition of the reactor (neutron flux and fuel temperature and others). To solve these problems, a high-sensitive fuel failure detection system has been developed based on the following considerations:

1. To deduce the effect of long-life FPs accumulated in the primary cooling system and to detect the FPs are detected selectively.
2. The state equation, which identifies the concentration of short-life FPs in the primary cooling system, was established. This state equation was introduced into fuel failure detection system to distinguish the small change in short-life FPs concentration caused by the change in the reactor operation parameter, such as fuel temperature and local power density.

The experiment of fuel failure detection system was performed since the end of 1981 at Japan Material Test Reactor (JMTR). And these results satisfy the requirement to identify 10<sup>-4</sup>% of the fuel damage.

#### 2.10.2.1.5 In-core temperature monitoring system

Four thermocouples are arranged at each hot plenum block in order to monitor the primary coolant temperature. The maximum coolant temperature around the thermocouples reaches about 1100°C. N-type thermocouples (Nicrosil–Nisil) are used because the deviation of thermal electromotive force is small compared with other types of thermocouples under a high temperature environment.

The thermocouples for the in-core temperature monitoring system should have a long lifetime with high reliability. Stability of thermos-electromotive force of many thermocouples were checked at long-term performance test, which was performed under the condition that the temperature and its running time were 1200°C and 20,000 h, respectively. As a result of the test, N-type thermocouple was selected.

### 2.10.3 Process instrumentation

The process instrumentations of temperature, pressure, flow rate, radioactivity, etc. are required to monitor the plant parameter during the reactor operation. There are about 4000 sensors in the HTTR, and the signals from the sensors are centralized by the plant computer.

The process instrumentation is used to measure process parameters in the primary cooling system, secondary helium cooling system, pressurized water-cooling system, etc. The signals of process instrumentation are transferred to the safety protection system, reactor control system, and others. The process instrumentations used for the reactor protection system and the engineering safety features actuating system consist of three identical channels.

## **2.10.4 Control system**

The control system of the HTTR consists of an operational mode selector, a reactor power control system, and a plant control system. Microcomputers are used for the plant control system and the reactor power control system. An operational mode selector supervises them.

### **2.10.4.1 Operational mode selector**

The HTTR is designed to achieve several operational modes to perform rated operation, high temperature test operation, safety demonstration test, and others. The operational mode selector is used to specify the control system and the reactor scram point of instrumentation.

The reactor has several operational modes. The reactor outlet coolant temperature is set at 850°C or 950°C at the rated power. “Rated operation” stands for the operation at 850°C and “high temperature test operation” stands for the operation at 950°C.

The reactor has two loop operational modes, one is called the “parallel-loaded operation” and the other one is the “single-loaded operation.” The IHX and PPWC are operated simultaneously during the former mode. On the other hand, only the PPWC is operated to remove the heat of 30 MW during the single-loaded operation. The maximum heat capacity of the IHX and PPWC is 10 and 20 MW, respectively, during parallel-loaded operation. The HTTR has several safety demonstration test operational modes, one is the “primary coolant flow rate decreasing test mode” and the other one is the “control rod withdrawing test.”

The operational mode selector has select switches for selecting the operational modes. The demand values of the control system and the set point of the safety protection system are changed automatically according to the operational mode selector.

### **2.10.4.2 Reactor power control device**

The reactor power control device consists of a reactor power control system and a reactor outlet coolant temperature control system. The reactor power and reactor outlet coolant temperature control systems are cascade connected: the latter is an upper control system to give demand to the power control system.

#### **2.10.4.2.1 Reactor power control system**

The signals from each channel of power range monitoring system are transferred to three controllers using microprocessors. In the case that there is a deviation between the process and set values, a pair of control rods is inserted or withdrawn at control rods speed from 1 to 10 mm/s according to the deviation. The relative position of 13 pairs of control rods, except for three pairs of control rods used only for the scram, are controlled within 20 mm by the control rods pattern interlock to prevent any abnormal power distribution.

#### **2.10.4.2.2 Reactor outlet coolant temperature control system**

The reactor outlet coolant temperature control system is used at about 100% of the rated power. In the case that there is a deviation, this control system gives a demand

to the power control system and changes the reactor outlet coolant temperature by moving the position of the control rods.

### 2.10.4.3 Plant control device

The plant control device controls the plant parameters, such as the reactor inlet coolant temperature, the primary coolant pressure, and the differential pressure between the primary cooling system and the pressurized water-cooling system or secondary helium cooling system. The schematic diagram of the plant control device is shown in Fig. 2.75.

#### 2.10.4.3.1 Reactor inlet coolant temperature control system

The reactor inlet coolant temperature control system is used in the power range from 30% to 100% and is cascade connected with a pressurized water temperature control system. In the case that there is a deviation, the reactor inlet coolant temperature is controlled by adjusting the pressurized water coolant inlet temperature of the pressurized water.

#### 2.10.4.3.2 Intermediate heat exchanger primary coolant flow rate control system

The IHX primary coolant flow rate control system controls the primary coolant flow rate in the IHX at constant value by adjusting the helium gas circulator.

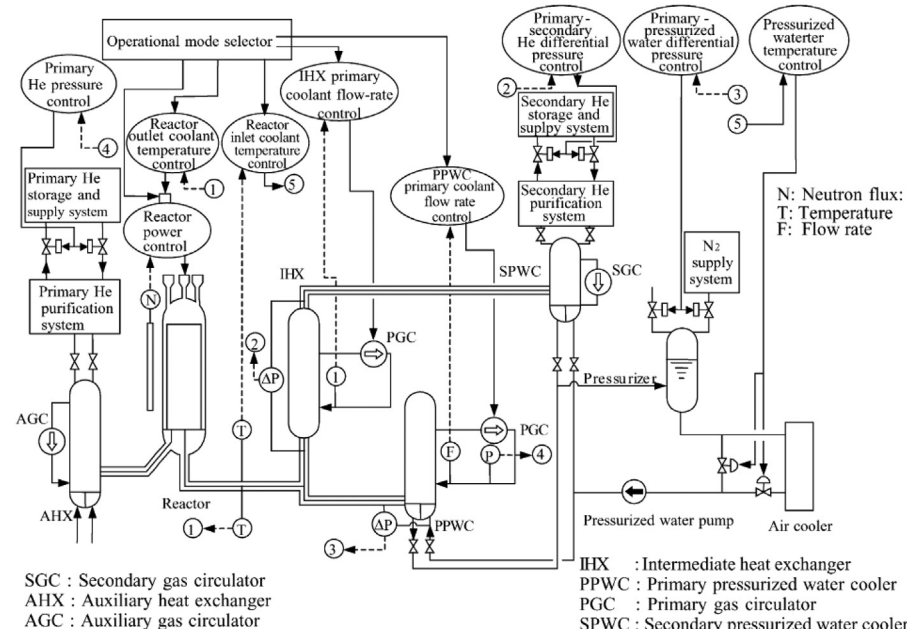


Figure 2.75 Schematic diagram of control system of HTTR [13].

#### 2.10.4.3.3 Primary-pressurized water cooler primary coolant flow rate control system

The PPWC primary coolant flow rate control system controls the primary coolant flow rate in the PPWC at the constant value by adjusting the revolution of the three helium gas circulators.

#### 2.10.4.3.4 Primary helium pressure control system

The primary helium pressure control system controls the primary helium pressure by activating the valves of the helium storage and supply system for primary cooling system. This system is used at about 100% of the rated power.

#### 2.10.4.3.5 Primary—secondary helium differential pressure control system

The primary—secondary helium differential pressure control system controls the differential pressure between primary and secondary helium by activating the valves of the helium storage and supply system for secondary helium cooling system. The secondary helium pressure is controlled higher than that of the primary by this system so as to prevent any release of FPs into the secondary helium cooling system.

#### 2.10.4.3.6 Primary-pressurized water differential pressure control system

The primary-pressurized water differential pressure control system controls the differential pressure between primary helium and pressurized water by activating the valves of the pressurizer in the pressurized water-cooling system. The pressurized water pressure is controlled lower than that of the primary helium by this system so as to prevent any water from entering into the primary cooling system.

#### 2.10.4.3.7 Pressurized water temperature control system

The pressurized water temperature control system controls the inlet pressurized water temperature of PWC by adjusting the flow rate of the pressurized water in the air cooler. The flow rate into the air cooler is adjusted by a bypass flow control valve and an outlet system is given by the reactor inlet coolant temperature control system, which is the upper control system in the cascade.

### **2.10.5 Safety protection system**

The safety protection system consists of the reactor protection system and engineered safety features actuating system. The reactor protection system ensures the integrity of the core and reactor coolant pressure boundary under abnormal operational conditions. The engineered safety features actuating system prevents FPs from being released into the environment due to an accident, such as a rupture of the primary concentric hot gas duct.

#### **2.10.5.1 Reactor protection system**

The reactor protection system inserts the control rods into the core to ensure the integrity of fuel and protect the reactor coolant pressure boundary under abnormal operating conditions. The logic circuits of this system have two trains, which

receive the signals from the reactor and process instrumentation, and send the signals in case of reactor scram.

The logic trains of reactor protection system are set with two parallel systems and each logic train is connected to the circuit breaker with two series. Each logic train sends a signal in case of a reactor scram independently.

In case of a reactor scram except for a depressurization accident, the control rods are inserted into the replaceable reflector region at first, and then the remaining control rods are inserted into core when the reactor outlet coolant temperature decreased to about 750°C or 40 min has elapsed after reactor scram. In the case of depressurization accident, all control rods are inserted into the core simultaneously.

### ***2.10.5.2 Engineered safety features actuating system***

The engineered safety features actuating system sends the signals actuating the engineered safety features, such as the isolation valves of containment vessel, the auxiliary cooling system, and the emergency air purification system. The engineered safety features protect the reactor, the reactor coolant pressure boundary, and the containment vessel boundary and prevent large amounts of FPs from being released outside the reactor facility. This system consists of logic circuits having two trains, which receive the signals from the reactor and process instrumentation, and actuates the engineered safety features.

#### ***2.10.5.2.1 Signal isolating containment vessel***

The signal isolating the containment vessel activates to close the isolation valve of the containment vessel in order to prevent FPs releases in a depressurization accident. These signals also activate to stop the air supply and exhaust in the ventilator and air conditioner in the reactor building system and to start up the emergency air purification system.

#### ***2.10.5.2.2 Signal starting up auxiliary cooling system***

The signals starting up the auxiliary cooling system, which are the signals for a reactor scram, activate to start up the auxiliary cooling system so as to remove residual heat in case of a reactor scram except for the case of the depressurization accident or an auxiliary heat exchanger heat transfer tube rupture accident.

#### ***2.10.5.2.3 Signal isolating auxiliary cooling water line***

The signals isolating the auxiliary cooling water line activate to stop the auxiliary cooling system and to close the valves of the containment vessel connected to the auxiliary heat exchanger and the valve of the primary coolant pressure boundary connected to the primary helium purification system.

## ***2.10.6 Performance test results***

In the “rise-to-power test,” many performance tests were carried out in order to confirm the characteristics of the instrumentation and control system of the reactor.

### 2.10.6.1 Characteristics of the neutron flux monitoring system

The wide range monitoring system and the power range monitoring system are used in the power range from  $10^{-8}\%$  to 30% and 0.1% to 120% of the rated power, respectively. The measurement range of the power range monitoring system should overlap the measurement range of the wide range monitoring system in order to continuously monitor the neutron flux. Therefore it is very important to confirm that the measurement range of the wide range monitoring system and the power range monitoring system overlap.

[Fig. 2.76](#) shows the calibrated result of the wide range monitoring system and the power range monitoring system from 0.1% to 30% of the rated power. It can be found that response values of the power range monitoring system are nearly equal to those of the wide range monitoring system within the reactor power range from 1% to 10%. This result satisfies the design requirement concerning the overlap between the wide range monitoring system and the power range monitoring system.

### 2.10.6.2 Primary-pressurized water cooler primary coolant flow rate control system

The PPWC primary coolant flow rate control system controls the primary coolant flow rate in the PPWC at a constant value by adjusting the revolution of three helium gas circulators. This control system has been designed as P-I control system with delayed time, and is required to be stably controlled for a  $\pm 10\%$  stepwise change.

In order to confirm the stability of this control system,  $-10\%$  stepwise change from 15.1 to 13.6 t/h was set at the set value of the primary coolant flow rate. [Fig. 2.77](#) shows the test result. The primary coolant flow rate gradually decreased, and reached

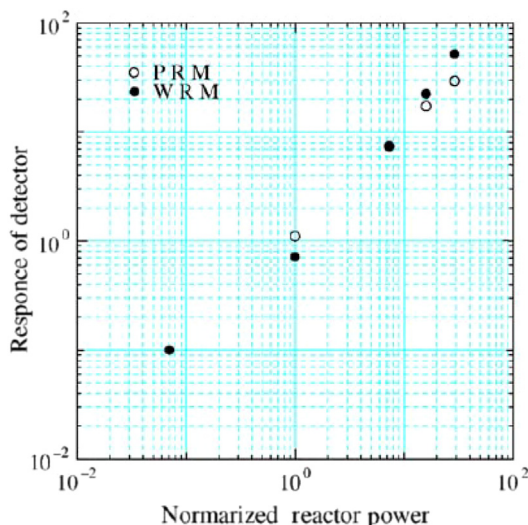


**Figure 2.76** Calibrated result of wide range monitoring and power range monitoring systems [\[73\]](#).

13.6 t/h without undershoot. The test result shows that the PPWC primary coolant flow rate control system has stable response characteristics against disturbances.

### 2.10.6.3 Reactor outlet coolant temperature control system

The reactor outlet coolant temperature control system gives a signal to the power control system and controls the reactor outlet coolant temperature by controlling the position of the control rods.

The response test for this control system has been carried out to confirm the behavior against ramp-wise change under actual operational condition. [Fig. 2.78](#) shows the

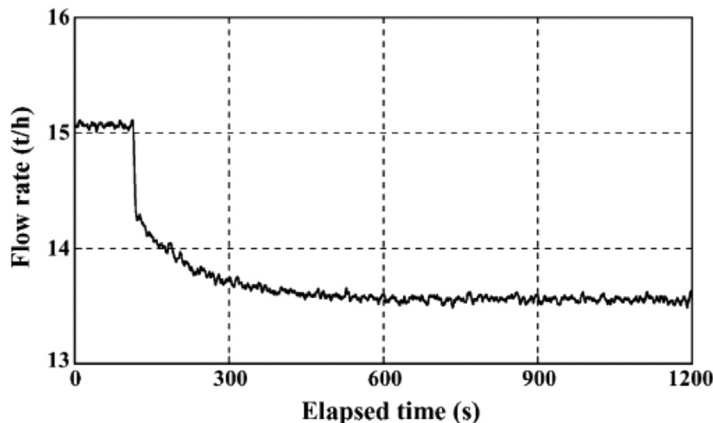


**Figure 2.77** Test result of primary-pressurized water cooler primary coolant flow rate control system [73].

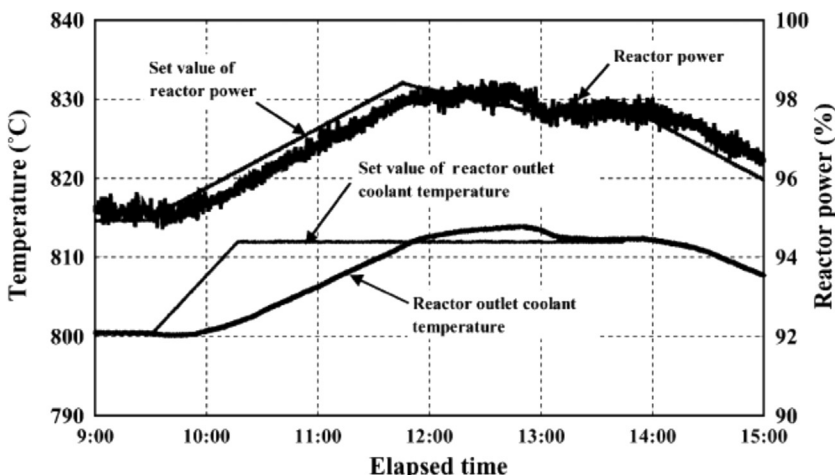


**Figure 2.78** Test result of the reactor outlet coolant temperature control system under the ramp-wise change from 800°C to 812°C [73].

transient behavior for a  $+15^{\circ}\text{C}/\text{h}$  ramp-wise change from  $800^{\circ}\text{C}$  to  $812^{\circ}\text{C}$ . The reactor outlet coolant temperature control system gives a demand for a reactor power increase to the reactor power control system. The set value of reactor power is increased up gradually from 95% to 98% at the rated power according to the deviation between the reactor outlet temperature and the set value of reactor outlet temperature. In proportion to the rise in the set value the reactor power rises gradually by withdrawing the control rods. Then, the reactor outlet coolant temperature rises gradually with the reactor power rise. The reactor outlet coolant temperature has been reached at  $812^{\circ}\text{C}$  stably. The test result shows that the reactor outlet coolant temperature control system has the capability of controlling the reactor outlet temperature stably.

## 2.11 Containment structures

### 2.11.1 Introduction

The containment structures of the HTTR consist of the reactor containment vessel, the service area, and the emergency air purification system, which minimize the release of FPs during accidents with FP release from the reactor facilities. The reactor containment vessel is designed to withstand the temperature and the pressure transients and to be leak-tight within the specified limits in the case of a rupture of the primary concentric hot gas duct (depressurization accident). The pressure inside the service area will be maintained at a negative pressure by the emergency air purification system. Radioactive materials are released from the stack to the environment via the emergency air purification system during accident conditions. The emergency air purification system will remove airborne radioactivities and will maintain the design pressure in the service area [74].

### 2.11.2 Reactor containment vessel

#### 2.11.2.1 Design and construction

The reactor containment vessel is comparatively small to minimize the amount of air, which may react with graphite components in the event of a rupture of the primary pressure boundary. The reactor containment vessel is made of carbon steel 30.3 m in height, with 18.5 m inner diameter, and  $2800 \text{ m}^3$  free volume. Its configuration is shown in Fig. 2.79. The personal air lock, which has an inner door and outer door, is provided for entrance into the reactor containment vessel. The maintenance hatch is equipped for carrying tools and machineries for annual inspections. Elastic plugging material is installed between the reactor containment vessel and base mat of the reactor building to absorb any thermal expansion in case of accidents [75]. Fig. 2.80 shows the sketch of the reactor containment vessel with its penetrations.

The reactor containment vessel is made to be pressure-proof during depressurization accidents and the pressure-proof test is performed 1.125 times its maximum pressure of 0.4 MPa. The reactor containment vessel is also made to be leak-tight

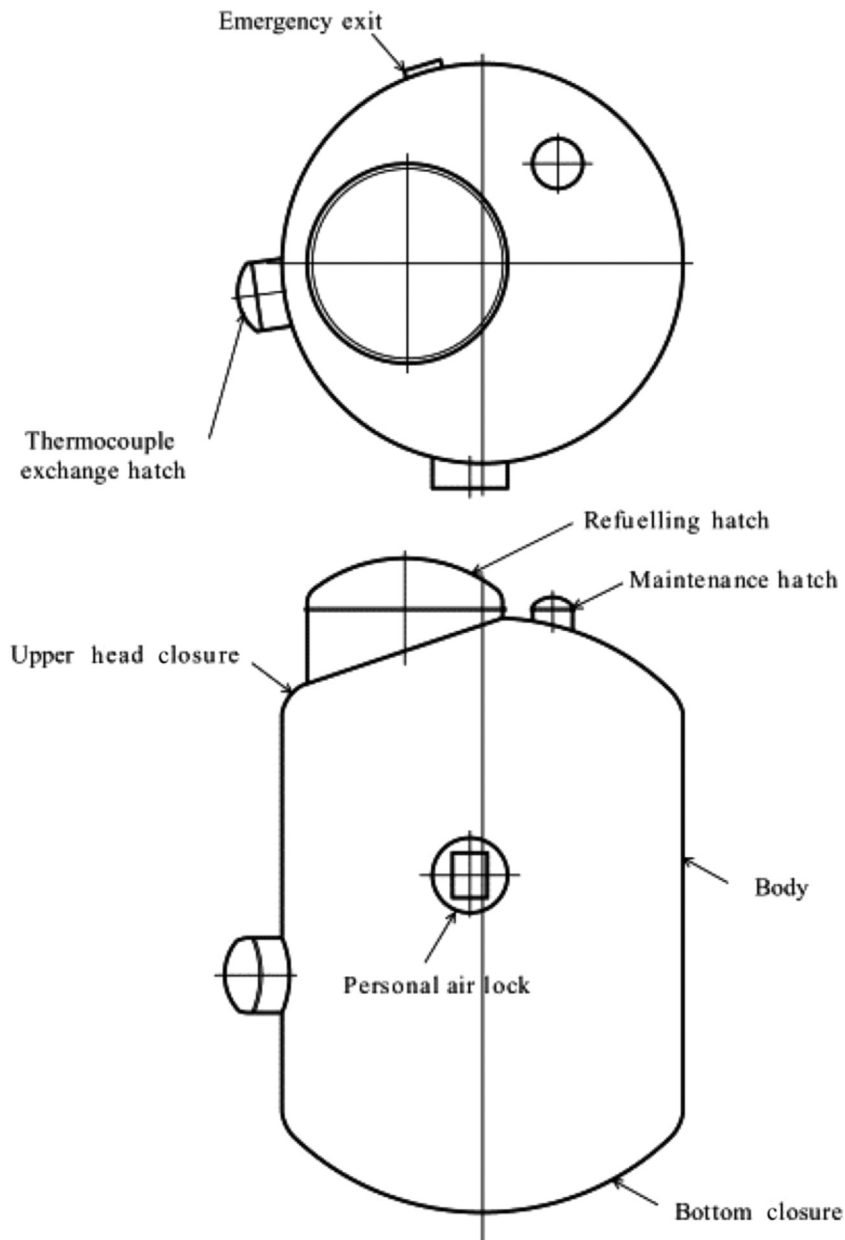
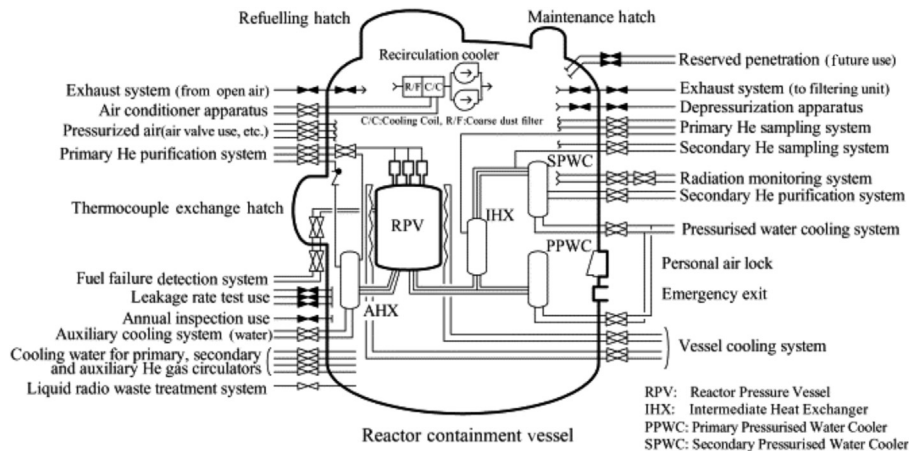


Figure 2.79 Schematic view of reactor containment vessel and its attached equipment [75].



**Figure 2.80** Schematic view of reactor containment vessel with its penetrations [75].

and its leakage rate is designed to be less than 0.1% of the total free volume of  $2800 \text{ m}^3$  per day at room temperature, air atmosphere, and 0.9 times its maximum pressure (0.36 MPa). During a depressurization accident, the peak pressure is 0.36 MPa, which appears 9 s after the initiation of an accident, and the temperature rises to  $85^\circ\text{C}$  after 1 s [13]. In the safety case, a leakage rate of 0.25 %/day was used for the calculation to simulate the accident condition as the increase of temperature and pressure and the difference between helium and air. The specification of the reactor containment vessel is listed in Table 2.26.

The construction of the reactor containment vessel started in 1991 at the factory. After various kinds of inspections, including material inspections, such as fracture toughness tests, had performed the reactor containment vessel was transported by parts using ships to the HTTR site. At the HTTR site, performance tests were conducted in order to confirm its initial pressure-proof and leakage characteristics. Fig. 2.81 shows a photo of the reactor containment vessel taken during its initial pressure-proof test in November 1992. After the whole body was constructed, penetrations were equipped with their isolation valves and the reactor containment vessel was completed in 1996 [75].

### 2.11.2.2 Leakage-rate test

In Japanese LWRs, the leakage-rate test of the reactor containment vessel was performed with an open reactor coolant pressure boundary to simulate an accident. In HTGRs, the leakage-rate test is planned with a closed reactor coolant pressure boundary to avoid the release of FPs into the environmental of the reactor containment vessel. It is necessary to establish other test method in order to estimate the leakage rate of the reactor containment vessel with closed reactor coolant pressure boundary.

In the HTTR, the leakage-rate test was performed with a closed reactor coolant pressure boundary and additional corresponding tests were conducted. First is the

**Table 2.26** Specification of reactor containment vessel [74].

Containment type	Steel containment
Maximum pressure in service (MPa)	0.4
Maximum temperature in service (°C)	150
Major size	
Inner diameter (m)	18.5
Overall height (m)	30.3
Body thickness (mm)	30
Upper head closure thickness (mm)	38
Refueling hatch diameter (m)	8.5
Maintenance hatch diameter (m)	2.4
Personal air lock diameter (m)	2.5
Free volume (m <sup>3</sup> )	2800
Material	Carbon steel
Leakage rate	Less than 0.1 %/day at the room temperature and 0.9 times the maximum pressure of 0.4 MPa

**Figure 2.81** Photo of reactor containment vessel (30.3 m in height, 18.5 m in inner diameter, and 2800 m<sup>3</sup> of free volume) taken during initial pressure-proof test in November 1992 [74].

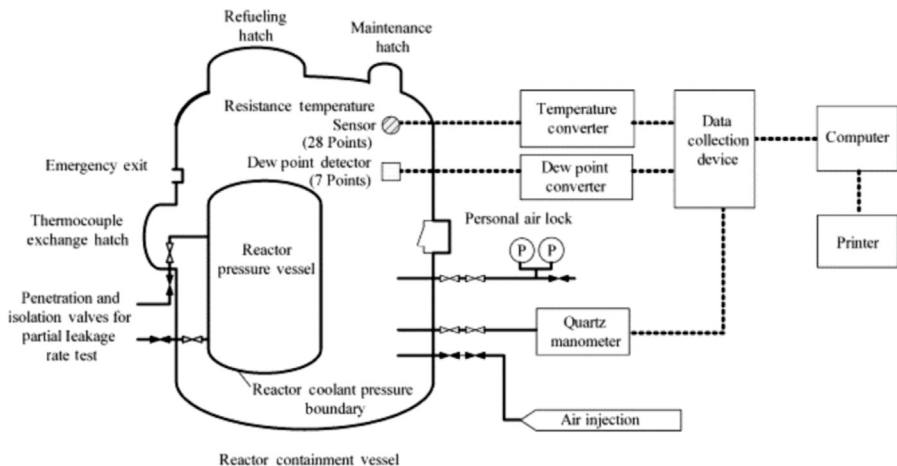


**Figure 2.82** System configuration of whole leakage-rate test of reactor containment vessel [75].

partial leakage-rate test. The partial leakage-rate tests were inspected at penetrations and isolation valves connected to the primary coolant pressure boundary. In an accident, such as a rupture of the hot gas duct, the penetrations and isolation valves connected to the primary coolant pressure boundary, which are also the reactor containment vessel boundary, will be pressurized. Adding these values of partial leakage rate of penetrations and isolation valves to the whole leakage rate can simulate an accident, such as a rupture of the hot gas duct. Second is the lower set pressure of the reactor coolant pressure boundary. The reactor coolant pressure boundary is kept at a pressure below the test pressure during the whole leakage-rate test of the reactor containment vessel in order to avoid a decrease of the measured value in the whole leakage test. The test chart of the whole leakage-rate test of the reactor containment vessel is shown in Fig. 2.82.

The allowance value of leakage rate  $L_{do}$  is regulated as

$$L_{do} (\%/\text{day}) = L_d (1 - A_1) = 0.1 \times (1 - 0.1) = 0.09, \quad (2.1)$$

where  $L_d$  is the leakage rate at the room temperature and 0.9 times its maximum pressure of 0.4 MPa, as shown in Table 2.26, and  $A_1$  is the factor of deterioration. The deterioration factor is regulated by the Japanese test standard (JEAC4203), and when the test is planned annually, the deterioration factor is 0.1 and for an inspection every 2 years, it is 0.2.

The term “leakage rate” is used with the follow meanings:

1. Partial leakage rate  $L_P$  is the leakage of penetrations and isolation valves connected to the reactor coolant pressure boundary.
2. Conversion leakage rate  $L_{CV}$  is the converted value of the partial leakage rate  $L_P$  to that of the whole leakage rate.

3.  $H$  hours leakage rate  $L_H$  is the leakage rate from beginning to  $H$  hours elapsed at the whole leakage-rate test.
4. Average leakage rate  $L_{AV}$  is the leakage rate of the measured value of the whole leakage-rate test with 95% confidence limit as for statistical processing and it is shown such as  $a \pm b$ .
5. Leakage rate  $L$  is the total value of the leakage rate and it is the sum of  $L_{CV}$  and upper value of  $L_{AV}$  ( $a + b$ ).

### 2.11.2.2.1 Partial leakage-rate test

The partial leakage-rate tests are performed for the penetrations and isolation valves of the primary helium purification system, primary helium sampling system, and fuel failure detection system, which are connected to the reactor coolant pressure boundary. The partial leakage-rate test was executed in accordance with the pressure drop method regulated by the Japanese test standard (JEAC4203). The specification of detectors is shown in [Table 2.27](#).

The partial leakage-rate test is conducted at the pressure above 0.36 MPa, which is 0.9 times the maximum pressure of 0.4 MPa. The partial leakage rate  $L_P$  and conversion leakage rate  $L_{CV}$  are calculated by the following equations:

$$L_P (\text{%/day}) = \frac{24}{H} \frac{P_1 - P_2}{P_1} \times 100 = \frac{24}{H} \frac{\Delta P}{P_1} \times 100, \quad (2.2)$$

$$L_{CV} (\text{%/day}) = L_P \times \frac{V_i}{V_0}, \quad (2.3)$$

where  $P$  is the gauge pressure Pa at arbitrary time,  $V_0$  is the free volume of the reactor containment vessel ( $2800 \text{ m}^3$ ),  $V_i$  is the free volume of the partial leakage-rate test area  $\text{m}^3$ ,  $H$  is the elapsed time h,  $\Delta P$  is the pressure drop ( $=P_1 - P_2$ ) Pa, subscript 1 is the starting value, and subscript 2 is the value after  $H$  hours elapsed.

The total value of conversion leakage rate  $\Sigma L_{CV}$  was  $1.43 \times 10^{-4} \text{ %/day}$  measured in 1996, and the other years' results had almost same value [\[76\]](#).

### 2.11.2.2.2 Whole leakage-rate test

The whole leakage-rate test was performed for the reactor containment body and its attached equipment, such as personal air lock, refueling hatch, and maintenance hatch. The whole leakage-rate test was executed in accordance with the absolute pressure method regulated by the Japanese test standard (JEAC4203). The specification of detectors is shown in [Table 2.28](#).

**Table 2.27** Detectors of partial leakage-rate test for penetrations and isolation valves [\[1\]](#).

Item	Detector	range	Accuracy	Number
Pressure	Pressure gauge	0–0.59 MPa	$\pm 0.5\%$ of full scale	2

**Table 2.28** Detectors of whole leakage-rate test for body and its attached equipment [74].

Item	Detector	Range	Accuracy	Number
Absolute pressure	Quartz manometer	0–0.67 MPa	± 0.01% of full scale	1
Temperature	Resistance temperature sensor	0°C–50°C	± 1°C	28
Humidity	Dew point detector	0.3–12 kPa	± 0.02% of full scale	7

In the absolute test method, pressure, temperature, and humidity are obtained. The average temperature  $T$  and average dew point  $P_C$  are:

$$T(\text{°C}) = \sum_i T_i D_i, \quad (2.4)$$

$$P_C(\text{°C}) = \sum_i P_{ci} E_i, \quad (2.5)$$

where  $T_i$  is individual temperature measured by resistance temperature sensors,  $P_{ci}$  is individual dew point, and  $D_i$  and  $E_i$  are the factors which depend on room volume.

The amount of leakage  $Q$ , which is the value of weight percent (wt.%) between air in the reactor containment vessel and leaked air, and  $L_H$ , which is the  $H$  hours leakage rate %/day, are calculated by:

$$Q(\%) = \frac{G_1 - G_2}{G_1} = \left( 1 - \frac{Pm_2 T_1}{Pm_1 T_2} \right) \times 100, \quad (2.6)$$

$$L_H(\%/\text{day}) = \frac{24Q}{H} \times 100, \quad (2.7)$$

where  $G$  is the air weight kg in the reactor containment vessel,  $Pm$  is the absolute pressure of air Pa in the reactor containment vessel, which is the difference value of the measured pressure value by the quartz manometer and the measured humidity value by the dew point detector, and  $T$  is the temperature K in the reactor containment vessel.

The regression line is analyzed for the Eq. (2.6) and its variance analysis is performed in order to clarify the significant difference between the amount of leakage and the elapsed time. The average leakage rate  $L_{AV}$  %/day can be calculated with its 95% confidence limit to  $L_H$ , and  $L_{AV}$  is shown as:

$$L_{AV}(\%/\text{day}) = 24(b \pm 2.07\sigma), \quad (2.8)$$

where  $b$  is the amount of leakage in 1 h, which is calculated by statistical processing and  $\sigma$  is also the statistic value.

[Fig. 2.83](#) shows the transient of pressure and amount of leakage  $Q$  measured during the whole leakage-rate test performed in 1999. The pressure inside the reactor containment vessel was raised by air compressors until the pressure reaches its test pressure of 0.36 MPa. After stability condition was confirmed, the measurement of leakage rate was begun. At the measurement duration, the amount of leakage  $Q$  was increased by the leak from the reactor containment vessel, and this amount was converted to the leakage rate with statistical processing. The leakage rates were obtained from 0.017 to 0.034 %/day at eight times testing confirmed from 1996 to 2012 as shown in [Table 2.29](#). These values are well below the set limitation of 0.09 %/day, which includes the deterioration factor.

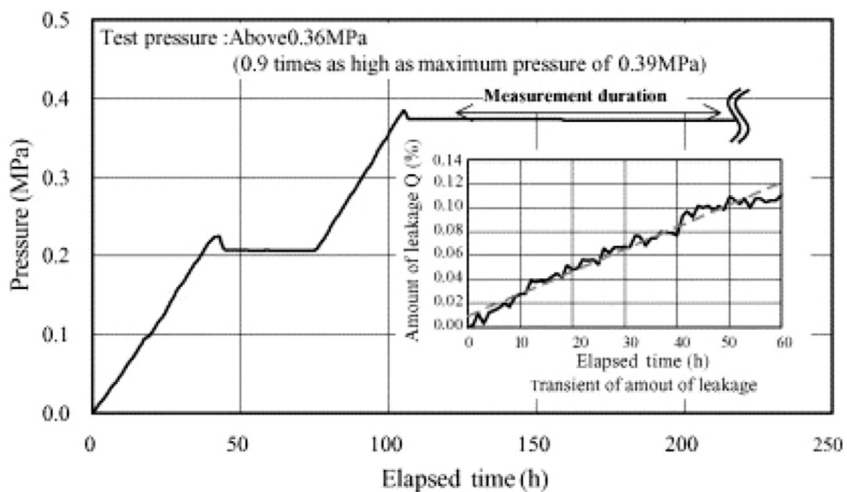


**Figure 2.83** Transient of pressure and amount of leakage  $Q$  during second whole leakage-rate test [\[74\]](#).

**Table 2.29** Leakage-rate test results of reactor containment vessel [\[74\]](#).

	1st	2nd	3rd	4th	5th
Time of whole leakage-rate test	Oct. 1996	Sep. 1999	Dec. 2000	Sep. 2001	Dec. 2002
Leakage rate $L$ (%/day)	0.018	0.017	0.034	0.018	0
	6th	7th	8th	9th	10th
Time of whole leakage-rate test	Dec. 2003	Dec. 2004	Dec. 2006	Dec. 2000	Mar. 2012
Leakage rate $L$ (%/day)	0	0.015	0	0.029	0.017

## 2.11.3 Service area

### 2.11.3.1 Design

The service area, as shown in Fig. 2.84, is the space surrounding the reactor containment vessel where the fuel handling and storage systems, the primary helium purification system, etc. are located. The service area is kept at a negative pressure during accidents by an emergency air purification system, which operates under the isolated reactor containment vessel condition. During normal operation, the service area is also kept at a negative pressure by the ventilation and air conditioning system. In operation floor at the ground level TP 36.5 m, the fuel handling and storage systems are equipped.

### 2.11.3.2 Commissioning tests

As a commissioning test, an airtight test of the service area is conducted. During an accident, like a failure of the primary helium purification system located inside the

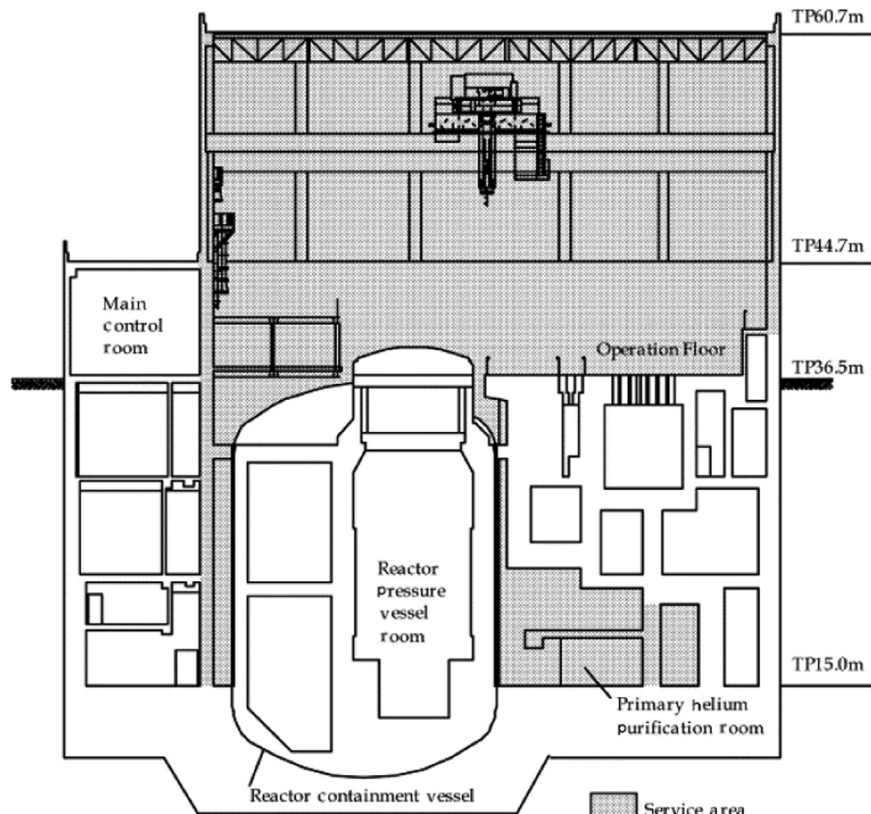


**Figure 2.84** Schematic view of service area [74].

**Table 2.30** Relationship between air pressure in service area and the elapsed time after start-up of emergency air purification regulation damper opening at 55% [74].

	Elapsed time (min)					
	0	1	2	3	4	5
Air pressure in service area at operating emergency air purification system A (Pa)	17	-75	-86	-82	-85	-87
Air pressure in service area at operating emergency air purification system B (Pa)	18	-71	-79	-81	-81	-81

service area, the service area is isolated automatically by an isolation signal. The service area maintains its air pressure of less than  $-59$  Pa by the emergency air purification system. In the airtight test of the service area, the opening of air regulation damper of the emergency air purification system changes from 20% to 55% as a parameter. [Table 2.30](#) shows the relationship between air pressure in the service area and elapsed time after the start-up of the emergency air purification system. During the emergency air purification system operating, air pressure of the service area was kept well below its allowable limitation of  $-59$  Pa within 1 min from the start-up of the emergency air purification system.

## 2.11.4 Emergency air purification system

### 2.11.4.1 Design

The emergency air purification system is an engineered safety feature and has two independent systems. It removes airborne radioactivity and maintains design pressure in the service area of below  $-59$  Pa during accidents. Each independent system is composed of an exhaust filtering unit, exhaust blower, and automatic butterfly valves. The exhaust filtering unit discharges the purified air to atmosphere through an exhaust duct. [Table 2.31](#) shows the major specifications and [Fig. 2.85](#) shows the schematic diagram of the emergency air purification system.

### 2.11.4.2 Commissioning tests

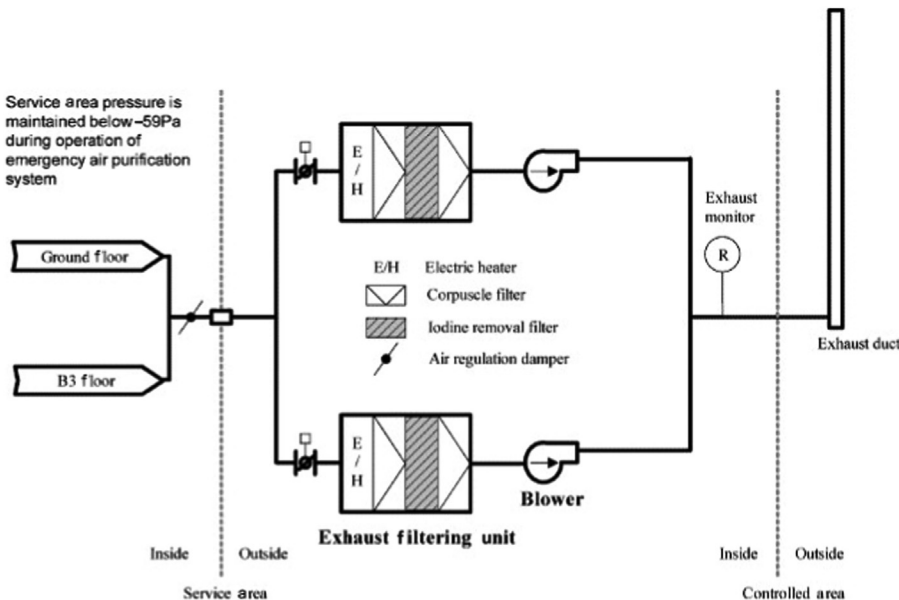
#### 2.11.4.2.1 Start-up test

The emergency air purification system is installed to mitigate the influence of a failure of primary helium purification system in the service area, etc. In the safety case, the start-up time of the emergency air purification system is important to prevent the public from suffering excessive radiation exposure. Considering the radiation exposure conservatively, the start-up time was set to be 13 min.

The start-up test was conducted with the following sequence, which demonstrates a failure of primary helium purification system. This failure is initiated by a rupture in the piping. The reactor containment vessel is isolated by closing the

**Table 2.31** Major specifications of emergency air purification system [74].

Exhaust filter unit	
Type	Corpuscle and iodine removal filter
Number	2
Volume velocity	3360 m <sup>3</sup> /h
Charcoal layer thickness	50 mm
Allowable limit of removal efficiency	
Corpuscle	More than 99%
Iodine	More than 95%

**Figure 2.85** Schematic diagram of emergency air purification system [77].

isolation valves, running down the pumps of the pressurized water-cooling system, etc. after detecting the increase in the primary helium purification flow within 5 s after a rupture. At the same time, the emergency air purification system is actuated. The reactor is automatically scrammed by detecting a signal of “pressurized water flow rate of the primary pressurized water cooler (PPWC) is low”; isolation valves of the reactor containment vessel are closed, and the auxiliary cooling system starts automatically to remove the residual heat of the core. The sequence of this accident is shown in Fig. 2.86.

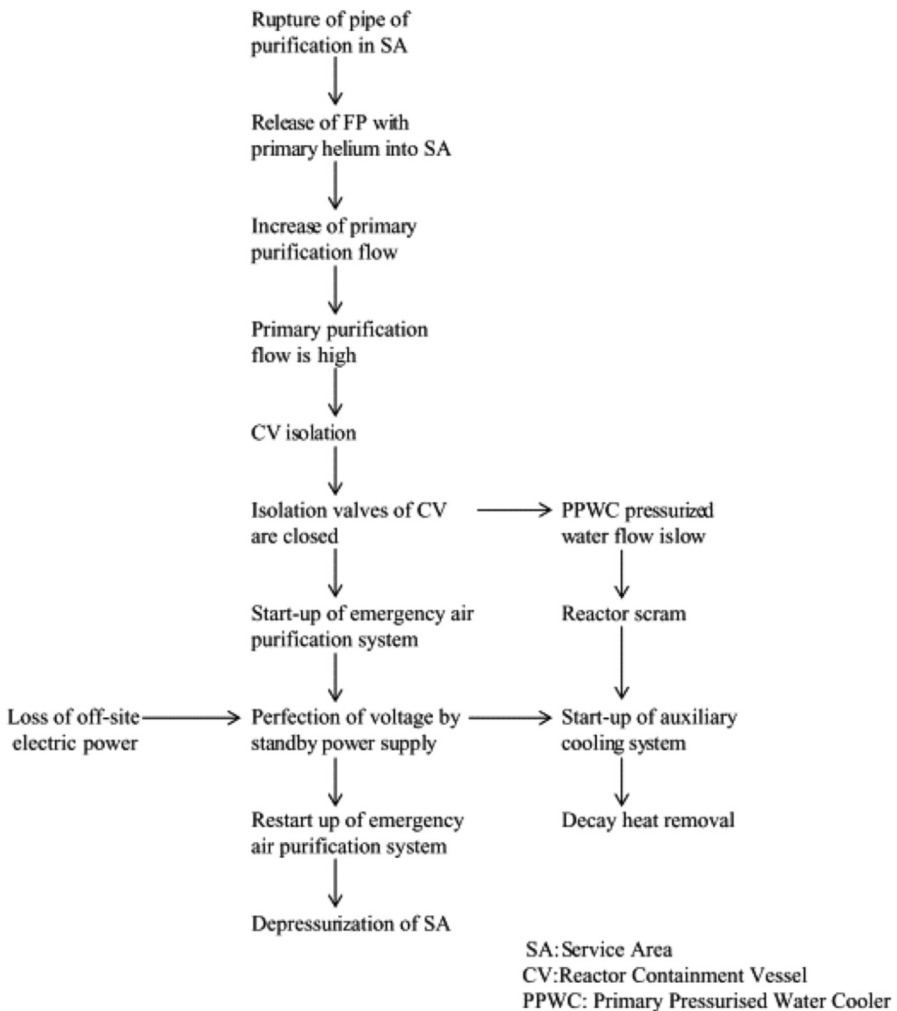


**Figure 2.86** Sequence of failure of primary helium purification system [74].

For this sequence, the following times were regulated in the safety case:

1. From the start-up command to the start-up of the blowers and electric heaters of the emergency air purification system.
2. From the start-up time of the blowers and electric heaters to the achievement of 4°C temperature difference between inlet and outlet of the electric heaters.
3. From the loss of off-site electric power simulation to the restart of the emergency air purification system by the stand-by power supply.
4. From the restart-up time of the blowers and electric heaters to the achievement of 4°C temperature difference between inlet and outlet of the electric heaters.

**Table 2.32** Start-up test result of emergency air purification system [74].

		Elapsed time (min)		
		Regulation value	Measured value	
			System A	System B
1	Time from the start-up command to the start-up of blowers and electric heaters of the emergency air purification system	—	0.09 s	0.08 s
2	Time from the start-up time of the blowers and electric heaters to the achievement of 4°C and electric heaters of the emergency air purification system	5	1	1
3	Time from the loss of off-site electric power simulation to the restart-up of the emergency air purification system by the stand-by power supply	1	49.8 s	53.8 s
4	Time from the restart up time of the blowers and electric heaters to the achievement of 4°C temperature difference between inlet and outlet of the electric heaters	5	1	1
	Total	13 <sup>a</sup>	>3	>3

<sup>a</sup>Total time of 13 min is the sum of item 2 (5 min), item 3 (1 min), item 4 (5 min), and a safety margin of 2 min.

The test result is shown in [Table 2.32](#). The start-up of the emergency air purification system was less than 3 min, which was well below the allowable limitation of 13 min.

#### 2.11.4.2.2 Filter efficiency measurement

Filter efficiency of the emergency air purification system for removal of radioactive particles and iodine was confirmed. The allowable efficiency limits of the particle removal and iodine removal are more than 99% and 95%, respectively. The concentration of the smoke of dioctyl phthalate (DOP) particles of 0.7 µm, generated by the temporary testing equipment upstream and downstream of the filter, was detected in order to measure the efficiency for corpuscle removal. The iodine removal efficiency was evaluated by the adsorption efficiency of active carbon and the leakage rate of Freon gas (R-112) through a bypass filter. The corpuscle removal efficiency  $E_C\%$  and iodine removal efficiency  $E_I\%$  are calculated by:

$$E_C(\%) = \left( 1 - \frac{C_d}{C_u} \right) \times 100, \quad (2.9)$$

$$E_l(\%) = A \times \left( 1 - \frac{D_f - D_a}{U_f - U_a} \right), \quad (2.10)$$

where  $C_d$  and  $C_u$  are DOP concentrations ppm downstream and upstream of the filter, respectively,  $A$  is the adsorption efficiency of active carbon%, which is the inspected value,  $U_f$  and  $D_f$  are the Freon gas concentrations ppm upstream and downstream of the filter, respectively, and  $U_a$  and  $D_a$  are the air concentrations ppm upstream and downstream of the filter.

As a result of the filter efficiency test, the corpuscle removal and iodine removal efficiency were estimated to be 99.99% and 99.59%, respectively, which were well over the allowable limitation of 99% and 95%, respectively.

## 2.12 Other systems

### 2.12.1 Introduction

Chemistry control is important for the helium coolant of high temperature gas-cooled reactors because impurities cause oxidation of the graphite used in the core and corrosion of high temperature materials used in the heat exchanger, etc. The helium purification systems are installed in the primary and secondary helium cooling systems in order to reduce the quantity of chemical impurities. The helium sampling systems monitor the concentration of impurities. The helium storage and supply systems keep the steady pressure of the helium system during the normal operation [13].

The new and spent fuels should be handled and stored safely and reliably by the fuel handling and storage system. The fuel handling system is utilized to keep the helium boundary without entering air to the helium system during the refueling, which will be performed every 3 reactor years [13].

This section describes the outline of the auxiliary helium and fuel systems.

### 2.12.2 Auxiliary helium systems

#### 2.12.2.1 Helium purification system

The helium purification system is installed in the primary cooling system and secondary in order to reduce the quantity of chemical impurities such as hydrogen, carbon monoxide, water vapor, carbon dioxide, methane, oxygen, and nitrogen. The primary helium purification system is mainly composed of a precharcoal trap, an inlet heater, two copper oxide fixed beds, coolers, two molecular sieve traps, two cold charcoal traps, and gas circulators as shown in Fig. 2.87 [78]. The flow diagram of the secondary helium purification system is almost same as that of the primary system except for the absence of a precharcoal trap.

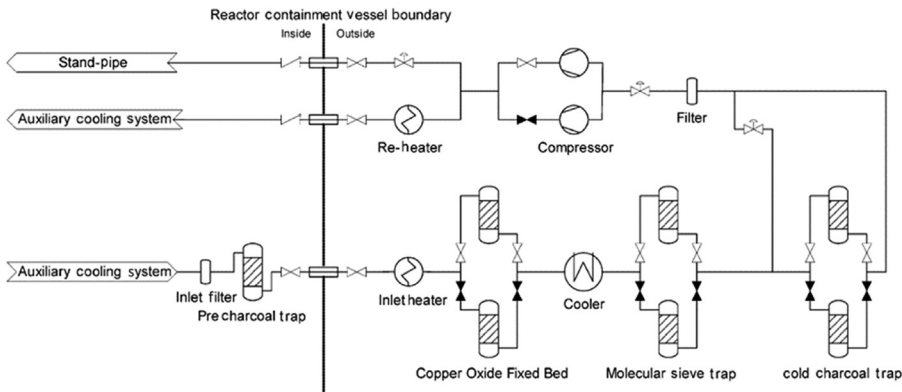


**Figure 2.87** Flow diagram of primary helium purification system [78].

**Table 2.33** Main specifications of primary helium purification system [13].

Item	Type	Number	Helium flow rate (kg/h)
Precharcoal trap	Vertical cylinder	1	200
Copper oxide fixed bed	Vertical cylinder	2	200
Molecular sieve trap	Vertical cylinder	2	200
Cold charcoal trap	Vertical cylinder	2	50

The primary helium gas is introduced into the primary helium purification system through the auxiliary cooling system and the purified helium gas returns to the auxiliary cooling system and stand pipes. Main specifications of the primary helium purification system are shown in Table 2.33. The flow rate of the primary helium purification system is determined considering the following requirements:

1. To satisfy the concentration limit of impurity to reduce oxidation of core graphite structures (limited impurity concentration value is shown in Table 2.34).
2. To purify >10% of the helium inventory in the primary cooling system in 1 h.
3. To purge the stand pipes.

The primary helium purification system has three kinds of traps for reducing chemical impurities. Each trap has two identical systems for reliability of plant operation. The first trap is a copper oxide fixed bed where hydrogen and carbon monoxide are oxidized to water vapor and carbon dioxide, respectively. It is kept at a temperature of 280°C during its operation. The second trap is a molecular sieve trap where water vapor and carbon dioxide are removed by adsorption. The third trap is a cold charcoal trap where oxygen, nitrogen, methane, and noble gases are removed by adsorption; it is kept at a temperature of -195°C. The flow rate in the primary helium purification system is 200 kg/h. The flow rate through the cold charcoal trap

**Table 2.34** Upper impurity limit in primary coolant at 4 MPa and reactor outlet coolant temperature from 800°C to 950°C [78].

Item	Concentration (ppm)
H <sub>2</sub>	3.0
CO	3.0
H <sub>2</sub> O	0.2
CO <sub>2</sub>	0.6
CH <sub>4</sub>	0.5
N <sub>2</sub>	0.2
O <sub>2</sub>	0.04

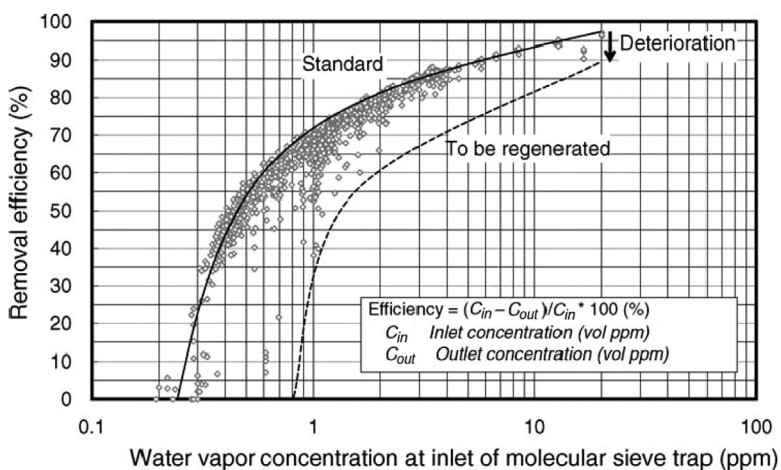


**Figure 2.88** Efficiency of water vapor removal at molecular sieve trap of primary helium purification system [78].

is 50 kg/h with a bypass flow for the rest of the gas. The efficiency of water vapor removal was confirmed in its commissioning test and is shown in Fig. 2.88. When the efficiency of the traps decreases during operation, the traps are changed manually to stand-by traps. The deteriorated traps can be used repeatedly after regeneration. Noble gases, absorbed by a cold charcoal trap, are stored for about 50 days and are then transferred to the gaseous radioactive waste treatment system.

The flow rate of the secondary helium purification system is 10 kg/h, which is determined in a similar manner to that of the primary helium purification system. The design of helium purification system takes credit of the experience obtained in the HENDEL loop [79].

### 2.12.2.2 Helium sampling system

The helium sampling systems detect chemical and radioactive impurities in the primary cooling system and secondary helium cooling system. The concentration of chemical impurities, hydrogen, carbon monoxide, water vapor, carbon dioxide, methane, nitrogen, and oxygen is measured by the gas chromatograph mass spectrometers. The primary helium sampling system, consisting of sampling equipment, a carrier gas supply system, and a standard gas supply system, automatically transmits the impurity concentration measurement to the main control room, as does the secondary helium sampling system.

The purpose of the primary helium sampling system is:

1. To monitor the chemical impurity level for the purpose of avoiding core graphite oxidation and carbon deposits, as well as the carburizing and decarburizing of Hastelloy XR in the IHX.
2. To detect the rupture of a heat exchanger tube in the PPWC and auxiliary heat exchanger.
3. To monitor the performance of the traps in the primary helium purification system.

The sampling locations of impurities except water vapor for the primary are the inlet and outlet of the reactor, the inlet and outlet of the primary helium purification system, and the inlet and outlet of the cold charcoal trap. Two detectors are installed for detecting water vapor. Sampling locations are as follows: the inlet to the reactor, the inlet and outlet of the primary purification system, and the inlet to the cold charcoal trap for the “No. 1” detector, the reactor outlet, the outlet of the PPWC, the outlet of the primary helium gas circulator for the PPWC and the IHX for “No. 2.”

The sources of the initial impurities in the primary coolant can be traced back to the core graphite, to the heat insulator in the primary hot gas duct, and to original impurities of the helium gas primary coolant. The total amount of water removed during the commissioning tests had been 0.75 kg.

### 2.12.2.3 Helium storage and supply system

The helium storage and supply systems are installed for the primary cooling system and secondary helium cooling system. The primary helium storage and supply system is composed of storage tanks, a supply tank, helium compressors, etc. The primary coolant is kept at a fixed pressure at about 4.0 MPa by the primary helium storage and supply system during normal operation.

The secondary helium storage and supply system stores and supplies helium gas and controls the pressure of the secondary helium gas to be higher than the primary coolant to aggravate the entry of primary coolant to the secondary coolant during an accident such as a rupture of the boundary between the primary and secondary helium cooling system.

The main specifications of the primary helium storage and supply system are shown in [Table 2.35](#). Six storage tanks with a capacity of 220 kg each and a supply tank with a capacity of 110 kg are installed. Two helium gas compressors are also installed in the system. One compressor is a stand-by system. The pressure of the primary helium gas is maintained at the design value by this system. The supply valve for the primary coolant opens and closes at a pressure of 3.92 and 3.99 MPa, respectively, and the exhaust

**Table 2.35** Main specifications of primary helium storage and supply system [13].

Item	Number	Tank volume (m <sup>3</sup> /tank)	Capacity (kg)	Max. pressure (MPa)
Storage tank	6	18	1320 (total)	8.6
Supply tank	1	10	110	8.6

valve opens and closes at a pressure of 4.00 and 3.96 MPa, respectively. The supply of helium gas to the primary coolant is also utilized for detecting the leakage rate of the primary coolant during operation when its automatic pressure control system is working. The very small leakage rate of the primary coolant can be detected by measuring the opening time of the helium gas supply valve.

The secondary helium storage and supply system is composed of a storage tank with a capacity of 25 kg, a supply tank with a capacity of 10 kg, two compressors, etc. This system is designed to control the pressure of the secondary helium gas to maintain the differential pressure between the primary and the secondary coolant. The supply valve for the secondary coolant opens and closes at a pressure difference of -29.4 and -9.8 kPa, respectively, and the exhaust valve opens and closes at a pressure difference of 29.4 and 19.5 kPa, respectively. The design pressure difference between the primary and the secondary coolant is 73.5 kPa.

### 2.12.3 Fuel system

The new fuel and the spent fuel should be handled and stored safely and reliably by the fuel handling and the fuel storage systems [80]. Each fuel element in the core will be discharged every three reactor years. The fuel elements keep their original position during their lifetime in the core.

#### 2.12.3.1 Fuel handling system

The fuel handling system is utilized to install and remove fuel elements, replaceable reflector blocks, top shielding blocks, control rod guide blocks, and control rods. The fuel handling system consists of a fuel handling machine, attached equipment, and auxiliary equipment. The fuel handling machine consists mainly of a shielded cask, a gripper, a fuel handling unit drive system, a rotating rack, and a door valve. The fuel handling machine has a shield sufficient to protect fuel handling personnel and a gas-tight boundary. With the fuel blocks stored to its capacity, the fuel handling machine maintains subcriticality. The door valve, connected with the bottom of the fuel handling machine, has a gas-tight shield structure along with the reactor isolation valve. The attached equipment used during refueling consists of a reactor isolation valve, connecting pipe, and control rod handling machine.

The fuel handling procedure is schematically shown in Fig. 2.89. The fuel elements are refueled column-wise through stand pipes by the fuel handling machine, which is able to handle the five fuel elements at one refueling step.

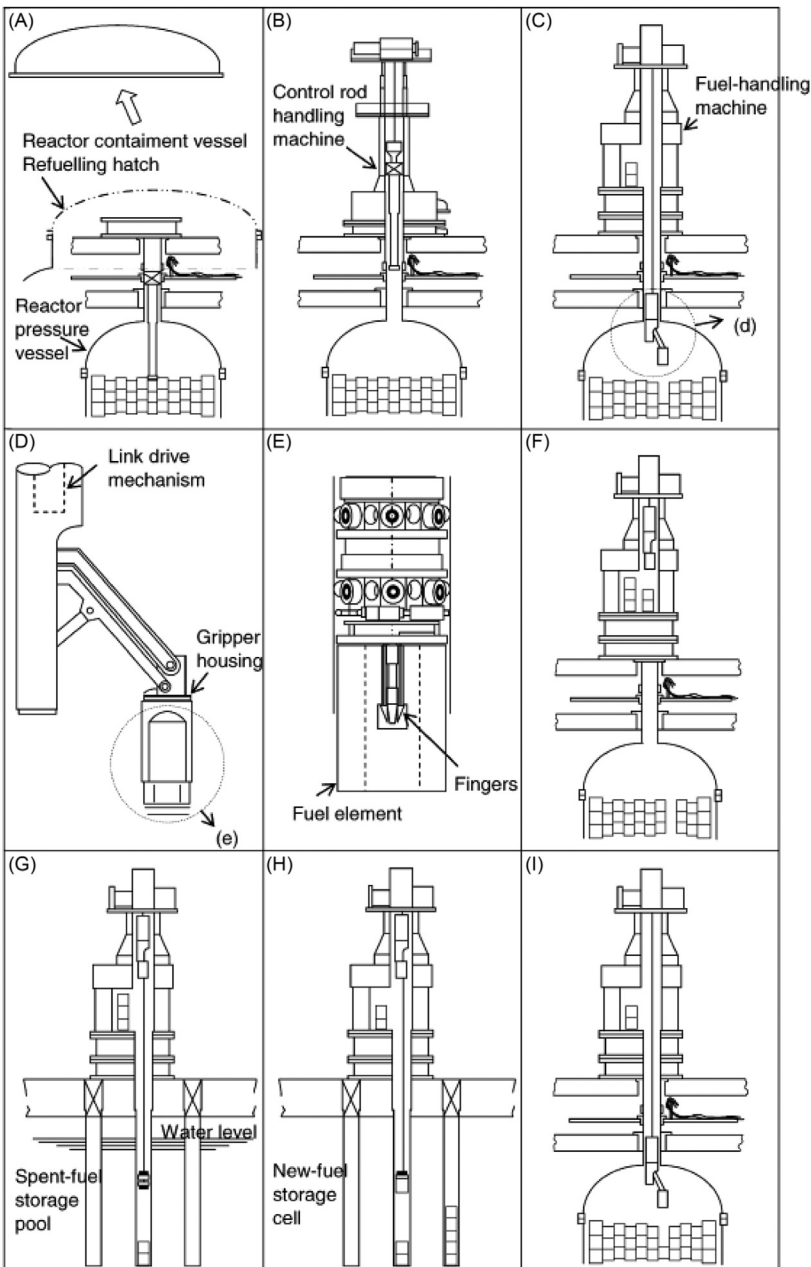


**Figure 2.89** Schematic plan of fuel handling procedure (A) Remove of reactor containment vessel. (B) Connection status of control rod handling machine to stand pipe. (C) Replacement of control rod handling machine with fuel handling machine. (D) Structure of gripper for fuel. (E) Insertion of finger of gripper into refueling hole of fuel block. (F) Removal of spent-fuel by lifting the gripper and storage in fuel handling machine. (G) Storage of spent-fuel in spent-fuel storage pool after moving fuel handling machine to pool. (H) Storage of new-fuel in fuel handling machine after moving it to new-fuel storage cell. (I) Installation of new-fuel into reactor with fuel handling machine [13].

Prior to the refueling operation, the reactor is shut down and depressurized, and the refueling hatch of the reactor containment vessel is removed ([Fig. 2.89A](#)). The connecting pipe, the reactor isolation valve, and control rod handling machine are installed on the stand pipe located above the region being refueled ([Fig. 2.89B](#)). The control rod handling machine removes the stand pipe closure and control rod drive mechanism. After removing the control-rod handling machine, the fuel-handling machine is connected to the reactor isolation valve in order to open the gate of reactor isolation valve ([Fig. 2.89C](#)). The gripper automatically descends into the RPV and comes to the position of the top shielding block on the fuel elements. Slowly lowered while the fingers of the gripper enter the handling hole in the block, the gripper positioning device is affixed to the machine to insert the gripper into the handling hole smoothly. After the fingers grab the block in the refueling hole, the gripper is lifted, and the block is put into the rotating rack of the machine ([Fig. 2.89C–F](#)). When all elements are in the rotating rack, the gate of the reactor isolation valve is closed and the fuel handling machine is transferred to the spent-fuel storage pool ([Fig. 2.89G](#)). Spent-fuel elements in the fuel handling machine are put into the rack in the pool. Then, the fuel handling machine is transferred to the new-fuel storage cell to put new-fuel elements into the rotating rack ([Fig. 2.89H](#)). The fuel handling machine is connected again to the reactor isolation valve and installs new-fuel elements into the RPV ([Fig. 2.89I](#)). The duration of the whole refueling is estimated about several months.

### 2.12.3.2 Fuel storage system

The HTTR has two fuel storage systems, one is the new-fuel storage system and the other is the spent-fuel storage system. The new-fuel storage system consists of fuel assembling and testing equipment, a new-fuel storage cell, and inert gas replacement equipment. The new-fuel storage cell can store about one and a half core inventories. The storage rack forming a vessel of a vertical cylinder with a plug has sufficient distance to the adjacent storage racks in order to keep subcriticality. The inert gas replacement equipment evacuates air in the rack and replaces it with pure helium gas to keep fuel elements in a dry condition. The functions of the new-fuel storage system are to inspect the new-fuel rods, to assemble the fuel elements, and to store new-fuel elements.

The spent-fuel storage system located inside the reactor building, consisting of a spent-fuel storage pool, water-cooling and purification system, and irradiated material storage pit, stores spent-fuel elements, control rod guide blocks, and replaceable reflector blocks. The spent-fuel storage pool has sufficient shielding and can store spent-fuel elements of about two core inventories. The inside of the spent-fuel storage pool is lined with stainless steel to prevent leakage of pool water. Leakage can be detected by monitoring the water from the leakage check ditch located within the lining. After 2 years cooling in the spent-fuel storage-pool, the spent-fuel is transferred to another spent-fuel storage system located neighborhood building of the HTTR.

## 2.13 Safety design

### 2.13.1 Introduction

As for the HTTR Licensing, in February 1989, the application for its installation permit was submitted to the prime minister of Japan by JAERI, which is the present JAEA. In November 1990, the safety review was terminated by Nuclear Safety Commission of the time and the prime minister issued the installation permit of the HTTR to JAERI. Up to now, the significant experimental data to validate the safety design of the HTTR have been accumulated through the following tests:

1. Long-term operation of 30 days at 850°C
2. Long-term operation of 50 days at 950°C
3. Safety demonstration tests
  - a. Reactivity insertion test by control rod withdrawal
  - b. Coolant flow reduction test by tripping of gas circulators
  - c. LOFC test

### 2.13.2 Basic safety design philosophy

[Fig. 2.90](#) shows a logical flow to establish the basic safety design philosophy of the HTTR. The top-level regulatory criteria for the HTTR is identical to that of the

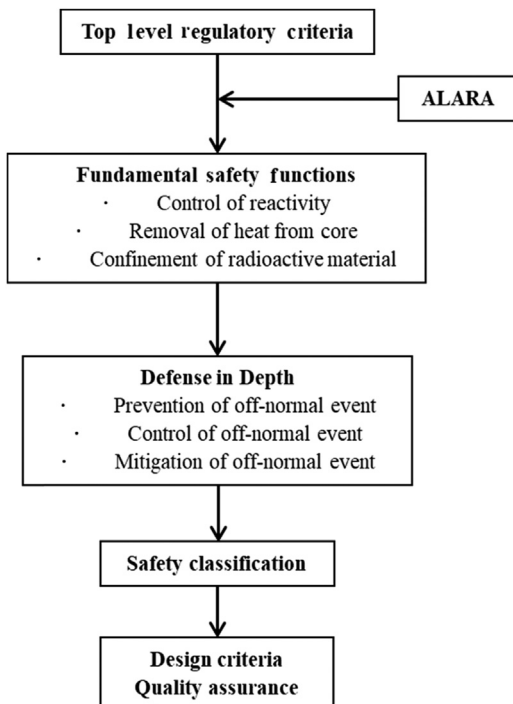


**Figure 2.90** Logical flow to establish a safety design philosophy of HTTR [81].

**Table 2.36** Summary of top-level regulatory criteria for HTTR [81].

Dose limits	Top-level regulatory criteria
Normal operation	<ul style="list-style-type: none"> <li>• 5 mSv of annual radiation exposure outside the site boundary</li> <li>• Based on “Examination Guide for Dose Goal outside the site boundary of Light Water Nuclear Reactor Facilities”</li> </ul>
Accident	<ul style="list-style-type: none"> <li>• No significant risk of radiation exposure to the public</li> <li>• Effective dose equivalent shall not exceed 5 mSv</li> <li>• Based on “Examination Guide for Safety Evaluation of Light Water Nuclear Power Reactor Facilities”</li> </ul>
Major accident	<ul style="list-style-type: none"> <li>• Effective dose equivalent to the whole body shall not exceed 0.25 Sv outside the site boundary</li> <li>• Effective dose equivalent to the thyroid shall not exceed 1.5 Sv for a child outside the site boundary</li> <li>• Based on “Examination Guide of Reactor Siting and Guidelines for Interpretation in their Application”</li> </ul>
Hypothetical accident	<ul style="list-style-type: none"> <li>• Effective dose equivalent to the whole body shall not exceed 0.25 Sv outside the site boundary</li> <li>• Effective dose equivalent to the thyroid shall not exceed 3.0 Sv for an adult outside the site boundary</li> <li>• The whole population dose shall not exceed <math>2 \times 10^4</math> man Sv</li> <li>• Based on “Examination Guide of Reactor Siting and Guidelines for Interpretation in their Application”</li> </ul>

LWR. **Table 2.36** provides the summary of the top-level regulatory criteria for both the HTTR and LWRs in Japan [81]. In addition, according to the International Commission on Radiological Protection (ICRP) recommendation [82], the principle of ALARA (as low as reasonably achievable) was applied to reduce the radiation dose to plant personnel and members of the public around the HTTR as low as reasonably achievable. To meet the Top Level Criteria and apply the principle of ALARA, the basic safety design philosophy of the HTTR was determined based on that of the LWR stipulated in “Guidelines for Safety Design of LWR Power Plant” considering inherent safety characteristics of the HTGR. In order to ensure safety, the well-known fundamental safety functions such as control of reactivity, removal of heat from the core, and confinement of radioactive materials shall be performed in normal and off-normal states. The strategy of the defense in depth [83] that provides a series of level of defense is implemented to ensure that the fundamental safety functions shall be reliably achieved in normal and off-normal states. The

level of the defense in depth consists of prevention of off-normal events, control of off-normal events, and mitigation of off-normal events. The newly considered premise to establish the basic safety design philosophy of the HTTR is that it considers an air ingress accident and following oxidation of the core. The HTTR safety design shall prevent the excessive oxidation of the core and FPs release to the environment.

### **2.13.3 Safety classification**

In compliance with the strategy of the defense in depth, all systems having safety functions in the HTTR were classified as Prevention System (PS)-1, PS-2, PS-3, Mitigation System (MS)-1, MS-2, or MS-3 depending on their roles and significance. The definition of each classification is shown as follows:

#### **PS-1**

- Structures, systems, and components whose failure or malfunction has the possibility to cause apparent damage in the core or a large amount of fuel failure.

#### **PS-2**

- Structures, systems, and components whose failure or malfunction does not have the possibility to cause the immediate apparent damage in the core or a large amount of fuel failure, however, has the possibility to cause the excessive amount of FP release outside the site boundary.
- Structures, systems, and components whose operation is expected in normal operation or anticipated operational occurrences and their malfunctions have the high possibility to damage the core cooling performance.

#### **PS-3**

- Structures, systems, and components are not classified as PS-1 and PS-2, and their failures or malfunctions have the possibility to trigger off-normal events.
- Every system to keep the amount of FPs in the primary circuit lower than the allowable level

#### **MS-1**

- Structures, systems, and components provided to stop the reactor rapidly, remove the residual heat, prevent the temperature and internal pressure increase of the primary pressure boundary, and prevent the excessive amount of radiation exposure to the members of public outside the site boundary.
- Other facilities indispensable to safety.

#### **MS-2**

- Structures, systems, and components provided to sufficiently reduce the radiation exposure to the public outside site boundary in the event caused by failure or malfunction of those classified as PS-2.
- Structures, systems, and components especially significant as countermeasures in off-normal states.

#### **MS-3**

- Structure, systems, and components provided to mitigate the anticipated operational occurrences together with those of classified as MS-1 and MS-2.
- Everything significant as countermeasures in off-normal states.

**Table 2.37** shows the safety classification of the HTTR.

**Table 2.37** Safety classification of HTTR [81].

Class	Function	Structure, system, component
PS-1	Primary pressure boundary	Components, pipes in primary circuit except small pipes such as pipes for instrumentation
	Prevention of insertion of excessive reactivity	Stand pipe Stand pipe closure
	Core constitution	Core structures (fuel block, reflector block, etc.) In-core graphite structure In-core metal structure
MS-1	Emergency stop of reactor	Control rod system
	Maintain subcriticality	Control rod system Reserve shutdown system
	Prevention of excessive pressure of primary pressure boundary	Safety valve in primary circuit
	Decay heat removal	Auxiliary cooling system Vessel cooling system
	Engineered safety system Core cooling	Auxiliary cooling system Vessel cooling system
	Containment of FP	Containment vessel Emergency air purification system
	Sending signal for engineered safety systems and reactor shutdown system	Engineered safety features actuating system
	The other systems having safety-related function	Emergency generator Control room Electric facility Auxiliary plant facility

(Continued)

**Table 2.37** (Continued)

Class	Function	Structure, system, component
PS-2	Containing primary coolant	Primary helium purification system
	Storage of radioactive waste	Gaseous radioactive waste treatment system Spent fuel storage pool, cell, rack
	Safety handling of fuel	Fuel handling machine
	Function related to irradiation test	Irradiation test facility
	Closing safety valve at proper pressure	Safety valve in primary circuit
MS-2	Decrease of FP release	Stack
	Postaccident measurement	Postaccident instrumentation
	Reactor shut down outside control room	Shut down system outside control room
PS-3	Containing primary coolant (which is not classified as PS-1 and PS-2)	Instrumentation pipe Primary helium sampling system Primary helium makeup system
	Circulation of primary coolant	Primary helium circulator
	Storage of radioactive waste	Liquid radioactive waste treatment system Solid radioactive waste treatment system
	Cooling of secondary helium circuit during normal operation	Secondary helium cooling system
	Maintain differential pressure between primary and secondary helium circuit	Secondary helium makeup system

*(Continued)*

**Table 2.37** (Continued)

<b>Class</b>	<b>Function</b>	<b>Structure, system, component</b>
	Plant control and instrumentation (except engineered safety features actuating function)	Reactor control system Reactor instrumentation system Process instrumentation system
	Plant auxiliary function	Compressed air system for control system
	Cooling of vessel cooling system during normal operation	Vessel cooling system
	Function related to irradiation test	Irradiation test facility (except ones classified as PS-2)
	Prevention of FP release to primary helium coolant	Coated layers of fuel Graphite sleeve for fuel
	Purification of primary coolant	Primary helium purification system
MS-3	Mitigation of reactor power increase	Interlock for control rod withdrawal Interlock for control rod pattern
	Mitigation of decreasing coolability in reactor core	Circuit breaker for primary water pump Interlock for inlet temperature of primary water in primary pressurized water cooler Interlock for water flow rate in secondary pressurized water cooler
	Mitigation of temperature increase of primary pressure boundary	Frequency converter for helium circulators
	Significant function for off-site emergency plan	Sampling system during accident, etc.

## ***2.13.4 Fundamental safety functions unique to HTTR***

### ***2.13.4.1 Control of reactivity***

The reactor is shut down safely and reliably from any operational state using the control rod system. Furthermore, the reserve shutdown system is provided, which is composed of boron-carbide/graphite ( $B_4C/C$ ) pellets. The power control and normal reactor shutdown of the HTTR are achieved with 16 pairs of control rods. The control rod system can achieve subcriticality from any operation state and maintain subcriticality in the cold core conditions even when a pair of control rods sticks at the operational position.

In the case of a scram during normal operation, nine pairs of control rods in the replaceable reflector region are inserted at first, and the rest of control rods are inserted after the core is cooled down to prevent exposure of the control rod cladding in a high temperature environment of above 900°C. The core temperature is determined by monitoring the outlet helium gas temperature. A pair of control rods is driven by the one-drive mechanism. The control rods are released from the drive mechanism and inserted by gravity when the reactor is scrammed.

### ***2.13.4.2 Removal of heat from core***

The main cooling system removes residual heat from the core during a normal reactor shutdown. In addition to the main cooling system, the HTTR has two other residual heat removal systems. The auxiliary cooling system is used for off-normal transients that coolant flow boundary is intact and a VCS is used for accidents that forced circulation of the coolant cannot be maintained.

The auxiliary cooling system automatically starts up when the reactor is scrammed in an anticipated operational occurrence and accident in which forced cooling is available, while the main cooling system is stopped. The auxiliary cooling system is classified as a safety system because it has safety function to cool heat transfer tubes in the PPWC in abovementioned off-normal states and keep their temperature lower than the allowable temperature. It consists of two helium gas circulators, the auxiliary water cooler and an affiliated water-cooling system. In terms of the core coolability, the residual heat can be removed by the VCS without using the auxiliary cooling system. However, it is needed from the viewpoint of operational flexibility because it takes a very long time to cool down the core without the auxiliary cooling system.

The VCS is used as a residual heat removal system when the forced circulation in the primary cooling circuit is no longer available due to a rupture of the inner pipe or both internal and external pipes in the coaxial double primary pipes. The VCS is also a safety system equipped with two completely independent systems, which are backed up with an emergency power supply. It is operated even during normal operation to cool the reactor shielding concrete wall.

### ***2.13.4.3 Confinement of fission product release***

The HTTR has multiple barriers to prevent FP release into the environment, fuel coatings, the reactor pressure boundary, the containment vessel, and the reactor building. The ceramic layers surrounding the fuel kernel act as the primary barrier for the FP

release. The integrity of these ceramic layers is sufficiently kept under 1600°C based on several experiments. JAERI carried out the irradiation test and postirradiation tests up to 33,000 MWd/t before the HTTR operation and continues to carry out irradiation tests for the HTTR initial loading fuel up to 70,000 MWd/t. So far, the heating up tests after the irradiation proved that the integrity of the fuel can be sufficiently maintained under 1600°C. It also showed that the fuel failure rate in the range from 1600°C to 1800°C is negligibly small.

This is the major specific feature of the HTTR as well as the other HTGRs in the world. While most of the HTGRs constructed or being designed in the world do not have a containment vessel, the HTTR has a containment vessel made of steel. Its functions are to contain FPs and to limit the amount of air ingress into the core. The containment vessel is installed in the reactor building, which acts as the confinement. The confinement is maintained at a slightly negative pressure to the environment by a ventilation and air conditioning system during both normal and off-normal states.

The off-site radiation dose limit in such accident as depressurization accident is remarkably reduced by the containment vessel together with the confinement.

### **2.13.5 Acceptance criteria**

Acceptance criteria for the HTTR are established fundamentally reflecting the safety requirements for LWR power plants and taking into account major features of HTGRs and the HTTR. Acceptance criteria for the anticipated operational occurrences and the accidents for the HTTR and LWRs are shown in [Table 2.38](#). The maximum fuel temperature is restricted to 1600°C to avoid fuel failure during the anticipated operational occurrences. Criteria for the temperature and the pressure of the primary pressure boundary and the containment vessel are determined considering the following items: (1) materials composing the pressure boundary and the containment vessel shall have stable strength, and their temperature range during the normal operation and abnormal condition is within the temperature range determined by the design code [31], (2) the materials such as 2½Cr–1Mo and Hastelloy XR have sufficient strength below the temperature of 550°C and 1000°C, respectively. However, the margin in their creep rupture strength decreases over 500°C for 2½Cr–1Mo and 980°C for Hastelloy XR. The temperature limits of their materials in anticipated operational occurrences are determined to be 500°C and 980°C, respectively, so that the reactor components can be reused without any repair after an anticipated operational occurrence occurs.

In the case of accidents, the core shall not be seriously damaged and shall maintain its geometry for sufficient coolability, that is, (1) the fuels shall be maintained in the graphite fuel block or sleeve and (2) the structural integrity of the graphite support structures such as support posts shall prevent the core from collapsing so as to maintain subcriticality. The radiation exposure is limited to 5 mSv as effective dose equivalent outside the site boundary of the HTTR. For the evaluation of the radiation exposure, external gamma ray exposure from the radioactive cloud containing noble gases and iodine, internal exposure by inhalation from the radioactive cloud, direct external gamma ray exposure, and external skyshine gamma ray exposure from FPs such as Cesium contained in the containment vessel are considered. The total radiation exposure, which is the sum of these exposures, shall be lower

**Table 2.38** Acceptance criteria for HTTR [81].

HTTR	LWR
<i>(1) Anticipated operational occurrence</i>	
<ul style="list-style-type: none"> <li>The peak fuel temperature shall be less than 1600°C</li> </ul>	<ul style="list-style-type: none"> <li>Minimum critical heat flux (MCHF) or MCHF ratio shall not exceed the limited value</li> </ul>
	<ul style="list-style-type: none"> <li>Fuel cladding shall not fail mechanically</li> </ul>
	<ul style="list-style-type: none"> <li>Fuel enthalpy shall not exceed the limited value</li> </ul>
<ul style="list-style-type: none"> <li>Pressure on reactor pressure boundary is less than 1.1 times of maximum pressure in service</li> </ul>	<ul style="list-style-type: none"> <li>Pressure on reactor pressure boundary is less than 1.1 times of maximum pressure in service</li> </ul>
<ul style="list-style-type: none"> <li>Maximum temperature of reactor pressure boundary</li> </ul>	
2½Cr—1Mo steel <500°C	
Austenite stainless steel <600°C	
Hastelloy XR <980°C	
<i>(2) Accident</i>	
<ul style="list-style-type: none"> <li>The reactor core shall not be seriously damaged and can be cooled sufficiently</li> </ul>	<ul style="list-style-type: none"> <li>Minimum critical heat flux (MCHF) or MCHF ratio shall not exceed the limited value</li> </ul>
	<ul style="list-style-type: none"> <li>Fuel cladding shall not fail mechanically</li> </ul>
	<ul style="list-style-type: none"> <li>Fuel enthalpy shall not exceed the limited value</li> </ul>
<ul style="list-style-type: none"> <li>The reactor core shall not be seriously damaged and can be cooled sufficiently</li> </ul>	<ul style="list-style-type: none"> <li>Pressure on reactor pressure boundary is less than 1.2 times of maximum pressure in service</li> </ul>
<ul style="list-style-type: none"> <li>Maximum temperature of reactor pressure boundary</li> </ul>	
2½Cr—1Mo steel <550°C	
Austenite stainless steel <650°C	
Hastelloy XR <1000°C	
<ul style="list-style-type: none"> <li>Maximum pressure on containment boundary is less than maximum pressure in service</li> </ul>	<ul style="list-style-type: none"> <li>Maximum pressure on containment boundary is less than maximum pressure in service</li> </ul>
<ul style="list-style-type: none"> <li>No significant risk of radiation exposure to public</li> </ul>	<ul style="list-style-type: none"> <li>No significant risk of radiation exposure to public</li> </ul>

than the limit of 5 mSv. Based on ICRP, in special case, 5 mSv of annual radiation exposure for the public is acceptable, though a limit of 1 mSv is recommended. For accidents, which have small frequencies of those occurrences, the value of 5 mSv is applied to judge the significant risk of radiation exposure for the public. The nearest site boundary from the HTTR facility is about 200 m and the site is about 5 km far from the center of Oarai town having about 20,000 inhabitants.

## 2.13.6 Selection of events

Abnormal events to be postulated as anticipated operational occurrences and accidents have been selected considering their frequencies of occurrence and based on the investigation of main causes, which affect each item of the acceptance criteria identified for the HTTR, that is, (1) fuel temperature, (2) core damage, (3) temperature of reactor coolant pressure boundary, (4) pressure at reactor coolant pressure boundary, (5) pressure at containment vessel boundary, and (6) risk of radiation exposure for the public. The initiating abnormal events have been classified into similar event groups according to “Examination Guide for Safety Evaluation of Light Water Nuclear Power Reactor Facilities.” Then the most severe events with respect to the acceptance criteria within each similar event group are selected as the representative postulated events. Examples of the selection of anticipated operational occurrences and accidents are shown in Figs. 2.91 and 2.92.

The main causes affecting the fuel temperature are increase of power and decrease of heat removal in the core. The increase of power is caused by reactivity addition, in which four event groups are postulated, namely, (1) malfunction of the reactivity control system, (2) malfunction of the experimental facility, (3) increase of the primary coolant flow, and (4) increase of heat removal by the secondary cooling system. Two initiating events are considered as the malfunction of the reactivity control system, namely (1) abnormal control rod withdrawal and (2) abnormal control rod insertion. The abnormal control rod withdrawal is the more severe event with respect to the fuel temperature, and is selected as the representative postulated event. The representative postulated events concerning other acceptance criteria are selected in the same way. The postulated events considered in the safety evaluation of the HTTR as anticipated operational occurrences and accidents are listed in Table 2.39. A major accident and a hypothetical accident are evaluated to ensure the safety of the public in the case of serious accidents. “Major accidents” are postulated assuming the occurrence of the worst-case accident from a technical standpoint considering the reactor characteristics and engineered safety features. “Hypothetical accidents” are postulated assuming the occurrence of an accident more serious than a “major accident,” which is unlikely to occur from a technical standpoint, and shall be based on the assumption that one or more engineered safety features fail to function. The acceptance criteria are established in “Examination Guide of Reactor Siting and Guidelines for Interpretation in their Application” as follows: (1) effective dose equivalent to whole body shall not exceed 0.25 Sv in a major accident or a hypothetical accident; (2) effective dose equivalent to thyroid shall not exceed 1.5 Sv for a child in a major accident and 3.0 Sv for an adult in a hypothetical accident; (3) whole population dose shall not exceed  $2 \times 10^4$  man Sv in a hypothetical accident. A double-ended rupture of coaxial double pipes of the primary cooling system

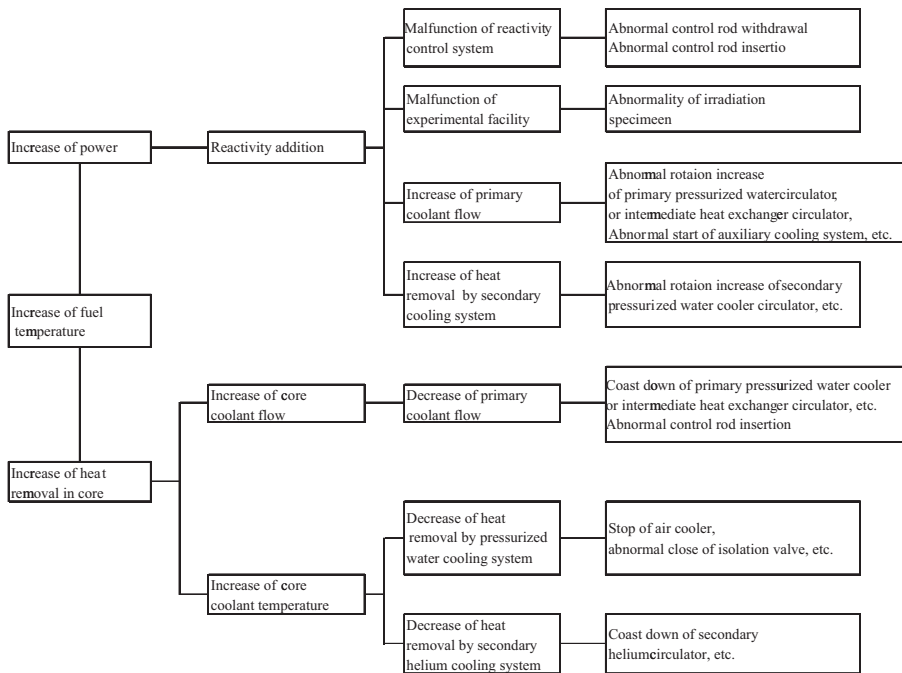


**Figure 2.91** Example of selection process of anticipated operational occurrence [81].

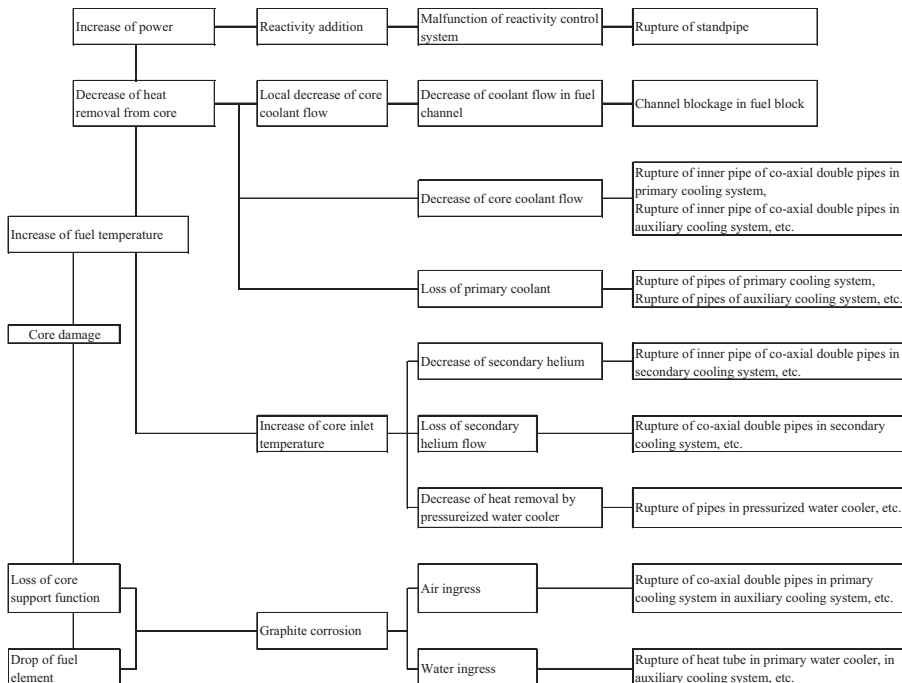


**Figure 2.92** Example of selection process of accident [81].

**Table 2.39** Selected events [81].

(1) Anticipated operational occurrence
Abnormal control rod withdrawal under subcritical condition
Abnormal control rod withdrawal during rated operation
Decrease in primary coolant flow rate
Increase in primary coolant flow rate
Decrease in heat removal by secondary cooling system
Increase in heat removal by secondary cooling system
Loss of off-site electric power
Abnormality of irradiation specimens and experimental equipment
Abnormality during safety demonstration tests
(2) Accident
Channel blockage in fuel block
Rupture of inner pipe of concentric pipe in primary cooling system
Rupture of inner pipe of concentric pipe in secondary cooling system
Rupture of concentric pipe in secondary cooling system
Rupture of pipe in pressurized water-cooling system
Rupture of concentric pipe in primary cooling system
Rupture of heat tube in pressurized water cooler
Rupture of pipe in primary coolant purification system
Rupture of pipe in processing facilities of radioactive gaseous waste
Rupture of sweep gas pipe in irradiation test facilities
Rupture of stand pipe

(depressurization accident) is postulated for the HTTR as the major and hypothetical accidents with respect to the risk of radiation exposure for the public.

### 2.13.7 Safety evaluation technologies

This section summarizes “Verified analysis codes accepted to licensing” [84]. Analytical tools for the safety evaluation were developed. All of them were validated by comparison between experimental results and analytical ones for the safety evaluation of the HTTR. **Table 2.40** shows the representative events in the safety evaluation of the HTTR and analytical tools. Analytical code is as follows:

**Table 2.40** Selected events and analytical codes.

Event name	BLOOST-J2	THYDE-HTGR	TAC-NC	RATSAM6	COMPARE-MOD1	GRACE	OXIDE-3F	FLOWNET/TRUMP
<i>Anticipated operational occurrence</i>								
Abnormal control rod withdraw under subcritical condition	Y							
Abnormal control rod withdraw under rated operation	Y							
Decrease in primary coolant flow rate		Y						
Increase in primary coolant flow rate		Y						
Decrease in heat removal by secondary cooling system		Y						
Increase in heat removal by secondary cooling system		Y						
Loss of off-site electric power		Y						
Abnormality of irradiation specimens and experimental equipment	Y							
Abnormality during safety demonstration tests		Y						

*(Continued)*

**Table 2.40** (Continued)

Event name	BLOOST-J2	THYDE-HTGR	TAC-NC	RATSAM6	COMPARE-MOD1	GRACE	OXIDE-3F	FLOWNET/TRUMP
<i>Accident</i>								
Channel blockage in fuel block								Y
Rupture of inner pipe of coaxial double pipes in primary cooling system			Y					
Rupture of inner pipe of coaxial double pipes in secondary cooling system		Y						
Rupture of coaxial double pipes in secondary cooling system		Y						
Rupture of pipe in pressurized water-cooling system		Y						
Rupture of coaxial double pipes in primary cooling system		Y	Y	Y	Y	Y		
Rupture of heat tube in pressurized water-cooling system		Y						
Rupture of pipe in primary coolant purification system							Y	
Rupture of pipe in processing facilities of radioactive gaseous waste								
Rupture of sweep gas pipe in irradiation test facilities								Y
Rupture of stand pipe	Y		Y	Y	Y			

The BLOOST-J2 code [85] is used to analyze the effects of reactivity and flow rate change on the reactor power and temperatures of the core. The BLOOST-J2 code was modified from BLOOST5 code [86] so as to adopt the configuration of the HTTR. The validation of the BLOOST-J2 code was conducted by comparing analytical results with the data of control rod withdrawal/insertion experiments with Fort St. Vrain (FSV) at 50% of rated power.

The THYDE-HTGR code [87] is used to analyze plant dynamics of the HTTR. The THYDE-HTGR code was modified from THYDE [88] code to treat helium gas behavior in transient conditions. The THYDE code was validated by a comparison with various experiments such as LOFT experiments [89]. A new function to evaluate thermal and hydraulic transient of helium gas was added in the THYDE-HTGR code. The other functions were the same as that of the THYDE code. The validation of the THYDE-HTGR code was conducted by comparing analytical results with the data of control rod withdrawal/insertion experiments with FSV at 50% of rated power. Thermal and hydraulics behavior of helium gas was validated by comparing experimental results obtained in Engineering Research Association of Nuclear Steelmaking (ERANS) and analytical ones.

The TAC-NC code [90] modified from TAC-2D [91] is used to calculate transient thermal and hydraulic characteristics in the core during LOFC accident such as the depressurization accident. The TAC-2D code was used for various calculations, and heat transfer calculations by conduction, convection, and radiation have a sufficient reliability. The function to analyze heat transfer by natural circulation in the core is added in the TAC-NC code. This function was validated by comparing with an air ingress experiment, which simulated a rupture of the coaxial double primary pipes of the HTTR.

The RATSAM6 code [92] is used to calculate the amount of mass and energy released from the reactor into the containment vessel with consideration given to heat transfer during the rupture of the coaxial double primary pipes. The validation of the code was performed by comparing the analytical results with experimental results, which are obtained by using a 1/8 scaled apparatus simulating the primary cooling system of the Colder Hall-type Reactor. The COMPARE-MOD1 code [93] is used to calculate pressure and temperature behavior in each compartment of the containment vessel during the depressurization accident. The code was certified by the US Nuclear Regulatory Committee as a code for safety analysis to calculate pressure and temperature behavior in the containment vessel.

The GRACE code [94] is used to calculate axial and radial distributions of oxidation of graphite materials and concentration distribution of oxygen in a mixed gas of air and helium by analyzing the oxidation reaction between ingressed air and the graphite structures. The validation of the code was performed by using results of a graphite oxidation experiment. Input conditions for the code such as mass transfer coefficient were obtained from the heat transfer correlations obtained in the experiments.

The OXIDE-3F code [95] is used to analyze the oxidation reaction of the graphite materials with steam ingress in the core by a rupture of the heat transfer tubes of the PPWC. The method to calculate the rate of graphite oxidation in the OXIDE-3F code is basically the same as that of the GRACE code.

The FLOWNET/TRUMP code [96] is used to calculate the temperature distribution in the fuel block when a coolant channel was blocked. The code is the combination of the FLOWNET and TRUMP codes. The FLOWNET code is a one-dimensional flow network evaluation code while the TRUMP code is a three-dimensional heat conduction code. The validation of the code was performed by comparing results of the uniform and nonuniform power distribution tests, which were carried out using the multichannel test rig of the HENDEL.

### 2.13.8 New safety criteria

After the 2011 off the Pacific coast of Tohoku Earthquake, Nuclear Regulatory Authority established a more stringent new regulation standard. On the new regulatory standards, the safety designs for the strengthened natural phenomena such as earthquakes and volcanoes, fire, and internal flooding were required. Furthermore, the mitigation measures against the beyond design basis accidents were required. The HTTR is considering changing the safety classification by considering safety functions such as radiant core cooling even if a loss of a forced cooling accident occurs. The safety review for the HTTR to confirm the conformity to the new regulation standard is undergoing.

## References

- [1] S. Shiozawa, et al., Overview of HTTR design features, Nucl. Eng. Des. 233 (2004) 11–21.
- [2] Y. Tachibana, et al., Procedure to prevent temperature rise of primary upper shielding in high temperature engineering test reactor, Nucl. Eng. Des. 201 (2000) 227–238.
- [3] K. Takamatsu, et al., High-temperature continuous operation of the HTTR, Trans. At. Energy Soc. Jpn. 10 (2011) 290–300.
- [4] M. Goto, et al., Long-term high-temperature operation in the HTTR (2) Core physics, in: Proceedings of the HTR 2010, Prague, Czech Republic, 2010.
- [5] S. Ueta, et al., Development of high temperature gas-cooled reactor (HTGR) fuel in Japan, Prog. Nucl. Energy 53 (2011) 788–793.
- [6] S. Hamamoto, et al., Chemical characteristics of helium coolant of HTTR (High Temperature engineering Test Reactor), in: Proceedings of the HTR 2012, Tokyo, Japan, 2012.
- [7] A. Shimizu, et al., Development of operation and maintenance technology of HTTR (High Temperature engineering Test Reactor), in: Proceedings of the HTR 2012, Tokyo, Japan, 2012.
- [8] Y. Tachibana, et al., Test Plan Using the HTTR for Commercialization of GTHTR300C, Japan Atomic Energy Agency, JAEA-Technology 2009-063, 2009.
- [9] K. Takamatsu, et al., Experiments and validation analyses of HTTR on loss of forced cooling under 30% Reactor power, J. Nucl. Sci. Technol. 51 (2014) 1427–1443.
- [10] M. Ono, et al., Comprehensive seismic evaluation of HTTR against the 2011 Off the Pacific Coast of Tohoku Earthquake, ASME J. Nucl. Rad. Sci. 4 (2) (2018). NERS-16–1104.
- [11] T. Nishihara, et al., Excellent Features of Japanese HTGR Technologies, Japan Atomic Energy Agency, JAEA-Technology 2018-004, 2018.

- [12] S. Nakagawa, et al., Performance test of HTTR, *Nucl. Eng. Des.* 233 (2004) 291–300.
- [13] S. Saito, et al., Design of High Temperature Engineering Test Reactor (HTTR), Japan Atomic Energy Research Institute, JAERI-1332, 1994.
- [14] N. Fujimoto, et al., Nuclear design, *Nucl. Eng. Des.* 233 (2004) 23–36.
- [15] K. Yamashita, et al., Nuclear design of the High-Temperature Engineering Test Reactor (HTTR), *Nucl. Sci. Eng.* 122 (1996) 212–228.
- [16] K.D. Lathrop, F.W. Brinkley, TWOTRAN-II: An Interfaced, Exportable Version of the TWOTRAN Code for Two-Dimensional Transport, Los Alamos, LA-4848-MS, 1973.
- [17] T.B. Fowler, et al., Nuclear Reactor Core Analysis Code: CITATION, Oak Ridge National Laboratory, ORNL-TM-2496, 1971.
- [18] N. Fujimoto, et al., Validation of the nuclear design code system for the HTTR using the criticality assembly VHTRC, *Nucl. Eng. Des.* 233 (2004) 155–162.
- [19] H. Yasuda, et al., Construction of VHTRC (Very High Temperature Reactor Critical Assembly), Japan Atomic Energy Research Institute, JAERI-1305, 1987.
- [20] E. Takada, et al., Core thermal–hydraulic design, *Nucl. Eng. Des.* 233 (2004) 37–43.
- [21] M. Ishihara, et al., Principle design and data of graphite components, *Nucl. Eng. Des.* 233 (2004) 251–260.
- [22] T. Iyoku, et al., Graphite core structures and their structural design criteria in the HTTR, *Nucl. Eng. Des.* 132 (1991) 23–30.
- [23] F.H. Ho, et al., Biaxial failure surface of 2020 and PGX graphites, in: Proceedings of the 7th International Conference on Structural Mechanics in Reactor Technology (SMiRT 7), Chicago, IL, 1983, L4/6, p. 127.
- [24] K. Kikuchi, et al., Failure of graphite short bars with hemispherical seats, *Eng. Fract. Mech.* 19 (1984) 1013–1024.
- [25] S. Yoda, et al., Effects of oxidation on tensile and compressive deformation behavior for nuclear grade isotropic graphite, in: International Carbon Conference 84, Bordeaux, France, 1984.
- [26] R.J. Price, L.A. Beavan, Strength of Nonuniformly Oxidized PGX Graphite, GA-A16270, 1981.
- [27] M. Eto, F.B. Growcock, Effect of Prestress and Stress on Strength and Oxidation Rate of Nuclear Graphite, NUREG/CR-2316, 1984.
- [28] American Society of Mechanical Engineers (ASME), The ASME Boiler and Pressure Vessel Code Case N-47-23 Class 1 Components in Elevated Temperature Service Section III Division I, ASME, New York, 1986.
- [29] M. Shindo, et al., Studies on improving compatibility of nickel-base alloys with a high-temperature helium-cooled reactor (VHTR) environment, in: Proceedings of the International Conference on Gas-Cooled Reactors Today, vol. 2, Bristol, British Nuclear Energy Society, 1982, pp. 179–184.
- [30] Y. Kurata, et al., Improvement of creep resistance of a nickel-base superalloy and its weld metal by controlling boron content, in: Proceedings of the International Conference on Creep, Tokyo, Japan, 1986, pp. 97–102.
- [31] Y. Tachibana, et al., Structural design of high temperature metallic components, *Nucl. Eng. Des.* 233 (2004) 261–272.
- [32] Y. Kurata, et al., Creep rupture characteristics in the HTGR simulated helium gas environment and their relevance to structural design, in: Proceedings of the Workshop Structural Design Criteria for HTR, Jülich, FRG, 1989, pp. 275–292.
- [33] E.L. Robinson, Effect of temperature variation on the longtime strength of steels, *Trans. ASME* 74 (1952) 780–781.
- [34] S. Taira, Lifetime of structures subjected to varying load and temperature, in: N.J. Hoff (Ed.), Creep in Structure, Springer Verlag, Berlin, 1962, pp. 96–119.

- [35] F. Garofalo, et al., Strain–time, rate–stress, and rate–temperature relations during large deformations in creep, in: Proceedings of the Joint International Conference on Creep, Institute Mechanical Engineering, London, 1963, pp. 1–31.
- [36] M.K. Booker, et al., Mechanical property correlations for 2½Cr–1Mo steel in support of nuclear reactor systems design, *Int. J. Press. Vessel. Pip.* 5 (1977) 181–204.
- [37] K. Hada, Influence of variations in creep curve on creep behavior of a high-temperature structure, *Nucl. Eng. Des.* 97 (1986) 279–296.
- [38] T. Iyoku, et al., Design of core components, *Nucl. Eng. Des.* 233 (2004) 71–79.
- [39] J. Sumita, et al., Reactor internals design, *Nucl. Eng. Des.* 233 (2004) 81–88.
- [40] K. Sawa, et al., Research and development on HTGR fuel in the HTTR project, *Nucl. Eng. Des.* 233 (2004) 163–172.
- [41] K. Hayashi, et al., Design Criteria, Production and Total Integrity Assessment of Fuels of the High Temperature Engineering Test Reactor, Japan Atomic Energy Research Institute, JAERI-M 89–161, 1989.
- [42] K. Fukuda, et al., Research and Development of HTGR Fuel, Japan Atomic Energy Research Institute, JEARI-M 89-007, 1989.
- [43] K. Sawa, et al., Fabrication of the first-loading fuel of the high temperature engineering test reactor, *J. Nucl. Sci. Technol.* 36 (1999) 683–690.
- [44] K. Minato, et al., Fission product palladium-silicon carbide interaction in HTGR fuel particles, *J. Nucl. Mater.* 172 (1990) 184–196.
- [45] K. Hayashi, et al., Assessment of Fuel Integrity of the High Temperature Engineering Test Reactor (HTTR) and Its Permissible Design Limit, Japan Atomic Energy Research Institute, JAERI-M 89–162, 1989.
- [46] M. Ishihara, T. Iyoku, Development of graphite design philosophy, *Nucl. Eng. Des.* 233 (2004) 251–260.
- [47] T. Iyoku, et al., Development of thermal/irradiation stress analytical code VIENUS for HTTR graphite block, *J. Nucl. Sci. Technol.* 28 (10) (1991) 921–931.
- [48] M. Ishihara, et al., Development of irradiation-induced stress analysis code system for graphite components in gas-cooled reactor, in: Proceedings of the 12th International Conference on Structural Mechanics in Reactor Technology (SMiRT 12), Stuttgart, Germany, 1993, C08/1.
- [49] T. Iyoku, et al., Seismic response of the high-temperature engineering test reactor core bottom structure, *Nucl. Technol.* 99 (1992) 169–176.
- [50] Nuclear Safety Commission, Guidelines for Aseismic Design of Nuclear Power Plants, 1981.
- [51] K. Iigaki, et al., Seismic design, *Nucl. Eng. Des.* 233 (2004) 59–70.
- [52] T. Iyoku, et al., R&D on core seismic design, *Nucl. Eng. Des.* 233 (2004) 225–234.
- [53] T. Iyoku, et al., Seismic study of High-Temperature Engineering Test Reactor core graphite structures, *Nucl. Technol.* 99 (1992) 158–168.
- [54] T. Ikushima, SONATINA-2V: A Computer Program for Seismic Analysis of the Two-Dimensional Vertical Slice HTGR Core, Japan Atomic Energy Research Institute, JAERI-1279, 1982.
- [55] M. Ishihara, T. Iyoku, M. Futakawa, Evaluation of aseismic integrity in HTTR core-bottom structure. III. Structural integrity of core support post component, *Nucl. Eng. Des.* 148 (1994) 91–100.
- [56] M. Ishihara, T. Iyoku, M. Futakawa, Evaluation of aseismic integrity in HTTR core-bottom structure. IV. Structural integrity of connecting elements between graphite components, *Nucl. Eng. Des.* 158 (1995) 83–95.
- [57] T. Furusawa, et al., Cooling system design and structural integrity evaluation, *Nucl. Eng. Des.* 233 (2004) 113–124.

- [58] M. Shindo, T. Kondo, Studies on improving compatibility of nickel-base alloys with high temperature helium-cooled reactor (VHTR) environment, in: BNES Conference, Gas-Cooled Reactors Today, Bristol, 1982.
- [59] T. Nishihara, et al., Demonstration test of hydrogen production using high temperature gas-cooled reactor, in: Proceedings of the 15th World Hydrogen Energy Conference, Yokohama, Japan, 2004.
- [60] Y. Tachibana, et al., Reactivity control system of the high temperature engineering test reactor, *Nucl. Eng. Des.* 233 (2004) 89–101.
- [61] S. Maruyama, et al., Temperature Analysis of Control Rod for HTTR, Japan Atomic Energy Research Institute, JAERI-M 90-104, 1990.
- [62] I. Nishiguchi, et al., General Criteria for the Structural Design of the HTTR Control Rods, Japan Atomic Energy Research Institute, JAERI-M 90-152, 1990.
- [63] K. Watanabe, T. Kondo, Y. Ogawa, Postirradiation tensile and creep properties of heat-resistant alloys, *Nucl. Technol.* 66 (1984) 630–638.
- [64] National Research Institute for Metals (NRIM) Creep Data Sheet No. 26 A, Data Sheets on the Elevated-Temperature Properties of Iron Base 21Cr–32Ni–Ti–Al Alloy Plates for Corrosion and Heat Resistant Applications (NCF 800H-P), National Research Institute for Metals, Tokyo, 1983.
- [65] National Research Institute for Metals (NRIM) Creep Data Sheet No. 27 A, Data Sheets on the Elevated-Temperature Properties of Iron Base 21Cr–32Ni–Ti–Al Alloy Tubes for Heat Exchanger Seamless Tubes (NCF 800H-TB), National Research Institute for Metals, Tokyo, 1983.
- [66] Y. Monma, et al., Assessment of elevated-temperature property data for alloy 800H, *Trans. Natl. Res. Inst. Met.* 26 (3) (1984) 33–47.
- [67] J. Fukakura, F. Matsumoto, T. Araki, Effect of strain hold time on fatigue life of alloy 800H at high temperatures, *Trans. Jpn. Soc. Mech. Eng.* 57 (540) (1991) 1700–1705.
- [68] R. Hino, Y. Miyamoto, H. Fukushima, Reliability test on control rod driving mechanism of HTTR with HENDEL, *J. At. Energy Soc. Jpn.* 33 (1991) 685–694.
- [69] A.L. Edwards, TRUMP: A Computer Program for Transient and Steady State Temperature Distribution in Multidimensional Systems, Lawrence Livermore Laboratory report, UCRL-14754, rev. 3, 1972.
- [70] M. Hirano, K. Hada, Development of THYDE-HTGR: Computer Code for Transient Thermal-Hydraulics of High Temperature Gas-Cooled Reactor, Japan Atomic Energy Research Institute, JAERI-M 90-071, 1990.
- [71] Y. Tachibana, et al., Integrity assessment of the High Temperature Engineering Test Reactor (HTTR) control rod at very high Temperatures, *Nucl. Eng. Des.* 172 (1997) 93–102.
- [72] Y. Shimakawa, et al., The plant dynamics analysis code ASURA for the high temperature engineering test reactor (HTTR), Specialist's meeting on uncertainties in physics calculations for gas cooled reactor cores, Villigen, Switzerland, 1990.
- [73] K. Saito, et al., Instrumentation and control system design, *Nucl. Eng. Des.* 233 (2004) 125–133.
- [74] N. Sakaba, et al., Leak-tightness characteristics concerning the containment structures of the HTTR, *Nucl. Eng. Des.* 233 (2004) 135–145.
- [75] M. Kondo, et al., Leakage Rate Test for Reactor Containment Vessel of HTTR, Japan Atomic Energy Agency, JAEA-Testing 2006-002, 2006.
- [76] K. Iigaki, et al., Performance tests of reactor containment structures of the HTTR, in: Proceedings of the 16th International Conference on Structural Mechanics in Reactor Technology (SMiRT 16), Washington, DC, 2001.

- [77] T. Aono, et al., Maintenance and Management of Emergency Air Purification System in HTTR, Japan Atomic Energy Agency, JAEA-Testing 2006-004, 2006.
- [78] N. Sakaba, et al., Short design descriptions of other systems of the HTTR, Nucl. Eng. Des. 233 (2004) 147–154.
- [79] Y. Inagaki, et al., Cooling performance of helium-gas/water coolers in HENDEL, Nucl. Eng. Des. 146 (1994) 301–309.
- [80] S. Nakagawa, et al., Development of the Unattended Spent Fuel Flow Monitoring Safeguards System (UFFM) for the High Temperature Engineering Test Reactor (HTTR) (Joint research), Japan Atomic Energy Agency, JAEA-Technology 2007-003, 2007.
- [81] K. Kunitomi, et al., Safety design, Nucl. Eng. Des. 233 (2004) 45–58.
- [82] ICRP, Recommendations of the International Commission on Radiological Protection, ICRP Publication 26, Program Press, Elmsford, NY, 1977.
- [83] International Atomic Energy Agency (IAEA), Basic Safety principles for Nuclear Power Plants 75-INSAG-3 Rev. 1, INSAG-12, 1999.
- [84] K. Kunitomi, et al., Safety evaluation of the HTTR, Nucl. Eng. Des. 233 (2004) 235–249.
- [85] S. Nakagawa, et al., Core Dynamics Analysis Code for High Temperature Gas Reactor BLOOST-J2, JAERI-M 89-0132, 1989.
- [86] M. Merrill, BLOOST-5: A Combined Reactor Kinetics—Heat Transfer Code for the IBM-7044; Preliminary Description, General Atomics, GAMD-6644, 1965.
- [87] M. Hirano, et al., Development of THYDE-HTGR: Computer Code for Transient Thermal-Hydraulics of High-Temperature Gas-Cooled Reactor, Japan Atomic Energy Research Institute, JAERI-M 90-071, 1990.
- [88] Y. Asahi, et al., THYDE-P2 Code: RCS (Reactor-Coolant System) Analysis Code, Japan Atomic Energy Research Institute, JAERI 1300, 1986.
- [89] M. Hirano, Analysis of LOFT Small Break Experiment L3-1 with THYDE-P Code: CSNI International Standard Problem No. 9 and THYDE-P Sample Calculation Run 50, JAERI-M 82-008, 1982.
- [90] K. Kunitomi, et al., Two-Dimensional Thermal Analysis Code “TAC-NC” for High Temperature Engineering Test Reactor and Its Verification, Japan Atomic Energy Research Institute, JAERI-M 89-001, 1989.
- [91] S.S. Clark, J.F. Petersen, TAC2D: A General Purpose Two-Dimensional Heat Transfer Computer Code—Mathematical Formulations and Programmer’s Guide, General Atomics, GA-9262, 1969.
- [92] R.K. Deremer, et al., RATSAM: A Computer Program to Analyze the Transient Behavior of the HTGR Primary Coolant System During Accidents, General Atomics, GA-A-13705, 1977.
- [93] R.G. Gido, et al., COMPARE-MOD1: A Code for the Transient Analysis of Volumes with Heat Sinks, Flowing Vents and Doors, Los Alamos, LA-7199-MS, 1978.
- [94] H. Kawakami, Air oxidation behavior of carbon and graphite materials for HTGR, Tanso 124 (1986) 26–33.
- [95] M.B. Peroominan, OXIDE-3: A Computer Code for Analysis of HTGR Steam or Air Ingress Accidents, General Atomics, GA-A 12493, 1975.
- [96] S. Maruyama, et al., Verification of Combined Thermal-Hydraulics and Heat Conduction Analysis Code FLOWNET/TRUMP, Japan Atomic Energy Research Institute, JAERI-M 88-173, 1988.